Dynamic Optimization Applied for Modelling and Optimal Control of a Packed Bed Reactor for Chemical-Looping Combustion

by

Marco Antonio Lucio Hernandez

A thesis
presented to the University of Waterloo
in fulfillment of the
thesis requirement for the degree of
Masters of Applied Science
in
Chemical Engineering

Waterloo, Ontario, Canada, 2019

AUTHOR'S DECLARATION

I hereby declare that I am the sole author of this thesis. This is a true copy of the thesis, including any required final revisions, as accepted by my examiners.

I understand that my thesis may be made electronically available to the public.

Abstract

Chemical-looping combustion (CLC) has recently emerged as a promising technology capable of curbing CO_2 emissions while also reducing the energy penalty entailed in carbon capture and sequestration (CCS). The novelty of CLC resides in its use of a metal oxide as an intermediate that serves the purpose of avoiding direct contact between fuel and air. The CLC process can be carried out in a packed bed reactor, in which the metal oxide supported in an inert material is intermittently exposed to both air and fuel streams. The oxidation stage produces a high temperature air stream that is used to feed a gas turbine and the reduction stage produces a highly concentrated CO_2 stream suitable for sequestration. The transient operation of the system is complex and temperature fluctuations and unconverted fuel at the reactor's exit is expected during the oxidation and reduction stages. To the author's knowledge, a study that specifies optimal control strategies focused on increasing the efficiency of every stage in the CLC PBR cycle is in critical need to advance this emerging technology.

The aim of this study is to adapt an existing 1-D mechanistic heterogeneous dynamic model, which considers mass and heat transport resistances in the particle (metal oxide and support) and the bulk fluid phases. The non-linear model is subject to validation against published data and a sensitivity analysis on key parameters during both reaction stages. Later, each reaction-stage simulation is formulated as an optimal control dynamic optimization problem that is solved using the direct transcription approach. The optimization results show improvements in the heat recovery process during the oxidation stage and a considerable reduction in fuel slip during the reduction stage, effectively producing more CO_2. Moreover, based on the outcome of the sensitivity analysis, an optimistic and a worst-case scenario are considered.

The dynamic optimization of the optimistic case shows even greater improvements in energy production during the oxidation stage and the results from the worst-case shows that a 97% rate of fuel conversion can be achieved within the reactor.

Acknowledgements

I would like to thank Professor Luis Ricardez-Sandoval, for giving me with the opportunity to pursue a MASc degree at the University of Waterloo and also for all the support and guidance throughout this work.

I would like to extend my appreciation to the readers of my thesis,

And a special acknowledgement to my father who always pushed me into pursuing a graduate degree. I would like to thank my mother, sister and brother for the unconditional support during these 2 years. And last but not least, to Rachel Allison for helping me feel loved and welcome in Canada.

Finally, I am thankful for the financial support provided by the Mexican Government across the Consejo Nacional de Ciencia y Tecnología (CONACYT)

Dedicated to my family

Table of Contents

List of Figures

List of Tables

Nomenclature

English symbols

1-D	One-dimensional
2-D	Two-dimensional
3-D	Three-dimensional
$a0_j$	Initial specific surface area of the OC
A_c	Cross-sectional area of the rector tube [m²]
Al_2O_3	Alumina
Ar	Argon
a_v	External particle surface area per unit volume reactor volume [1/m]
$C_{i,j}$	Concentration of gas species *i* in fluid phase at stage *j* [mol/m³]
$C_{c\ i,j}$	Concentration of gas species *i* in solid phase at stage *j* [mol/m³]
$C_{T\ j}$	Total gas concentration in fluid phase at stage *j* [mol/m³]
CCS	Carbon capture and sequestration
CFC	Chlorofluorocarbon
CFD	Computational fluid dynamic
CH_4	Methane
CLC	Chemical-looping combustion
CO	Carbon monoxide
CO_2	Carbon dioxide
C_{Fs}	Set-point for the fuel slip
$C_{\mathrm{pf}\ j}$	Heat capacity of the gas mixture in the fluid phase at stage *j* [J/mol/K]
$C_{p\ i,j}$	Heat capacity of component i in the gas mixture at stage j [J/mol/K]
$C_{pc\ j}$	Heat capacity of the gas mixture in the particle at stage *j* [J/mol/K]
$C_{ps\ j}$	Heat capacity of the OC at stage *j* [J/mol/K]
$C_{Tc\ j}$	Total gas concentration in the solid phase [mol/m³]
Cu	Copper

C_{MS}	Set-point of methane slip
$C'_{Ni,j}$	Initial concentration of Nickel in the OC [kgNi/kgOC]
$C'_{NiO,j}$	Initial concentration of Nickel oxide in the OC [kgNiO/kgOC]
C_{OS}	Set-point of oxygen slip
$D_{ax\ i,j}$	Axial dispersion coefficient of species *i* at stage *j* [m²/s]
$D_{e\ i,j}$	Effective diffusion coefficient of species *i* at stage *j* [m²/s]
$D_{k\ i,j}$	Knudsen diffusivity
$D_{m\ i,j}$	Diffusion coefficient of the component i in the mixture at j [m²/s]
$D_{w,i,j}$	Binary gas phase diffusivity [m²/s]
Dp	Particle diameter [m]
$E_{CH_4,j}$	Activation energy of the reduction reaction at stage j [J/mol]
$E_{a\ CO,j}$	Activation energy of the reduction reaction at stage j [J/mol]
$E_{a\ H_2,j}$	Activation energy of the reduction reaction at stage j [J/mol]
$E_{a\ O_2,j}$	Activation energy of the oxidation reaction at stage j [J/mol]
EOR	Enhanced oil recovery
Fe	Iron
Fe_2O_3	Hematite
Fe_2O_4	Magnetite
$F_{i,j}$	molar flow rate of gas species *i* [mol/s]
$F_{in\ j}$	molar flow rate of gas species *i* at the inlet [mol/s]
$F_{T\ j}$	Total molar flow rate of gas species *i* [mol/s]
G_j	Inlet mass flux at stage *j* [kg/m²/s]
GHG	Greenhouse gas
GRACE	Grangemouth Advanced CO_2 Capture Project
H_2	Hydrogen
H_2O	Water
$h_{f\ j}$	heat transfer coefficient between fluid phase and OC particle at stage *j* [W/m²/K]
HRSG	Heat recovery steam generation

IEA	International energy agency
IFBR	Interconnected fluidized bed reactor
IGCC	Integrated gasification combined cycle
k_j	Time element at j stage
$k0_{CH_4,j}$	Frequency factor of OC reduction with methane [m/s]
$k0_{CO,j}$	Frequency factor of OC reduction with carbon monoxide [m/s]
$k0_{H_2,j}$	Frequency factor of OC reduction with hydrogen [m/s]
$k0_{O_2,j}$	Frequency factor for OC oxidation reaction [m/s]
$k_{c\ i,j}$	Mass transfer coefficient between bulk phase and OC particle of species *i* at stage *j* [m/s]
M_i	Molecular weight of gas species *i*
MEA	Monoethanolamide
Me	Metal
Me_xO_y	Metal oxide
N_2	Nitrogen
NFE	Number of finite elements
Ni	Nickel
NiO	Nickel oxide
n_i	Reaction order for each gas species *i*
L	Reactor length [m]
O_2	Oxygen
OC	Oxygen-carrier
P	Pressure [bar]
PBR	Packed bed reactor
$Pe_{a\ i,j}$	Axial Peclet number of component *i* at stage *j*
Pr_j	Prandtl number at stage *j*
PSA	Pressure swing absorber
r	Reactor radial element
$R_{i\ j}$	Rate of reaction of component *i* at stage *j* [1/s]

$Re_{p\ j}$	Reynolds number based on initial superficial velocity at stage j
R_g	Gas constant [J/mol/K]
Rp	OC particle radius [m]
$Sc_{i,j}$	Schmidt number of component *i* at stage *j*
t	Time element
$T_{c\ j}$	Temperature of the solid phase at stage *j* [K]
T_j	Temperature of the fluid phase at stage *j* [K]
T_{exit}	Set-point for exit temperature [K]
TiO_2	Titanium dioxide
TIT	Turbine inlet temperature [K]
V	Volume
$v_{0\ j}$	superficial velocity [m/s]
X_j	Conversion of the oxygen-carrier at stage j
$y_{i,j}$	Mole fraction of the species *i* in the feed at stage *j*
$y_{ifeed\ j}$	Mole fraction of the species *i* in the feed
z	Length element

Greek symbols

$\Delta H_{i,j}$	Heat of reaction at stage *j* [J/mol]
ε_b	Bed porosity
ε_c	Oxygen-carrier porosity
φ_i	Stoichiometric coefficient of component i
$\lambda_{ax\ j}$	Axial heat dispersion coefficient at stage *j* [W/m/K]
$\lambda_{m\ j}$	Thermal conductivity of gas mixture at stage *j* [W/m/K]
$\lambda_{s\ j}$	Thermal conductivity of the oxygen-carrier at stage *j* [W/m/K]
μ_j	Viscosity of the gas mixture at stage *j* [N*s/m²]
$\rho_{\ j}$	Density of the gas mixture at stage *j* [kg/m³]
$\rho_{s\ j}$	Density of the oxygen-carrier at stage *j* [mol/m³]

τ	Tortuosity

Subscripts

i	Gas phase species
in	Initial
j	Stage of the CLC sequence
s	Solid phase

Chapter 1
Introduction

The temperature on Earth is highly dependent on the concentration of greenhouse gases (GHGs); without these gases, the average global temperature would be -20 °C instead of 15°C. The principal GHGs affecting the atmosphere include water (H_2O), carbon dioxide (CO_2), methane (CH_4), nitrous oxide (N_2O), chlorofluorocarbons (CFC's) and sulfur hexafluoride (SF_6). Carbon dioxide is a long-lived gas that persists semi-permanently in the atmosphere and does not respond either physically or chemically to changes in temperature. CO_2 affects physically or chemically all the others GHGs in the atmosphere, such as water; as well; causes increments in ocean acidity, sea levels, as well as drastic weather changes. Anthropogenic GHG emissions are responsible for 75% of the CO_2 produced globally; which , along with its long lifespan in the atmosphere (300 years), makes carbon dioxide the pivotal point of attention in climate-change endeavours [1].

Prior to the industrial revolution, the concentration of CO_2 in the atmosphere was 280 ppm. This value has increased significantly during the post-industrial era, reaching a level of 406 ppm in 2017 [2]. It is widely agreed that in order to prevent significant changes in the Earth's global climate, such as rising temperatures and melting of the artic, the concentration of CO_2 must not exceed 450 ppm. Thus far, technologic advances have intended to stop crossing this threshold by focusing on improving fossil-fired energy production systems, such as power plants; switching to renewable energy sources, such as nuclear, solar or wind; enhancing biological sinks and reducing non-CO_2 greenhouse gas emissions. However, these technologies are unable to fully replace fossil-fired power generation as the main source of energy, thus increasing the challenge of lowering CO_2 levels [3].

In light of these energy challenges, carbon capture and sequestration (CCS) is a promising alternative technology with the potential to curb CO_2 emissions. These technologies often involve CO_2 separation, pressurization, transportation and sequestration. According to the International Energy Agency (IEA), in order to stop drastic detrimental changes in the Earth's ecosystems, a 20% reduction of global CO_2 emissions would need to be achieved via CCS by 2050 [4]. Power generation is a suitable sector for the application of CCS since it is responsible for approximately 40% of all anthropogenic CO_2 emissions and it is more propitious in terms of the suitability of emissions types and existing infrastructure. Even so, an existing power plant (natural gas and/or integrated gasification combined cycle) without CCS would require an extra 10-25% energy input to capture the CO_2 generated. Despite its relatively large contribution to global CO_2 emissions, the automobile source sector would require more infrastructure to achieve a lower sequestration percentage than power generation [5].

Studies indicate that the number of large point sources of CO_2 is projected to increase in the future. By 2050, around 20-40% of global fossil fuel emissions would meet the criterion to be technically suitable for capture, 30-60% thereof would be CO_2 emissions produced by the power generation sector [5]. The inclusion of CCS and enhanced oil recovery (EOR) would increase production costs of electricity for a natural gas combined cycle by 40 %; whereas an integrated gasification combined cycle (IGCC) would only see a 16% increase in costs [5]. For this reason, investigating a cost-effective CCS technology is necessary in order to achieve a feasible CO_2 emissions control in fossil fuel-based power plants.

The most advanced technological pathways currently available for CCS in power generation are post-combustion, pre-combustion, and oxy-fuel combustion. Post-

combustion CO_2 capture has by far the greatest short-term potential for reducing GHGs as it is applicable to the majority of existing power plants. Pre-combustion and oxyfuel technologies are less common since they require extra adjustments in existing plant configurations. Moreover, commercially available CCS technologies face the obstacles of high capital costs alongside a high energy penalty, which results in reductions in process efficiency and increases in the price of the energy [3], [6].

Consequently, further research and development of low-cost CCS will be necessary in the upcoming years. Chemical-looping combustion (CLC) has been identified as one of the most promising options because of its potential to reduce the energy penalty; therefore, reducing the economic cost of CO_2 capture [7]. CLC is an emerging technology that has gained an increasing amount of attention and thus, important breakthroughs in its development. This technology can be categorized as an oxy-fuel alternative, as it avoids direct contact between air and fuel, while simultaneously producing power using a gas turbine. Hence, the production of nitrogen dilutions is circumvented, and a highly concentrated CO_2 stream is generated.

At its core, the CLC process can be viewed as an alternated batch process of oxidation and reduction of a metal or /metal oxide by an air and fuel stream, respectively. During the oxidation stage, the oxygen molecules are transferred to the metal; while a heat front is produced as product of the exothermic reaction. Consequently, in the reduction stage, a fuel stream reduces the same metal oxide forming CO_2 and H_2O as the main by-products.

In principle, CLC can be used with gaseous, liquid or solid fuels, with gaseous being the easiest to implement. The CLC process can be carried out using interconnected fluidized bed (IFBR) or packed bed reactors (PBR), which avoid solid-gas separation and allow the

specification of a more compact reactor design due to an increase in operating pressure [8]. On the other hand, implementing a packed bed reactor requires a multibed configuration to provide a high temperature stream to the downstream gas turbine; additionally, during the reduction process, fuel slip may occur and must be avoided to accomplish high CO_2 efficiency recovery. Thus, a sophisticated control system is required for packed bed operation.

1.1 Research objectives

There are limited studies on packed bed CLC reactor modelling, as only several have been published [9]–[14]. These current available models can describe the CLC phenomena in a PBR in various ways; the mechanistic models can include 1-D or 2-D spatial domains, consider heterogenous or homogeneous phases or even be expressed as an analytical solution. In recent years there was one study addressing dynamic optimization and control [13]; in that work, the authors presented a control scheme using dynamic optimization while the control actions remained constant during each stage of the CLC cycle. To the author's knowledge, a study that specifies optimal control strategies focused on increasing the efficiency of every stage in the CLC packed bed cycle (oxidation, reduction and purges) is in critical need to advance this emerging technology. By proposing optimal control frameworks, the objectives of this thesis include:

- Enhancing the heat recovery in the oxidation process
- Augmenting the fuel conversion into CO_2 by reducing the fuel slip at the reactor's exit
- Reducing the amount of inert gas used during the purge

The novelty of this work is that the aforementioned study will be accomplished by modelling a 1-D mechanistic heterogeneous model, which will be validated using data reported in the literature. The proposed modelling framework will be used to solve an optimal control problem which would be casted as a dynamic optimization formulation. The use of these types of control schemes would assist in having a more accurate control of the state variables at each stage. By presenting optimal control profiles for each reaction stage, the possibility of achieving the proper smooth operation of a large-scale CLC PBR is showed. A framework of this type would will advance this technology and more insight towards scale-up and commercialization of CLC technologies. Moreover, it is intended to encourage more attention on this technology as a feasible solution to the greenhouse effect.

This thesis is organized as follows:

In Chapter 2 a literature review of the technology in its current status is presented, including advances in its development and areas of focus in current research. The goal of this review is to identify the gaps in the literature on dynamic simulation for CLC in packed beds.

Chapter 3 focuses on presenting the adapted mechanistic dynamic model and a base-case scenario, which was validated against published data; moreover, a sensitivity analysis will also be included.

Chapter 4, the same mechanistic model structure is used aiming towards increasing the energy production and the fuel conversion into CO_2 during the oxidation and reduction stage respectively. These will be achieved by performing manual step changes, optimal control strategies and dynamic optimization of an optimistic and worst-case scenarios.

Chapter 5 will present the conclusions and a brief overview of potential areas for future works.

Chapter 2
Literature Review

This chapter presents the relevant literature on CLC technology. The scope of this review will include a general overview of the different available CCS technologies, a CLC process description and current technological status, relevant information on types of oxygen-carriers and reactor configurations, with their respective design and operational features and limitations. Additionally, this chapter will review the status of modelling and optimization on interconnected fluidized bed reactors and packed bed reactors for CLC. This review intends to highlight the need for further research in dynamic modelling of a CLC PBR; specifically, the features of implementing dynamic optimization to identify optimal control strategies for this process. In the context of this research gap, the intention of this thesis is to contribute to the dynamic control and dynamic operation field of a CLC PBR.

2.1 Overview of the CCS pathways

Carbon Capture and Sequestration (CCS) has proven to be a feasible clean energy approach for the power generation industry. Globally speaking, the high demand for energy generation through fossil fuels will remain constant in the foreseeable future, since other energy sources are not forecasted to meet up the global demand during the first half of the 21st century [15]. Therefore, the development of CCS technologies is utterly important in order to reduce the global concentration of CO_2.

The goal behind CCS is to produce a highly concentrated CO_2 stream from an industrial source, transport it and then store it away from the atmosphere. Regarding the

highly concentrated CO_2 stream, the three main pathways considered are: Post-combustion technologies, Pre-combustion decarbonization and Oxy-fuel combustion, as shown in Figure 1.

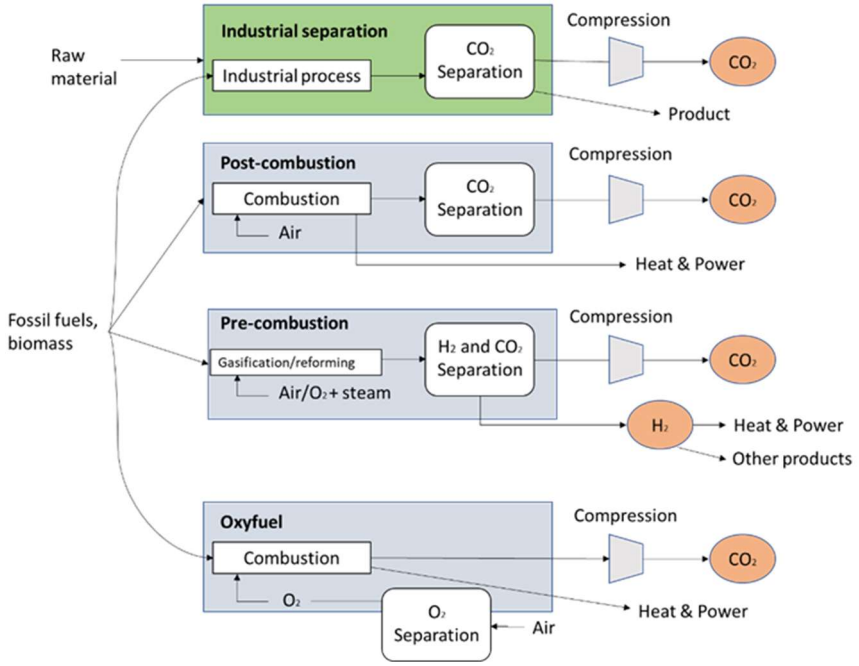

Figure 1. Schematic diagram of Carbon Capture and Storage (CCS) technology

Post-combustion capture is the separation of CO_2 from the flue gas after power generation, which means that it is the last step on the process flowsheet. The stripping of CO_2 from nitrogen and small quantities of oxygen and vapor is usually performed by one of the following methods: absorption using solvents or solid sorbents, pressure and temperature swing adsorption, cryogenic distillation, or selective membranes [16]. Existing power plants use air for combustion, which generates a flue gas that is at atmospheric pressure and typically has a low partial pressure of CO_2 (8-15 %vol). Therefore, the use of monoethanolamide (MEA) is preferred over physical absorption in this case, since the low-pressure operations allow for no pressure drop in the CO_2 separation process. The principal

advantage of this approach is that it has the greatest short-term potential for reducing GHGs because it can be applied to the majority of existing power plants. The limitations of post-combustion include a drop in net efficiency of 10-14 % due to its intrinsic low concentrations of CO_2, as well as its large volumes of flue gas, high compression ratios, and high energy expenditures in order to cool the CO_2 before it is captured [17]–[19].

Pre-combustion decarbonization capture is a process whereby CO_2 is recovered before the fuel is burned. The process involves reacting a fuel with oxygen and/or steam to produce a synthesis gas (syngas) or fuel gas composed mainly of carbon monoxide and hydrogen, which is then combined with steam in a catalytic reactor, called a shift converter, to form CO_2 and more hydrogen. The CO_2 is then separated from the hydrogen by physical or chemical absorption [20]. An example of a pre-combustion process is the integrated gasification combined cycle (IGCC) with a pressure swing absorber (PSA), which separates the CO_2 from H_2 and H_2O. The main advantage of the pre-combustion process is the fact that it produces a higher CO_2 concentration stream. Since this process can be operated at higher pressures and temperatures, the size and costs of the equipment for the CCS facilities, such as the PSA, are reduced. Moreover, the use of physical solvents can be implemented in IGCC as an alternative due the high partial pressure of CO_2. A main benefit of physical over chemical solvents is the less intensive energy penalty for regeneration, whilst the limitation is that they work better under low temperatures [20]. The main drawback of this CCS pathway is that the implementation of an IGCC incurs more capital cost than the add-on of a CO_2 stripper in post-combustion capture [21]–[23]. This financial drawback combined with the harsh operational conditions involved in the pre-combustion combined cycles indicate that more research and insight regarding the most effective separation mechanism are necessary.

Oxy-fuel combustion, refers to the process of burning fuel with almost pure oxygen, which in turn creates a purer CO_2 flue stream without nitrogen dilution. Consequently, the cost of CO_2 separation diminishes greatly, since only water vapor must be removed from the exhaust stream. Oxy-fuel combustion can be applied to several fuels, including coal, natural gas or blends of biomass and coal. The main drawbacks of this process are the fact that it is energy intensive due the separation of pure oxygen from air and the high combustion temperatures reached after using pure oxygen in the fuel blend require special alloy materials. The latter could be circumvented by recirculating the flue gas back into the burners to control the flame temperature. It is reported that the air separation unit requires 60% of the total CCS energy penalty for an oxy-fuel system, decreasing the overall plant efficiency by 7-9% [24].

Based on the above, all the three aforementioned CCS technological pathways face the obstacles of high capital costs alongside a high energy penalty, which results in reductions in process efficiency and increases in the price of the energy. Thus far, post-combustion capture technology is the most mature technology due to its easier installation on existing power plants; despite its high energy penalty, it remains as the pathway with the greatest short-term potential for reducing CO_2 emissions. Therefore, CLC, which can be considered as an oxy-fuel process, has been identified as one of the most promising technologies that has the potential to decrease the said energy penalty while still producing the highly concentrated CO_2 stream.

2.2 CLC progress through the years

In 1954, Lewis and Gilliard et al. were the first to identify a process capable of producing pure carbon dioxide. In their study on production of pure CO_2 they also introduced

novel concepts including: oxygen-carrier (OC), fuel flexibility to reduce CO_2, and the use of two interconnected fluidized beds as a framework to carry out the process [25]. Later, Richter and Knoche et al. developed a fuel oxidation scheme involving two intermediate reactions with a metal oxide, such as copper oxide, nickel oxide or cadmium oxide, acting as the OC, with the idea of enhancing the thermal efficiency in fossil fuel fired power plants [26]. Moreover, in 1987 Ishida et al. introduced the concept of chemical-looping combustion with the aim of reducing the exergy loss caused by the conversion of fuel energy into thermal energy. Later on, Jin et al. suggested the use of CLC as a way to capture CO_2 using metal OCs [27]–[29].

Up to that point, CLC was merely a concept that had been tested in a limited number of experiments. It was not until the Grangemouth Advanced CO_2 Capture Project (GRACE) in 2000, that more than 300 different particles were evaluated, two of which were produced in large quantities for testing in a 10 kWth chemical-looping combustor unit built specifically for the project [30], [31]. Subsequently, the fist demonstration of the technology was performed by Lyngfelt and Thunman et al., who presented the first 100 hours of continuous CLC operation using natural gas as fuel and a Ni-based OC, which ended up being capable of achieving 99.5% conversion efficiency [32].

Similar projects were launched in which a 300 Wth CLC reactor was built and operated over the time span of 30-70 h, the same reactor was used to evaluate the performance of three different OCs (i.e. nickel, iron and manganese-based OC) [33]. In addition, Ryu et al. operated a 50 kWth unit during 28 h using methane as fuel and tested nickel and cobalt-based OCs [34].

The first long term operation (120 h) was performed at the Institute of Carboquimica (IBC-CSIC) as reported by Adanez et al. in 2006. The experiment was carried out in a 10

kWth CLC plant using a copper-based OC, which effectively debunked the erroneous belief that copper-based materials were not adequate for operation in fluidized-bed reactors due to agglomeration. The results showed a 100% CO_2 capture at 800 °C, without agglomeration [35], [36]. Moreover, the investigation of the CLC process at a lab-scale capacity has been implemented by some research groups. Table 1 shows the prominent CLC units using gaseous and solid fuels that have been reported in the open literature.

Table 1 Prominent CLC lab-scale and pilot-scale units

Location	Unit size (kWth)	Configuration	Fuel	Reference
Chalmers University of Technology, Chalmers, Sweden	10	IFBR	CH_4, syngas, coke, coal	[37]
Institute of Carboquimica, ICB-CSIC, Spain	10	IFBR	CH_4	[35]
IFP-Total, France	10	IFBR	CH_4	[38]
Xi'an Jiaotong University, China	10	IFBR	Coke	[39]
Southeast University, China	10	IFBR	Coal, biomass	[40], [41]
ALSTOM Power Boilers, France	15	IFBR	CH_4, syngas,	[31]
Ohio State University, Ohio, USA	25	Interconnected moving bed	Coal	[42]
Korean Institute of Energy Research, Kier, Korea	50	IFBR	CH_4, CO, H_2	[34]
Technical University of Vienna, Tuwien, Austria	120	IFBR	CH_4, CO, H_2	[43], [44]
Darmstadt University of Technology, Germany	1,000	IFBR	Coal	[45], [46]
ALSTOM Windsor, Connecticut, USA	3,000	IFBR	Coal	[47], [48]

Thus far, the principal focus of research efforts investigating CLC has been directed to the improvement or development of OC materials suitable for the operation [49]. Since harsh operating conditions, such as high temperatures and pressures, are presented in the CLC process, the main goals are to increase reactivity and durability. Table 2 shows a summary of the operating hours for each material in continuous operation for studies up to 2018 [50]–[54].

Table 2. Experience summary time on CLC in continuous operation units [55], [56]

Oxygen-carrier material	**CLC operating hours**
Nickel	>2,114
Copper	>391
Iron	>445
Manganese	70
Cobalt	25
Mixed oxides	82

2.3 Process description

The CLC process is composed of an oxidation process (also known as air reactor) and a reduction process (also known as fuel reactor), as show in Figure 2. The use of a metal oxide as an intermediate serves the purpose of completing the cycle between the two reactors.

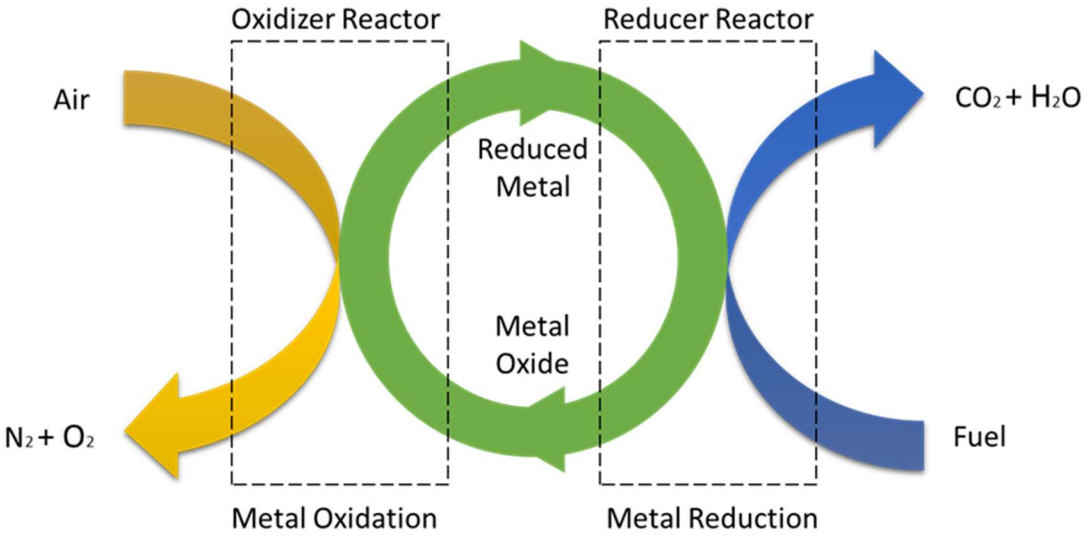

Figure 2. Diagram of the chemical-looping combustion (CLC) process

During the oxidation stage (see Equation 2.1), the metal is in direct contact with an air stream; thus, metal is oxidized by oxygen (exothermic reaction). The flue gas contains N_2 and unreacted O_2 and is heated up to a temperature between 900 and 1,200 °C by the packed bed, thus making it suitable for driving a gas turbine for power generation [8], [30], [57].

$$2Me_xO_{y-1} + O_2 \rightarrow 2Me_xO_y \quad (2.1)$$

In the reduction stage (see Equation 2.2), the fuel is oxidized to form CO_2 and H_2O by a metal oxide (Me_xO_y) that is reduced to a metal (Me). The H_2O presented in the product stream could be removed after a simple water condensation, leaving an almost pure CO_2 stream that is ready for transportation and storage. Hence, this technology would avoid the necessity of using extra separation equipment, which is required by other CCS technologies. Additionally, the net chemical reaction over the two steps, and therefore the combustion

enthalpy, is the same as conventional combustion; thus, the total amount of heat released in the CLC process is the same as in conventional combustion [3].

$$C_nH_{2m} + (2n + m)Me_xO_y \rightarrow (2\mathrm{n} + \mathrm{m})Me_xO_{y-1} + nCO_2 + mH_2O \quad (2.2)$$

The overall non-catalytic reduction reactions between the metal oxide and CH_4, CO, and H_2, which are the main compounds present in natural gas and syngas, are described by the following reactions:

$$2Me_xO_y + CH_4 \rightarrow 2Me_xO_{y-1} + CO_2 + 2H_2 \quad (2.3)$$

$$Me_xO_y + CH_4 \rightarrow Me_xO_{y-1} + CO + 2H_2 \quad (2.4)$$

$$Me_xO_y + CO \rightarrow Me_xO_{y-1} + CO_2 \quad (2.5)$$

$$Me_xO_y + H_2 \rightarrow Me_xO_{y-1} + H_2O \quad (2.6)$$

Other heterogeneous catalysed reactions can take place in the reduction phase, such as those catalyzed by the reduction of the support material [58]. The kinetics of the metal oxide reduction can differ widely depending on variables such as the reducing fuel, the selected metal oxide, the OC preparation method, and a variety of conditions during testing [59]–[62].

2.4 Oxygen-carrier characteristics

Identifying the proper solid compound capable of conveying the transfer of oxygen in a CLC process is an essential task. The main characteristics of an effective OC material are as follows [3], [49], [55]:

- High oxygen transport capacity
- High reactivity, to reduce inventories
- Favourable tendency towards high conversion of fuel gas to CO_2 and H_2O

- Resistance to attrition to minimize losses of OC material
- Cost-efficient
- Low environmental impact

Oxygen transport capacity is one key characteristic of the OC which is important for process design and operation. The oxygen transport capacity is one indicator of the amount of oxygen that can be transferred by the OC between reaction stages. Hence, the amount of active metal/metal oxide in the reactor necessary to carry away the mass balance is affected. Abad et al. [63] selected 16 kg/s-MW as the maximum circulation rate feasible in a interconnected fluidized bed reactor for CLC at atmospheric pressure; although the actual value would depend on the properties of the OC particles. On the other hand, there is not a work in the literature addressing the OC load per MW produced for a packed bed reactor.

The use of pure metals as OCs is not preferable as they tend to have lower oxygen transport capacities and reactivity rates that decrease after a few cycles. These limitations can be improved by bonding an inert support material to the metal oxide. The use of porous inert supports, such as alumina or silica, provide higher surface areas for reaction, and a binder for increasing their mechanical strength and attrition resistance [31], [64], [65]. The most studied active metal oxides for gaseous CLC applications are nickel-based, copper-based and iron-based.

Nickel-based OCs are the most widely studied in the literature as they are highly reactive in the reduction and oxidation environments, while also capable of maintaining stability at high temperature conditions (900-1,100°C). As well, this metal oxide has a oxygen transport capability of 0.21 and near complete CH_4 conversion is attainable during the reduction stage using a nickel-based OC; nevertheless, the formation of CO and H_2 creates thermodynamic restrictions [66]. Moreover, there are additional drawbacks when

using nickel; including its relatively low maximal operating temperature due to its melting point of 1,453 °C and the required safety measures due its toxicity. In addition, pure NiO particles have low reaction rates due to their low porosity [29], [64] and the use of alumina-based support materials hinders the reduction after the formation of the $NiAl_2O_4$ spinel compound [67], [68]. Despite these drawbacks, nickel-based OCs are still a viable option because their low reaction rates could be improved by using the right OC preparation method, such as spray drying or impregnation [69], [70]. Other compounds such as zirconia, bentonite, TiO_2 and MgO can also be used as support materials. However, studies have shown their relatively low reactivity, lack of mechanical strength and high carbon formation; hence, the focus has been mainly on alumina-based supports [61], [67], [71], [72].

Copper-based OCs have shown high reaction rates and adequate oxygen transfer capacities (0.20), exhibiting no thermodynamic restrictions to achieve full fuel conversion into CO_2 and H_2O. Furthermore, copper is cheaper than other CLC metal oxides, such as nickel, and it poses less of an environmental challenge. However, the main draw back of Cu-based OCs is its low melting point (1,085°C), which causes problems during the oxidation reaction, where requires high temperatures to obtain superior energetic efficiencies [73]–[76]. Additionally, the reaction rate of pure CuO quickly decreases as the number of oxidation cycles increases [31]. Therefore, different support materials such as silica, TiO_2 or γ-Al_2O_3, as well as different preparation methods, such as impregnation or co-precipitation, have been tested in search of curbing the reaction rate decay of copper-based OCs. Nevertheless, these studies have shown that changes in materials and preparation methods do not increase the reactivity or improve the mechanical strength of the OC [31], [74].

Despite their low CH_4 conversion and oxygen transport capacity (0.1), iron-based OCs are still an attractive option due to their low-cost and non-toxic characteristics [77]. The iron oxidation stages are arguably less suitable for CLC applications, especially when CH_4 is used as fuel. Moreover, Fe-based OCs have shown adequate reactivity when H_2 and CO are used as fuels while also having a low tendency to carbon formation [78]. In regards to preparation methods of iron-based OCs, there is a wide range including physical mixing, freeze granulation and impregnation. Although, the metal content in the aforementioned methods has to be in between 20% and 100% wt. due to its low oxygen transport capacity [77]. Iron-based OCs have been tested in different support materials including alumina, which has shown to enhance the oxygen transport capacity; whereas, the use of silica shows drastic decrements in reactivity as the number of regeneration cycles increase [79].

Economic analysis based on the lifetime of the particles have showed that the cost of the OC particles does not represent a limitation in the development of the technology [32], [77]. Based on the latter and the availability of kinetic data, Ni-based OCs are the most viable short-term option for gaseous fuels, especially when methane is used.

2.5 Reactor characteristics

The sequential nature of the gaseous CLC process requires the exposure of the OC to alternated oxidizing and reducing streams. The oxidation stage is achieved with air being fed to the reactor (air reactor) whereas the reduction takes place with fuel being fed to the reactor (fuel reactor). The alternated sequence can be carried out in different reactor configurations, with interconnected fluidized bed reactors (IFBR) [57] being the most widely investigated. Notwithstanding, packed bed (PBR) [8] and rotating [80], [81] reactors have

emerged as alternatives for the CLC reactor configuration. Figure 3 depicts a basic layout for IFBR and PBR.

Due to its intrinsically harsh and complex operating conditions, CLC requires special attention in some design and control aspects in order to maximize efficiency in the system. Some of these include:

- Effective contact time between fuel and air with the OC to maximize conversion
- Adequate control at the air reactor exhaust stream, which directly affects the downstream turbine efficiency
- High pressure operation to increase power generation
- Limited CO_2 leakage from the fuel reactor

The aforementioned aspects will be addressed for the gaseous operation in IFBR and PBR reactor configurations in the following section.

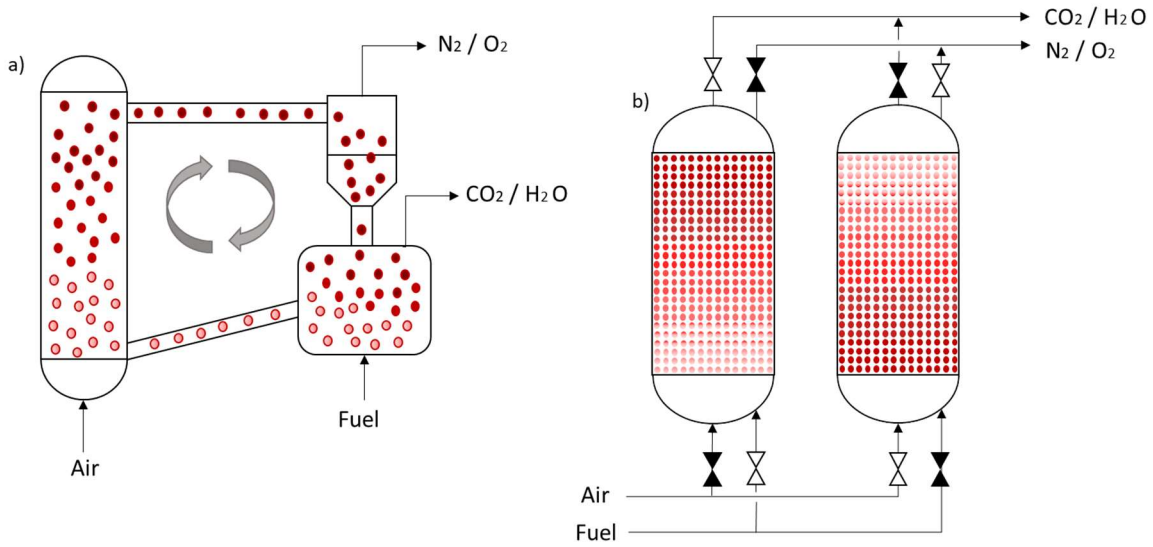

Figure 3. Reactor configuration for CLC system: a) interconnected fluidized bed reactor b) packed bed reactor

2.5.1 Interconnected Fluidized Bed Reactor (IFBR)

Figure 3(a) shows a schematic diagram of the IFBR which mainly consists of a high velocity fluidized bed (riser) and a low velocity bubbling bed. The OC is simultaneously oxidized and transported by an air stream within the riser. The OC particles are then sent into the cyclone separator by a loop seal, which avoids gas leakage, where nitrogen and unreacted oxygen are separated from the OC particles. Subsequently, the oxidized OC particles go inside the low velocity bubbling bed to be reduced by a fuel stream; the laminar flow allows the separation of the OC particles and the product stream (CO_2 and H_2O) to take place without the need of an extra cyclone separator. The velocity inside each reactor (air or fuel) depends greatly on the OCs reactivity, especially for the reduction reaction which requires larger residence time [32], [34]. Nevertheless, some authors have considered both reactors as bubbling-beds [35], [72]

It is possible to achieve a continuous production of hot air stream in a single IFBR, thus avoiding feeding problems with the downstream turbine. The operation of this configuration relies on the cyclone separator high efficiency, especially since the separation of the OC particles from the hot air stream directly impacts the downstream turbine due to formation of fines [82](mainly caused by attrition of the OC particle [32]). The fine formation has been contemplated in studies where the determination of the long-term attrition effect of different OC materials was analyzed [83]. Similarly, models using scaled-up pilot plant experimental data have been used to predict attrition rates for large IFBRs [84]. The results showed that most of the attrition is formed in the cyclone separator due to the extremely harsh conditions, such as high velocity and temperatures, which means that more research in OC support materials is required in order to minimizes attrition rates. Therefore, the

implementation of a CLC IFBR requires special design considerations in the solid separation system to avoid the feeding of fines into the downstream turbine, hence jeopardizing its safe operation.

CLC in an IFBR is the most mature technology and its effectiveness in producing a continuous hot air stream during the oxidation stage is intrinsic in its design. However, in order to achieve efficient and competitive energy usage, the IFBR needs to operate between 10-30 bar. This pressure range requirement entails some process difficulties in terms of maintaining a stable OC solid circulation between the interconnected reactors, such as two-phase flow pattern issues [85], [86]. Due to this and the fine formation caused by attrition inside the cyclone separator, the PBR configuration for CLC is a promising option.

2.5.2 Packed bed reactor (PBR)

Unlike the IFBR configuration which requires continuous transport of OC particles, Noorman et al. [8] presented a concept based on stationary OC particles inside the reactor and they are alternately exposed to oxidation and reduction streams. As shown in Figure 3, at least two packed beds are required to supply a constant high temperature stream to the downstream turbine; the sequential operation of each packed bed requires a switching system after each reaction stage is completed. The idea is that while the oxidation is taking place in one reactor, the other reactor is being used to perform the reduction process.

For instance, in the oxidation stage, the packed bed would be oxidized by an air stream and the resulting exit gas stream would only be composed of nitrogen and unreacted oxygen. Moreover, the exothermic reaction heats the exit gas stream until the conversion of the OC particles begin to decay. Feeding to the downstream turbine would be stopped when

the exit gas temperature diminishes to the point that the safe operation of the downstream turbine is no longer possible.

In the packed bed configuration, the reduction comes after a brief purge by an inert gas stream, which avoids the contamination of the fuel and oxygen in the overall process [8]. Once the purge is completed, a fuel stream is fed to the reactor in order to regenerate the OC particles. The reduction stage is defined by the formation of an exit gas stream composed mainly of CO_2 and H_2O. During this last phase, the amount of fuel slip, which is unreacted fuel leaving the reactor due to an increment in the OC reduction, starts to increase; hence, the end of the reduction stage is denoted by the exit mole concentration of the fuel matching its equivalent at the reactor inlet.

An advantageous feature of the PBR scheme is the avoidance of the cyclone separator, which effectively circumvents the cumbersome task of recovering the OC particles from the hot air effluent stream, as required in the IFBR configuration. Moreover, a multi-PBR configuration would allow the operation of the CLC process at higher pressures with a constant hot stream production. This effectively translates into higher overall energy efficiency and thus, lower energy penalty due to CCS, making this technology economically attractive [85], [87]. Furthermore, in the PBR scheme the two-phase flow operational problems would be avoided, resulting in a more compact reactor as well as more inlet mass flux flexibility. Increased flexibility, could improve the use of the OC oxygen transport capacity since full OC conversion could be attained [8].

The sequential stages in the operation of a CLC PBR could be a drawback since different feeding streams to the reactor need to be fed; hence, a high temperature and high flow gas switching system is required [88]. A full-scale power plant using this technology would need a sophisticated system of valves for different feeds and outlet gases; thus, exact

knowledge of each stage's culmination is necessary to avoid low feeding temperatures to the downstream turbine and fuel slip during the oxidation and reduction stages, respectively [8], [89]. Similarly, this technology cannot use solid fuels which limits their applicability and exposure [90].

The experimental demonstration of the exothermicity inside a PBR configuration was carried out by Noorman et al. [88] inside a reactor measuring 30 mm ID X 1,500 mm long, using Cu-based OC supported in alumina. The experiment was performed at 2.5 bar pressure and observed a 125°C rise in temperature. Other tests have been carried out in a PBR working at 7 bar and using syngas as fuel with ilmenite as OC [91]; the results from these studies showed that a maximum temperature rise of 340°C could be obtained, which agrees with the theoretical prediction presented before the experiments. Furthermore, a sensitivity analysis was performed by Noorman et al. [92] on a micro-scale reactor in which parameters such as oxidation and reduction temperatures as well as feeding compositions were varied. The results showed that the conversion rate of the OC is directly proportional affected by both, temperature and feeding composition. Similarly, in the same study, the oxygen concentration in the inlet air stream affected the time at which the maximum temperature was reached.

In summary, the PBR can successfully perform the CLC process as can the IFBR; but most importantly, it can operate at higher pressures, which would translate into more enthalpy available for the downstream gas turbine during the oxidation stage. As well, the segregation of the OC particle from the gaseous streams is avoided which immediately creates savings in the operational cost of the cyclone separator. In conclusion, these features make the PBR a more energy efficient concept than the IFBR, while at the same time still producing the desired highly concentrated CO_2 stream.

2.6 Modelling and optimization of the PBR

Modelling of the air and fuel reactors is a key aspect in the research and development of CLC technology as it is a suitable path towards design, optimize and scale-up of the CLC system. Modelling is also the best way to improve the dynamic operability and controllability in various reactor configurations, which aid in dynamic cycle switching and thus smooth operation. The modelling of the IFBR and PBR reactors mainly consists of fluid dynamics, mass and heat transfer and reaction kinetics.

This section addresses the current reactor models and published works on dynamic optimization, which includes information on the necessary control strategies to employ during CLC IFBR and PBR operations.

2.6.1 IFBR simulation and modelling

The mathematical modelling and dynamic simulation of the CLC process will provide insights to improve the design and operation of the complex fluid dynamics and kinetics taking place inside the reactor, particularly for scaling-up purposes; since changes in two-phase flow patterns might occur. The most investigated configuration scheme for CLC is IFBR; it has the most kinetic and empirical data available in the literature.

The computational fluid dynamic (CFD) models are an alternative in the modelling of the IFBR in CLC. They do not require detailed assumptions in the modelling procedure because they are based on the first principles of momentum, heat and mass transfer. These models can simulate the behaviour of the reactor during transient operation until steady state is achieved. Thus far, most of the CFD studies have been limited to the fuel reactor [93] [94] [95]. Moreover, these studies effectively demonstrated the reaction selectivity for CO_2 and

H_2O, such as the desired gas composition distribution, and the flowing regimes within the bubbling bed.

In later years, simulations based on semi-empirical models, which are defined as a combination of a mechanistic model and some empirical equation obtained from experimental data, have been used to model either the fuel or the air reactor. Abad et al. [96] carried out the modelling of a high velocity fluidized bed fuel reactor of a 1 MWth CLC unit. The fuel reactor used coal as fuel and ilmenite as the OC. The model's framework included the fluid dynamics of the reactor, axial profiles of the gas and solid compositions, the conversion of the OC and carbon formation inside the reactor. The results of the simulation showed that the high carbon formation, which is caused by the high operating temperatures at the bottom of the bed, thwarts the fuel conversion; this is due to a decrement in the surface area of the OC. Moreover, the same model was used to simulate a fuel reactor of 100 kWth CLC of coal with an in-situ gasification unit. The results pointed out the most significant operating conditions affecting the oxygen demand that were necessary in order to achieve 98.5% carbon capture efficiency; these included reactor temperature, solid circulation flow rate an solid inventory. [97]. The semi-empirical model previously presented by Abad et al. [98] was adjusted to different design conditions to achieve oxygen demand reduction in an in-situ gasification CLC process; the model showed that in order to increase gas-solid contact in the fuel reactor, a secondary reactor is needed [99].

Optimization of a CLC IFBR has not been studied thoroughly. The work of Abad et al. [100] is the only one regarding optimization. Their objective was to maximize the carbon capture of a 1 MWth CLC unit, using coal as fuel and ilmenite as the OC. After performing a sensitivity analysis on certain parameters, such as temperature inside the reactor, OC inventory, OC-fuel ratio and coal particle size, the optimization was performed by making

changes in key sensitive variables until a target value was satisfied. The results of that study indicated that carbon capture at a rate of 97% could be achieved by increasing the OC inventory to 3000 kg/MWth.

Despite their usefulness, semi-empirical models are not capable of capturing the complete range of operation and therefore may not accurately depict the intricacies of the IFBR process. Furthermore, the complexity of the fluid dynamics inside the CLC IFBR inhibits the simultaneous modelling of both reactor (air and fuel) with the CFD models. Thus far, executing CFD models is computationally expensive making the use of semi-empirical models the only feasible option, despite their limitations. Moreover, experimental results have shown that the operating conditions of one reactor affects the behaviour of the other one [101]. Hence, the solids (OC and/or solid fuel) circulation rate affects the OC conversion rate which also affect the temperature and the fluid dynamics of the system in transient basis [102]. Hence, the simulation of both reactors is of great importance if control and optimization want to be performed; otherwise, a sub-optimal solution could be found. The latter situation is avoided in a CLC PBR modelling, control and optimization studies, since the sequential operation in a packed bed somehow makes each reaction stage independent from the other; nevertheless, the initial conditions for each reaction stage are based on the concluded phase.

2.6.2 PBR simulation and modelling

Various studies have shown that increasing the efficiency of the power cycle using gaseous fuels can be achieved by operating the CLC system at high pressures. Subsequently, operating pressurized CLC plants using IFBRs presents various technical difficulties related to the maintenance of stable solid circulation rates between reactors [85],

[86]. PBRs have thus emerged as an attractive alternative for CLC operations at high pressures.

Various modelling studies for PBRs have also been conducted, including that by Noorman et al. [8], who showed that the high temperatures of the CLC process can also be reached in a packed bed. Using an analytical and a numerical solution of the 1-D mechanistic model, they were able to show the exothermic nature of the oxidation. Their results indicated that the maximum temperature is independent of the oxidation kinetics and that inactivation of the OC due to carbon deposition would not hinder the reaction rate. Similarly, Hamers et al. [103] developed a 1-D mechanistic model using syngas as fuel and CuO/Al_2O_3 as OC. Their model showed good accuracy against experimental data at high flow rates. Moreover, Noorman et al. [9], [10] presented a particle and reactor mechanistic dynamic model in which various sensitivity analyses were performed. The advantages of using large OC particles to diminish the pressure drop in the packed bed was explicitly described in their study. At the same time, their results point to the fact that mass and heat transfer limitations in the interphase could be considerable. Han et al. [11], [12] studied the dynamic behaviour of a CLC PBR using 1-D and 2-D homogeneous and heterogenous mechanistic models. The diffusion limitation within the OC particle was analyzed which showed its impact on the kinetic parameters, particularly with small OC particle diameters. In addition, the heterogenous model was extended to optimize the particle size and to perform kinetic parameter estimation [104]. Additionally, Han et al. [13] used the previously presented heterogenous model to perform multi-period optimization of the full CLC cycle (oxidation, reduction, purge). In that work, the authors presented a control scheme using dynamic optimization while the control actions remained constant during each stage of the CLC cycle. This study was able to increase the time of the heat recovery process during the

oxidation stage; similarly, a fuel conversion greater than 98% was maintained during the reduction stage.

The above-mentioned studies have shown, despite potential challenges, that the use of PBR for CLC is a promising alternative even though some solutions to certain operating and controlling problems are necessary to further demonstrate the technical feasibility of this technology for large-scale (industrial) applications. To the author's knowledge, there is no study in the literature that addresses transient operation and dynamic controllability of a PBR for CLC. However, operating parameters and design considerations have been presented in the literature [8], [13], [87], with the most pertinent for large-scale operation of the process including the following:

- The inherent nature of the PBR dynamic operation creates exit gas temperature oscillations during the oxidation phase which have the potential to damage the downstream turbine, which is not able to withstand such sudden changes[87]; thus, to protect this equipment the exit gas temperature should be kept as steady as possible.
- The investigated OCs in CLC operation can operate at temperatures between 800-1,200 °C [105]; whereas the range of operation for gas turbines is approximately 827-1,627°C [106].
- The temperature within the reactor should always be kept below the melting point of the metal oxide.
- The fuel concentration at the reactor's outlet has to be kept as low as possible in order to obtain a higher fuel conversion into CO_2, a 98% fuel conversion is often set as target during the reduction stage [107], [108].

- The pressure drop across the reactor bed must be below 8% of the inlet pressure [87].
- The PBR need to be coupled with a high temperature and high flow switching system to ensure a smooth transition between reaction stages (e.g. oxidation to purge or purge to reduction) [89].

To summarize this chapter, most of the research to date has focused on the development of suitable OCs, with the goal of achieving selectivity and durability. Moreover, in regards to the modelling and optimization of the reactor, attention has been directed to IFBR and fewer works focusing on PBR have been developed.

Researchers have identified that PBR for CLC has great potential because its design intrinsically avoids solid separation and enables it to operate at higher-pressures, effectively increasing its energy efficiency. The main disadvantage the PBR concept is that its high temperatures also necessitate the implementation of a complex high flow gas switching system. A full-scale power plant would require a set of valves and prominent control systems to guarantee smooth transitions, especially in the operation of the gas turbine.

Due to the novelty and the complexity of CLC technology, there is no work on dynamic optimization that comprises every reaction stage in the CLC PBR operation. In this regard, dynamic modelling of a large-scale PBR for CLC would greatly assist in the identification of each reaction stage's ending point, which ultimately would define the beginning of the subsequently stage in the CLC operation. Likewise, optimization of the dynamic model would enhance energy recovery during the oxidation stage while also maintaining pseudo-steady exit gas temperature. In the same manner, the optimization of the reduction stage would minimize the amount of unreacted fuel, thus increasing the fuel conversion within the reactor and effectively producing more CO_2. In this thesis, an attempt

to contribute to the research body by modelling a large-scale PBR for CLC is presented; in order to understand the transient behaviour of each reaction stage and identify their beginnings and ends is presented.

Chapter 3
Model implementation and validation of a PBR

Modelling the PBR reactor has previously been performed [8]–[11], [104]. In those works, dynamic homogeneous and heterogenous models were introduced; being the latter type, the most accurate descriptive model for the CLC phenomena taking place inside the PBR. For these reasons, a 1-dimensional heterogenous model, which includes the effects of reaction kinetics in association with mass and heat transport in both the particle and the bulk phases, is adapted from the literature for implementation in this study. Additionally, the proposed model is coupled with pressurized reaction kinetics that were also adapted from the literature [109]. The simulation results were validated using published data [13], [110] and by conducting a sensitivity analysis on key model parameters. Moreover, this model will serve as framework for the dynamic optimization problem discussed in Chapter 4. Part of the work presented in this chapter has been published in the open literature [111].

3.1 Operating philosophy

Since the CLC reaction stages work as a batch process, more than one PBR is required to supply a constant hot air stream to the downstream turbine. According to Spallina et al. [89], a heat management strategy for a high-pressure multi-packed bed CLC cycle sequence could begin with oxidation, followed by heat removal, purge, reduction and a final purge, as shown in Figure 4. Although this might not be the optimal operation sequence for the reactor, since the heat removal can be performed after the reduction [89], it does

exemplify the challenge of identifying the beginning and end of each stage and the transient operation due to changes in the inlet feed of the CLC PBR scheme.

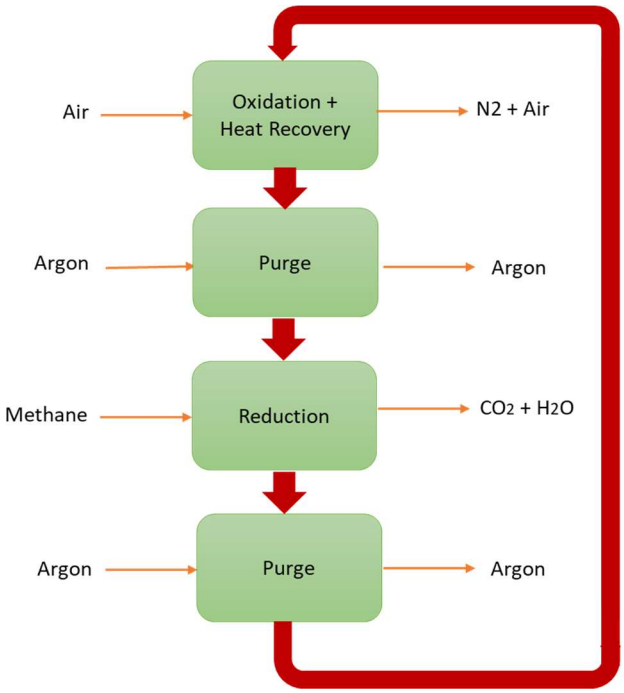

Figure 4. Cycle sequence strategy for a Packed bed CLC reactor

The packed bed CLC sequence can be adapted to a combined cycle power plant in many different configurations. The conventional scheme is that the CLC reactor would replace the gas combustor. Figure 5 shows a simplified layout of a combined cycle with CLC where air and fuel (methane) are pressurized to 20 bar and sent to the oxidation and then reduction stages in the multi-bed configuration. In addition, the flue gas from the oxidation stage is used to drive the gas turbine; the exhaust from the gas turbine is then sent to a heat recovery steam generation (HRSG) system for additional power production. In addition, the flue gas from the reduction stage could be utilized to drive a secondary gas turbine and/or preheat any of the air or fuel streams. Multiple energy efficiency studies have been

performed using many configurations [112]–[114]; those works have shown that the CLC configuration achieved a higher net efficiency than the conventional natural-gas fired combined cycle with post-combustion CO_2 capture. Therefore, the CLC PBRs operating conditions are highly dependant on the surrounding process equipment; the performance of the secondary equipment will define inlet and outlet temperatures which are key parameter in the oxidation and reduction stages of the CLC PBR. Despite the net optimization of the complete system shown in Figure 5 is beyond the scope of this work, the present optimization study for a single CLC PBR identifies feasible operating conditions for a combined cycle power generation system.

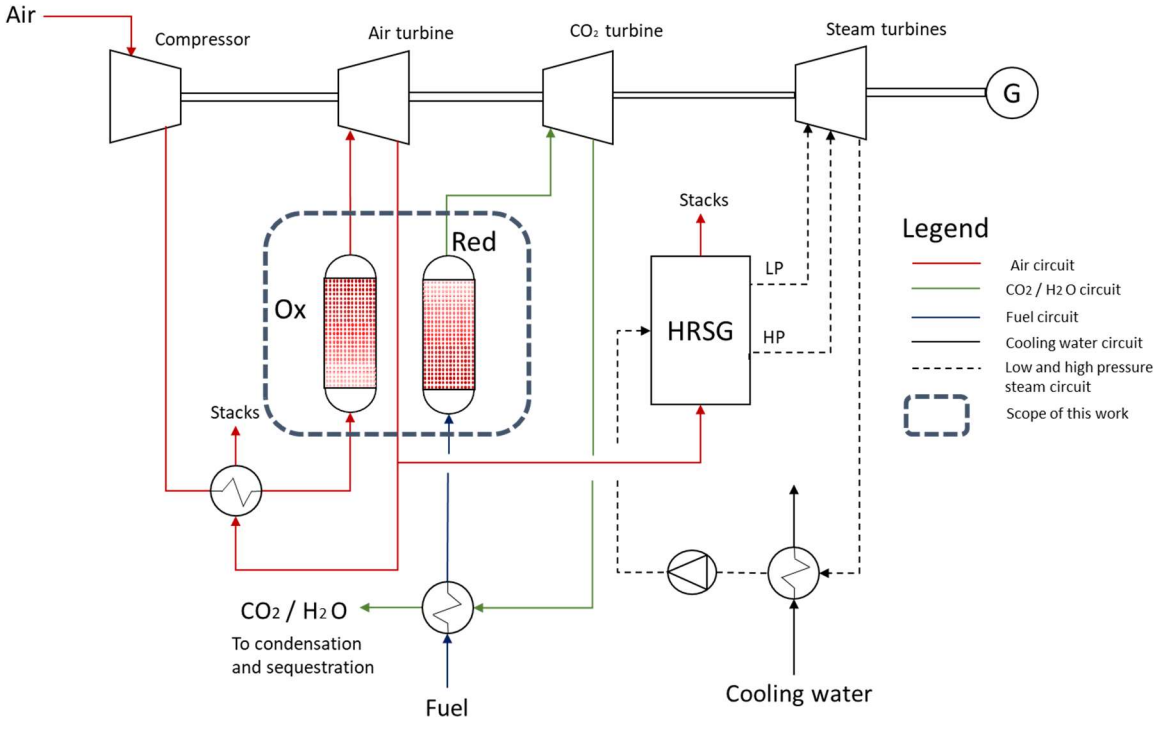

Figure 5. Schematic diagram of a gaseous fuel CLC-combined cycle [112]

3.2 PBR model

The model for a CLC PBR considered in this study is composed of two domains involving the OC particle and the axial reactor position [11]. A set of partial differential equations describes the motion of gaseous bulk fluid across the packed bed and within the OC particle, where intraparticle and interfacial transport limitations occur. Moreover, the use of a heterogeneous model is able to depict the interfacial resistance, which is related to the thickness of the boundary layer between gas-solid phases and while intraparticle limitations are related to the pore size of the OC particle [11].

The assumptions considered in the development of this model are as follows:

- The OC particle is modelled as spherical particles
- OC particles have a constant volume
- OC particles have a macroscopically uniform structure that is not affected by the reaction
- Uniform metal oxide distribution within the OC particle
- Uniform OC particles distribution within the reactor
- The gas concentrations and temperature inside the pores of the OC particle are assumed to be functions of the radial and axial directions in the particle and reactor models, respectively
- At any point, the gas inside the particle is at the same temperature as the OC particle
- The thermal conductivity of the gas is negligible compared to the OC particle
- Perfectly well distributed feed stream in the cross-sectional area of the reactor
- Pressure drop across the packed bed gas is neglected

The model was developed such that it can be used with any type of OC particle in combination with any gaseous fuel [11]. However, the present study used methane (CH_4) as fuel in the reduction stage and Ni/NiO with alumina as the OC because of the availability of experimental data in the open literature [104], [109], [115].

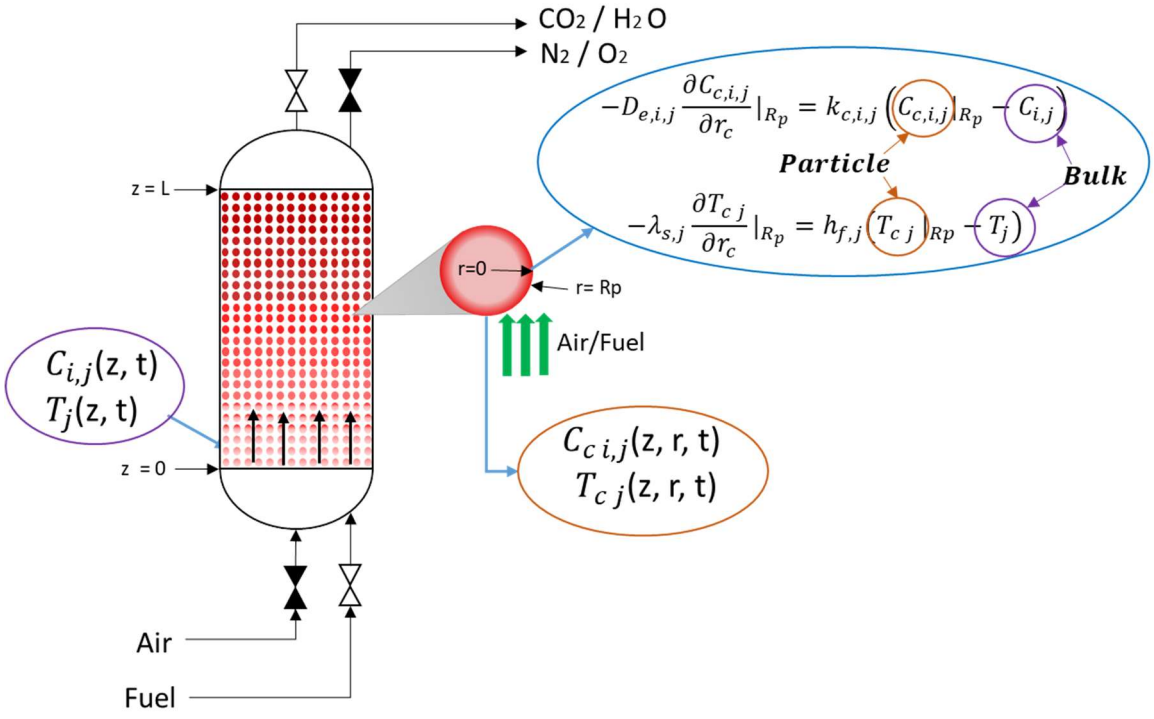

Figure 6 Schematic of the packed bed CLC reactor

Figure 6 shows a schematic diagram of the packed bed CLC reactor illustrating the interactions between the reactor model and the OC particle model across the boundary conditions. The mass and heat balances of the reactor and particle are presented next. Similarly,

Table 3 and Table 4 present the model parameters used for each stage in the CLC sequence. The definition for each of the model parameters considered in the presented model are provided in the nomenclature section.

The mass and energy balances for the reactor model:

$$\varepsilon_b \frac{\partial C_{i,j}}{\partial t} + \frac{\partial F_{i,j}}{\partial V} = \varepsilon_b \frac{\partial}{\partial z}\left(D_{ax\,i,j} \frac{\partial C_{i,j}}{\partial z}\right) + k_{c\,i,j}\, a_v\left(C_{c\,i,j}|_{Rp} - C_{i,j}\right) \quad (3.1)$$

$$\varepsilon_b C_{pf\,j} C_{T\,j} \frac{\partial T_j}{\partial t} + C_{pf\,j} F_{T\,j} \frac{\partial T_j}{\partial V} = \varepsilon_b \frac{\partial}{\partial z}\left(\lambda_{ax\,j} \frac{\partial T_j}{\partial z}\right) + h_{f\,j}\, a_v\left(T_{c\,j}|_{Rp} - T_j\right) \quad (3.2)$$

The boundary and initial conditions for the bulk phase:

$$\varepsilon_b D_{ax\,i,j} \frac{\partial C_{i,j}}{\partial z}|_{z=0} = \left(F_{i,j}|_{z=0} - y_{ifeed\,j} F_{in\,j}\right)/A_c \quad (3.3)$$

$$\varepsilon_b \lambda_{ax\,j} \frac{\partial T_j}{\partial z}|_{z=0} = \left(T_{c\,j}|_{z=0} - T_{in\,j}\right) C_{pf\,j} F_{T\,j}/A_c \quad (3.4)$$

$$\frac{\partial C_{i,j}}{\partial z}|_{z=L} = \frac{\partial T_j}{\partial z}|_{z=L} = 0 \quad (3.5)$$

$$G_j = \frac{F_{in\,j}}{A_c} \frac{\rho_{in,j}}{C_{in,j}} \quad (3.6)$$

The spatial and time domains included in the reactor model are as follows:

- The axial bed position is described by: $z \quad \forall \quad 0 \leq z \leq L,\ L = reactor\ length$
- The time variation is described by: $t\ \forall\ 0 \leq t \leq t_{j,final},\ \forall\ j = \{oxidation,\ reduction,\ purge_1, purge_2\}$

The state variables included for the reactor model are:

- Concentration of gas species *i* in the fluid phase:
  - $C_{i,j}(z,t), \forall\ i = \{O_2, CH_4, H_2,\ CO, CO_2, H_2O, Ar\},\ j = \{oxidation,\ reduction,\ purge_1, purge_2\}$
- Temperature in the fluid phase:
  - $T_j(z,t), \forall\, j = \{oxidation,\ reduction,\ purge_1, purge_2\}$

The reactor model, shown in Equation 3.1 and 3.2, explicitly considers the following mass and heat terms: time dependent, convection, axial diffusion and transfer between the reactor's bulk phase and each OC particle. The boundary conditions shown in Equation 3.3 and 3.4 describe the mass and heat feeding stream conditions at the reactor's inlet; whereas, Equation 3.6 describes the inlet mass flux at each *j* stage. Additionally, Equation 3.5 describes the mass and heat insulation at the reactor's exit.

Table 3. List of coefficients and parameters used for the reactor model

	Oxidation	*Reduction*	*Purge$_1$ after Ox*	*Purge$_2$ after Red*
ε_b	0.37 [a]	0.37 [a]	0.37 [a]	0.37 [a]
$D_{ax\,i,j}$ *(m²/s)*	1.62e-3 [a]	2.3279e-5 [a]	1.6492-5 [a]	1.9945e-5 [a]
$k_{c\,i,j}$ *(m/s)*	0.48271 [a]	0.0785 [a]	0.07253 [a]	0.06882 [a]
a_v *(1/m)*	2700.0 [a]	27000 [a]	27000 [a]	27000 [a]
$y_{ifeed\ j}$	0.23 O_2, 0.77 N_2 [a]	1.0 CH_4 [a]	1.0 Ar [a]	1.0 Ar [a]
$F_{in\ j}$ *(mol/s)*	21097 [b]	610 [d]	488 [b]	610 [b]
$C_{pf\ j}$ *(J/mol/k)*	31.63 [c]	58.55 [c]	20.28 [c]	20.28 [c]
$\lambda_{ax\ j}$ *(W/m/K)*	3.4304 [a]	1.3777 [a]	0.4375 [a]	1.1377 [a]
$h_{f\ j}$ *(W/m²/K)*	855.5 [a]	1603.8 [a]	694.9 [a]	2085.7[a]

a. Han et al. [11], b. Spallina et al. [87], c. Perry's handbook [116], d. Han et al. [13]

The mass and energy balances for the particle phase:

$$\varepsilon_c \frac{\partial C_{c\,i,j}}{\partial t} = \frac{1}{{r_c}^2}\frac{\partial}{\partial r_c}\left(D_{e\,i,j}{r_c}^2\frac{\partial C_{c\,i,j}}{\partial r_c}\right) + \rho_{s\ j}\Sigma R_{i\ j} \tag{3.7}$$

$$((1-\varepsilon_c)\rho_{s\ j}C_{ps\ j} + \varepsilon_c C_{pc\ j}C_{Tc\ j}\frac{\partial T_{c\,j}}{\partial t} = \frac{\lambda_{s\,j}}{{r_c}^2}\frac{\partial}{\partial r_c}\left({r_c}^2\frac{\partial T_{c\,j}}{\partial r_c}\right) + \rho_{s\ j}\Sigma R_{i,j}\left(-\Delta H_{i,j}\right) \tag{3.8}$$

The boundary conditions for the particle phase:

$$\frac{\partial C_{c\,i,j}}{\partial r_c}|_{r_c=0} = \frac{\partial T_{c\,j}}{\partial r_c}|_{r_c=0} = 0 \tag{3.9}$$

$$-D_{e\,i,j}\frac{\partial C_{c\,i,j}}{\partial r_c}|_{R_p} = k_{c,i,j}\left(C_{c\,i,j}|_{R_p} - C_{i,j}\right) \quad (3.10)$$

$$-\lambda_{s\,j}\frac{\partial T_{c\,j}}{\partial r_c}|_{R_p} = h_{f\,j}\left(T_{c\,j}\,|_{Rp} - T_j\right) \quad (3.11)$$

The spatial and time domains included in the particle model are the following:

- The particle radial spatial position is described by: r_c , $\forall\ 0 \le r_c \le R_p$, $R_p = particle\ radius$

The state variables included for the OC particle model are:

- Concentration of gas species *i* in the OC particle:
  - $C_{c\,i,j}\,(z,r,t), \forall\ i = \{O_2, CH_4, H_2,\ CO, CO_2, H_2O, Ar\},\ j = \{oxidation, reduction, purge_1, purge_2\}$
- Temperature inside the OC particle:
  - $T_{c\,j}\,(z,r,t), \forall\, j = \{oxidation,\ reduction, purge_1, purge_2\}$
- Conversion of the OC particle:
  - $X_j(z,r,t), \forall\, j = \{oxidation,\ reduction, purge_1, purge_2\}$

Table 4 List of coefficients and parameters used for the particle model

	Oxidation	*Reduction*	*Purge$_1$ after Ox*	*Purge$_2$ after Red*
ε_c	0.5 [a]	0.5 [a]	0.5 [a]	0.5 [a]
$D_{e\,i,j}$ *(m²/s)*	3.4015e-7 [a]	8.27e-7– 3.06e-6 [a]	3.2408e-7 [a]	1.46e-6 [a]
$\rho_{s\,j}$ *(kg/m³)*	4480 [a]	4330 [a]	4330 [a]	4480 [a]
$C_{pc\,j}$ *(J/mol/k)*	31.63 [b]	58.55 [b]	20.28 [b]	20.28 [b]
$\lambda_{s\,j}$ *(W/m/K)*	8.6462 [a]	7.7512 [a]	8.6462 [a]	7.7512 [a]
$\Delta H_{i,j}$*(J/mol)*	-479,400 [c]	156,500 / -2100 / -43,300 [c]	---	----

a. Han et al. [11], b. Perry's handbook [116], c. Iliuta et al. [115]

The particle model, shown in Equation 3.7 and 3.8, explicitly considers the following mass and heat terms: time dependent, radial diffusion and reaction. The boundary conditions shown in Equation 3.10 and 3.1 describe the mass and heat transfer between the reactor's bulk phase and the OC particle; note that these boundary conditions are evaluated along the axial domain of the reactor. Equation 3.9 describes the mass and heat insulation at the center of OC particle.

A complete description of the relevant physical properties used in this model are described in the Appendix A. The reaction kinetic terms that appear in the model $(R_{i,j})$ are presented next.

3.3 Reaction kinetic model

Nickel-based OCs have shown very high reactivity for the combustion of methane. The use of NiO supported in 21% γ-alumina and CH_4 as fuel had been previously tested in continuous CLC pilot plant experiments that were performed for 40 h of reaction time [117]. The results showed no major changes in the porosity, density or mechanical strength of the OC; however there were some thermodynamic limitations preventing full conversion of methane in CO_2 and H_2O due to the presence of small amounts of CO and H_2 at equilibrium conditions [105]. On the other hand, the use of a Ni-based OC enables oxidation to work at temperatures between 1200-1400 K due to its high melting point (1728 K). Moreover, the ubiquity of Ni-based OC experimental data for CLC is the main reason why a Ni/NiO metal is selected for this work.

The kinetics parameters for the oxidation reaction were taken from those presented by Dueso et al. [62]. In that study, the kinetics were determined in the TGA at temperatures of 1223 K and 1173 K while keeping a constant atmospheric pressure and using different

concentrations of O_2 ranging from 5% vol to 21% vol. The experiment was performed during 5 cycles; the kinetic constant was determined assuming an Arrhenius model.

The oxidation step (Equation 3.12) can be accurately described by the shrinking core model [118]; moreover, the correction equation presented by Nordness et al. [109] for higher operating pressures in the CLC PBR is implemented alongside the previously selected Dueso's kinetic parameters. Equation 3.13 describes the reaction rate for the oxidation used in this work. The kinetic parameters are presented in Table 5.

$$2\mathrm{Ni} + O_2 \rightarrow 2\mathrm{NiO} \tag{3.12}$$

$$r_{O_2,j} = \frac{a0_j}{P^{1.02}}\, k0_{O_2,j}\, e^{\frac{-E_{a\,O_2,j}}{Rg^{*}T_{c\,j}}} \left(1 - X_j\right)^{\frac{2}{3}} C_{O_2,j}\, C'_{Ni,j};\ \ \forall\ j = \{oxidation, purge_1\} \tag{3.13}$$

The kinetics for the reduction stage were taken from Nordness et al. [109], where the kinetics of the NiO OC reduced with methane were analyzed at high pressure in a packed bed reactor using the nucleation and nuclei model (NNM) [119], [120]. Equations 3.14-3.19 show the reaction mechanisms and rates for total CH_4 oxidation, H_2 oxidation and CO oxidation, respectively. The kinetic parameters are presented in Table 5.

$$2CH_4 + 3NiO \rightarrow 3Ni + CO_2 + 4H_2 + CO \tag{3.14}$$

$$H_2 + NiO \rightarrow Ni + H_2O \tag{3.15}$$

$$CO + NiO \rightarrow Ni + CO_2 \tag{3.16}$$

$$r_{CH_4,j} = \frac{a0_{\mathrm{j}}}{P^{1.01}}\, k0_{CH_4,j}\, e^{\frac{-E_{CH_4,j}}{Rg^{*}T_{c\,j}}}\ n_{CH_4}\left(1 - X_j\right)^{\frac{2}{3}} \left(-\ln\left(1 - X_j\right)\right)^{1-\frac{1}{n_{CH_4}}} C_{CH_4,j}\, C'_{NiO,j};\ \ \forall\ j = \{reduction, purge_2\} \tag{3.17}$$

$$r_{H_2,j} = \frac{a0_{\mathrm{j}}}{P^{1.39}}\, k0_{H_2,j}\, e^{\frac{-E_{a\,H_2,j}}{Rg^{*}T_{c\,j}}}\ n_{H_2}\left(1 - X_j\right)^{\frac{2}{3}} \left(-\ln\left(1 - X_j\right)\right)^{1-\frac{1}{n_{H_2}}} C_{H_2,j}\, C'_{NiO,j};\ \forall\ j = \{reduction, purge_2\} \tag{3.18}$$

$$r_{CO,j} = \frac{a0_j}{P^{1.21}}\, k0_{CO,j}\, e^{\frac{-E_{a\,CO,j}}{Rg^{*}T_{c\,j}}}\; X_j\, n_{CO}\left(1-X_j\right)^{\frac{2}{3}}\left(-\ln\left(1-X_j\right)\right)^{1-\frac{1}{n_{CO}}}\, C_{CO,j}\, C'_{NiO,j}\,;\ \forall\ j = \{reduction, purge_2\} \quad (3.19)$$

Table 5. List of kinetic parameters

	Oxidation/Purge₁ *i=O_2*	*Reduction/Purge₂* *i=CH_4/H_2/CO*
$a0_j$ *(m²/s)*	0.002 [a]	102 [b]
$k0_{i,j}$ *(m/s)*	4.6e-1 [a]	8.16e-6 / 2.13e-5 / 2.26 e-5 [b]
$E_{a\,i,j}$ *(J/mol)*	22,000 [a]	77,410 / 23,666 / 26,410 [b]
R_g *(J/mol/K)*	8.3145 [a]	8.3145 [a]
P *(bar)*	20 [c]	20 [c]
n_i	--	0.8 / 0.6 / 0.8 [b]
$C'_{Ni,j}$ / $C'_{NiO,j}$	0.21	0.21

a. Taken from Dueso et al. [62], b. Taken from Nordness et al. [109], c. Taken form Noorman et al. [8]

The conversion rate for the OC is as follows:

$$\frac{dX_j}{dt} = \left(\sum_i r_{i,j}\right) / C'_{NiO}\,, \forall\ j = \{oxidation,\ reduction, purge1, purge2\} \quad (3.20)$$

The mass balance for Ni and NiO, assuming no migration of the Ni particles:

$$\frac{dC_{NiO\,j}}{dt} = \left(1-X_j\right) M_{NiO}\ \ \forall\ j = \{oxidation,\ reduction, purge1, purge2\} \quad (3.21)$$

$$\frac{dC_{Ni\,j}}{dt} = X_j M_{Ni}\ \forall\ j = \{oxidation,\ reduction\ purge1, purge2\} \quad (3.22)$$

Recalling equation 3.12, $\Sigma R_{i,j}$ can be written as follows:

$$\sum R_{i,j} = \varphi_i\, r_{O_2}\,, \forall\ i = \{O_2, CH_4, H_2,\ CO, CO_2, H_2O, Ar\},\ j = \{oxidation, purge1\} \quad (3.23)$$

$$\sum R_{i,j} = \varphi_i\, r_{CH_4,j} + \varphi_i\, r_{H_2,j} + \varphi_i\, r_{CO,j}\,, \forall\, i = \{CH_4, H_2,\ CO, CO_2, H_2O, Ar\},\ j = \{reduction, purge\ 2\} \quad (3.24)$$

where ϕ_i is the stoichiometric coefficient of component *i* in the reaction.

Since the purges are performed with an inert gas, such as argon, it is then assumed that the remaining reactants inside the PBR, after the culmination of the oxidation or the reduction stages, are still reacting with the unconverted OC particles. Therefore, the kinetics considered for each one of the purges used the same set of equations as in the corresponding previous reaction stage (oxidation or reduction), as shown in equation 3.23 and 3.24.

3.4 Base case operating condition

Commercial availability of CLC technology is hindered by a lack of studies on large-scale reactors and pressurized conditions; increasing focus in these research areas would boost confidence levels regarding use of this technology. In order to address this gap in the literature, the current work was based on a large-scale reactor working under high pressure. The nominal design of the reactor was selected from a study conducted by Spallina et al.[87], which included a sensitivity analysis on the reactor length and diameter. That analysis helped those authors to select the total number of reactors required for continuous operation for a 168.9 MW gas turbine. Although that work was carried out with a Fe-based OC, some of the conditions used for that study can also be applied for a large-scale Ni-based OC reactor; for instance, the reactor's dimensions, such as length and diameter, were defined based on pressure loss and diffusion limitations at a corresponding mass flux.

The base case and operating conditions for this work are shown in Table 6. Reactor and OC characteristics and dimensions Table 6 and Table 7, respectively.

Table 6. Reactor and OC characteristics and dimensions

Reactor configuration		Sources
Parameter		
Length (m)	11	[87]
Diameter (m)	5.5	[87]
OC active material	Ni/NiO supported in alumina	[62]
OC diameter (mm)	1.4	[115]
Weight fraction of metal oxide in OC (wt.%)	0.21	[62]
Solid porosity (εc)	0.5	[14]
Melting point of reduced metal (°C/K)	1455/1728	

Table 7. Feed streams, base case

Oxidation + Heat removal		Sources
Gas stream	Air	
Total mass flux (kg/s/m²)	3.2	[87]
Pressure (bar)	20	[8]
Inlet Temperature (°C)	450	[87]
Initial conditions (t=0)	$C_{i,j} = 0, T_j = 600, X_j = 0$	[10]
Reduction		
Gas stream	Methane	
Total mass flux (kg/s/m²)	0.545	[13]
Pressure (bar)	20	[8]
Inlet Temperature (°C)	450	[13]
Initial conditions (t=0)	$C_{i,j} = 0, T_j = 900, X_j = 0$	[10]
Purge		
Gas stream	Argon	
Total mass flux (kg/s/m²)	1.3	[87]
Pressure (bar)	20	[8]
Inlet Temperature (°C)	450	[13]
Initial conditions (t=0)	*Based on previous stage's state variables values*	

In summary, a 1-D mechanistic dynamic model representing the phenomena inside a PBR for CLC has been introduced. This model contains a set of partial differential equations for the OC particle and another for the bulk phase of the reactor. The state variables, such as concentration of the gas species and temperature in both the particle and bulk phases, are coupled between both sets of equations across boundary conditions. Furthermore, the reaction kinetic model was presented for each reaction stage. Additionally, a base case scenario was selected from the literature and will be used as benchmark to study this system.

3.5 Model implementation

The dynamic model presented in the previous section was implemented in PYOMO with a version of Python 3.6.5 [121]. The set of partial differential-algebraic equations were discretized using centered finite differences, which has also been used in previous works for similar models [8], [11]. The resulting set of non-linear algebraic equations was solved using the interior-point optimization algorithm combined with the linear solver MA97 in the PYOMO environment [122]. The number of discretization elements per domain was determined *a priori* from trial and error simulations. Due to the model's non-linearity, the ratio of finite elements (NFE) in the spatial domain to those in the time domain is also affected. Such small changes in the model necessitate further cumbersome adjustments that could effectively hinder the development and ubiquity of this type of solution technique in the CLC field. The number of NFE in each domain (spatial in r, spatial in z, and time t) was determined by increasing the number of points until no further improvement in the model predictions were observed, while maintaining a reasonable computational time. Accordingly, for the base-case operating condition reported above, discretization elements are needed for the

reactor's axial domain (*z*) and the particle's radial domain (*r*). A summary of the NFE employed in this work is presented in Table 8.

Table 8. NFE for each stage in the CLC sequence

NFE	Radial (r)	Axial (z)	Time (t)	Total # of equations
Oxidation	14	18	26	97,906
Reduction	8	10	22	63,417
Purge 1	12	12	20	55,146
Purge 2	6	9	15	36,355

Each stage was solved individually and the resulting state variables profiles, such as concentrations, temperatures and OC conversion, were used as an initial condition for the next stage of the CLC sequence. The resulting set of nonlinear algebraic equations belonging to each stage were solved simultaneously. Each of the resulting problems was solved using the direct transcription dynamic optimization approach. Each simulation required on average 1,000 CPU seconds (2.5GHz i5-7200U processor).

3.6 Model validation

Due to the scarcity of studies regarding dynamic operation of large-scale CLC PBR, a direct comparison between the results obtained by the present 1-D model and published data cannot be performed. Therefore, comparison in terms of concentrations, temperatures and conversions profiles against data available in the literature, either in previous simulations and/or in experimental works, was performed with the aim to validate the model proposed in this study.

The data reported by Han et al. [13] was used for the temperature profile validation. Figure 7 shows the temperature profiles of the exit gas at various times throughout the complete cycle sequence.

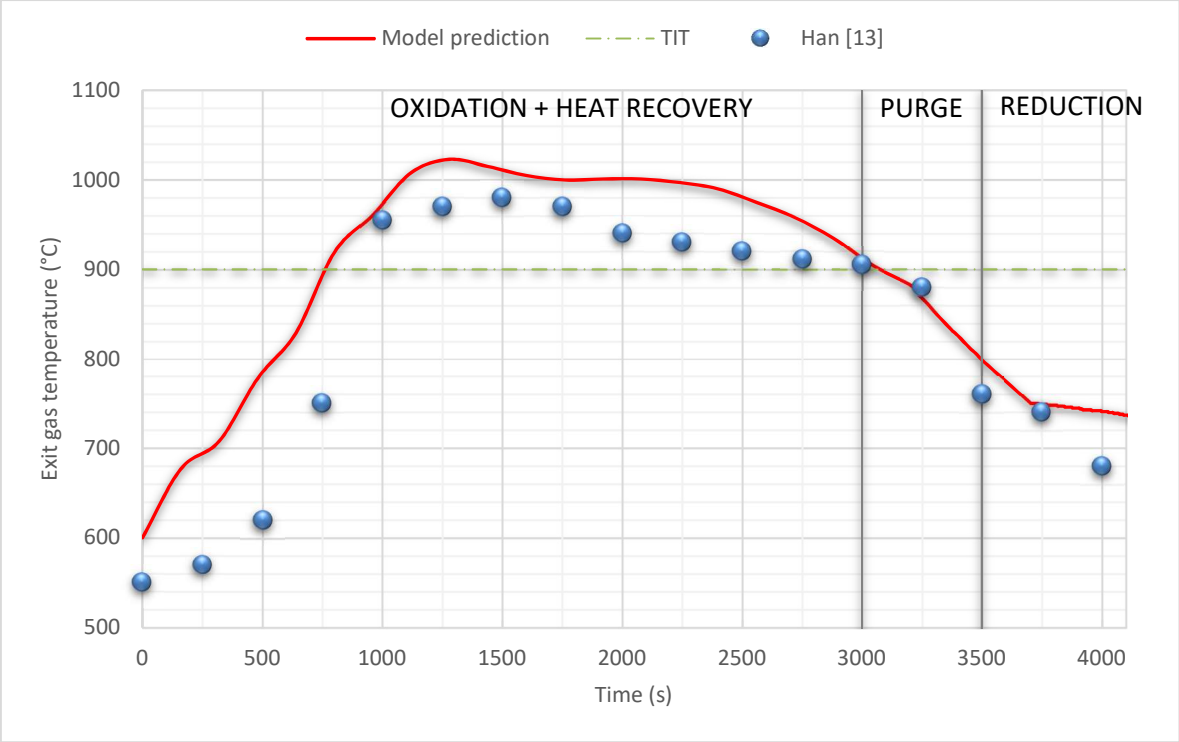

Figure 7. Exit gas temperature for the complete CLC cycle sequence: data by Han et al. [13]

In order to ensure the effective functioning of the model, it was decided to compare our temperature profiles against those reported in the study by Han et al. [13] at various stages of the CLC PBR sequence. Han's study is an adequate benchmark because they use a similar large-scale reactor as well as their choice of a Ni-based type OC and CH_4 as fuel in the reduction stage also corresponds to the present study. Han's study was implemented using different kinetic data for the oxidation reaction, which was not presented in that study [11]. Despite the latter, the exit gas temperature profile shown in Figure 7 is still

fairly similar to the one presented in that study, including the duration of the heat recovery process which is approximately the same (3,000 s). Additionally, the exit gas temperature decrement during the purge and the reduction against Han's work was benchmarked; the results follow the expected tendencies, because the exothermic reaction is over and the cooling of the bed due to convection is imminent. Moreover, Figure 7 confirms the results first indicated by Noorman et al. [8] during the oxidation, i.e. the exit gas temperature reaches and surpasses the minimum turbine inlet temperature (TIT) [82], effectively demonstrating that a CLC PBR can provide a suitable air hot stream to feed the downstream turbine.

The goal of the reduction stage is to ensure that all the feeding fuel is converted into CO_2 and H_2O in order to ensure maximal CO_2 sequestration. A key aspect of this stage is that the OC reduction time should be kept as short as possible; accordingly, a sufficiently high temperature would allow the reaction to take place quickly (approximately a minimum of 600°C [115]). Moreover, the operation strategy for the reduction stage is to reduce the OC particle while keeping a low CH_4 mole fraction, also known as a fuel slip, at the reactor's outlet. Figure 8 shows the exit gas fraction at different times during the reduction stage; the results of the present simulation are compared against those reported by Han et al. [13].

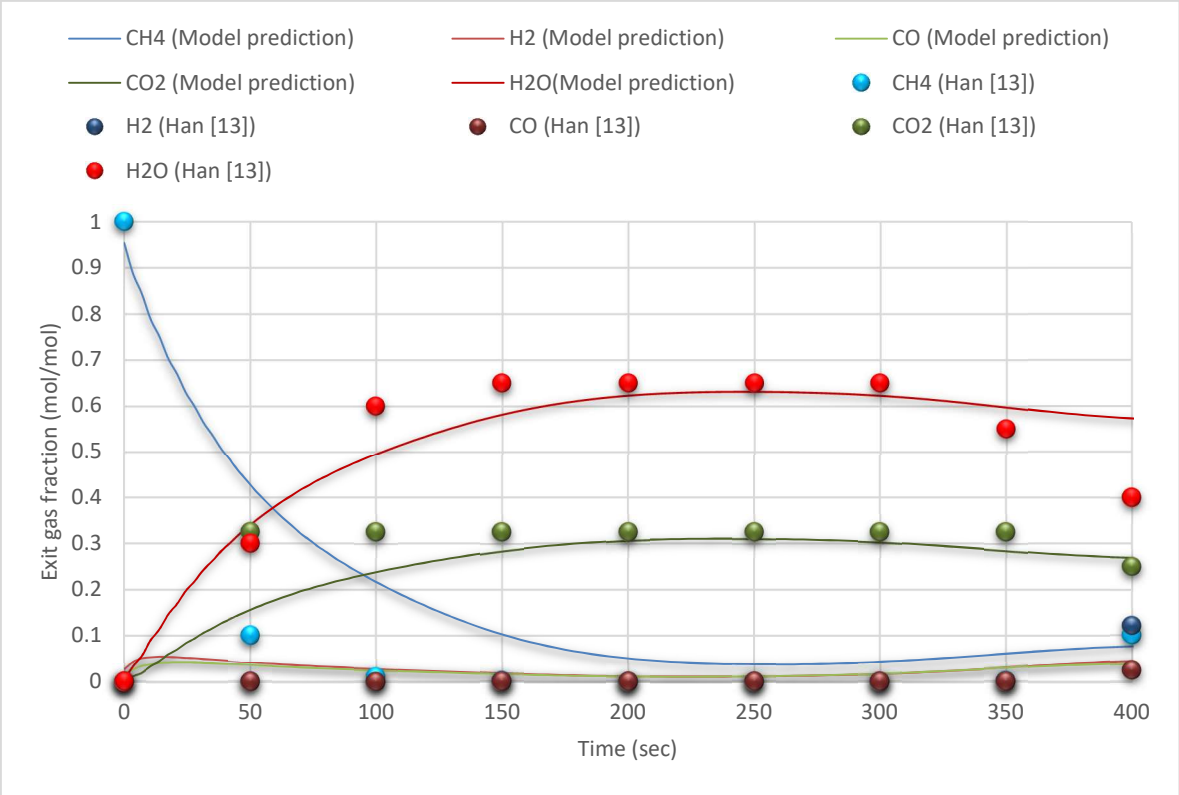

Figure 8. Gas mole fraction at the exit of the reactor during the reduction stage: data by Han et al. [13]

The selectivity towards CO_2 conversion of the Ni-based OC is crucial for the production of a highly concentrated stream. As shown in Figure 8, the selectivity is achieved by producing a stream with approximately 60% H_2O and 30% CO_2, which is expected according to Iliuta et al. [115]. The duration of the reduction stage (approx. 420 s) and the mole fractions estimated by the current model at the exit of the reactor are also in agreement with Han's work [13]. Moreover, the present model is able to predict the time at which the OC conversion has almost achieved a full reduction; indicated by the increment of fuel slip as well as the decrement of H_2O and CO_2 at the end of the reduction stage process [8].

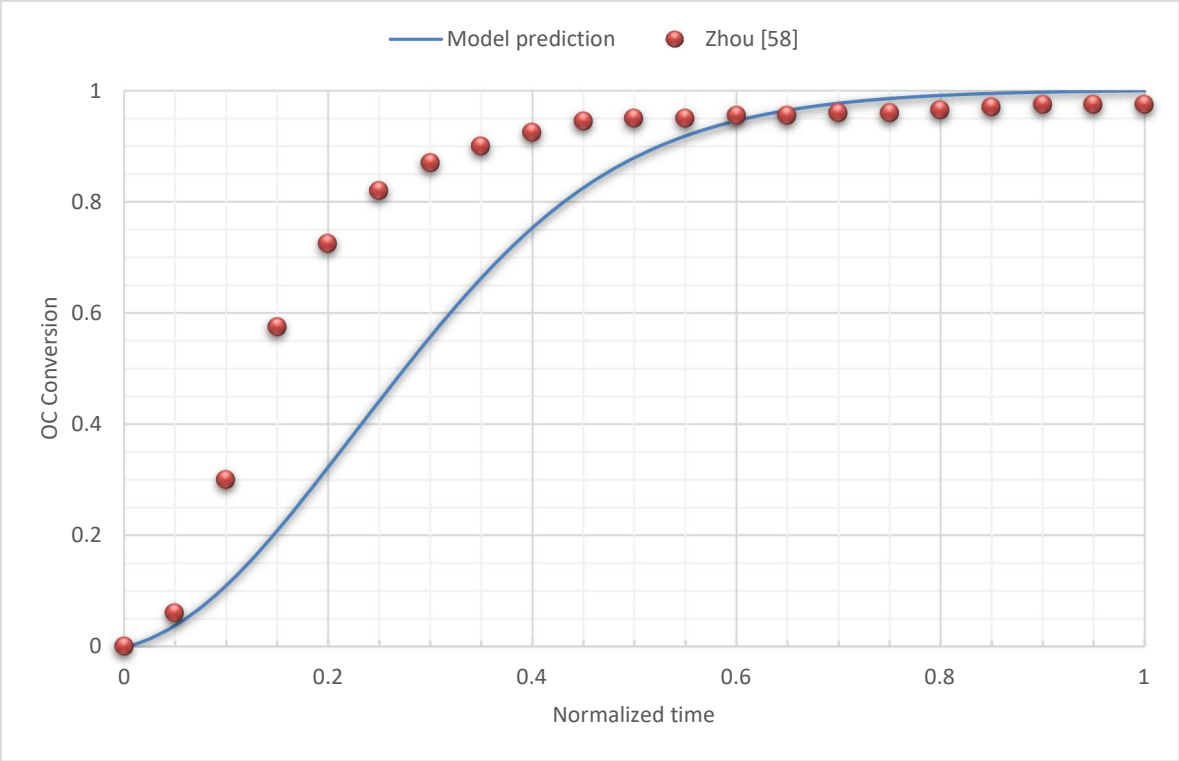

Figure 9 Time profile of the OC conversion during the reduction stage: data by Zhou et al. [58]

The results form the present model have explicitly demonstrated a non-linear behaviour in the OC conversion profile during the reduction stage. This same phenomena was presented in a previous study performed by Zhou et al.[58]. Figure 9 highlights the OC conversion time profile comparison against Zhou's work in which a Ni-based OC was reduced with CH_4. Zhou achieved a maximal conversion of the OC particles of 98%, whereas this work achieved 100%. Despite the different system's dimensions (e.g. reactor length) and operating conditions (e.g. pressure), the transient conversion profile in both studies follow a similar behaviour.

3.7 Sensitivity analysis

To gain a better understanding of the model parameters and variables, as well as the way they impact the dynamic model, a sensitivity analysis was performed for the oxidation and reduction stage. The analysis will aid in the selection of suitable control variables for the CLC process.

Using the information mentioned above in Table 6 and Table 7 for the base case, this study evaluated the following parameters: inlet mass flux, inlet stream temperature, reactor's length and operating pressure. These parameters were selected based on their design flexibility; variations in these parameters would automatically affect either the OC load in the packed bed or the gas phase concentrations. The sensitivity of each one of these parameters to model performance is discussed next.

3.7.1 Effect of the inlet mass flux

The inlet mass flux plays a key role in the performance of the reactor throughout the CLC process stages. For instance, during oxidation, the OC's melting point might be reached at low mass fluxes, thus damaging the fixed bed. Whereas at higher mass fluxes, the outlet gas temperature may fall beneath the minimum required for the gas turbine to operate properly. Thus, the maximum achievable temperature in the reactor is highly sensitive to the inlet air mass flux. In order to analyse its effect on the reactor's performance, a change in the air mass flux of +/- 10% was considered.

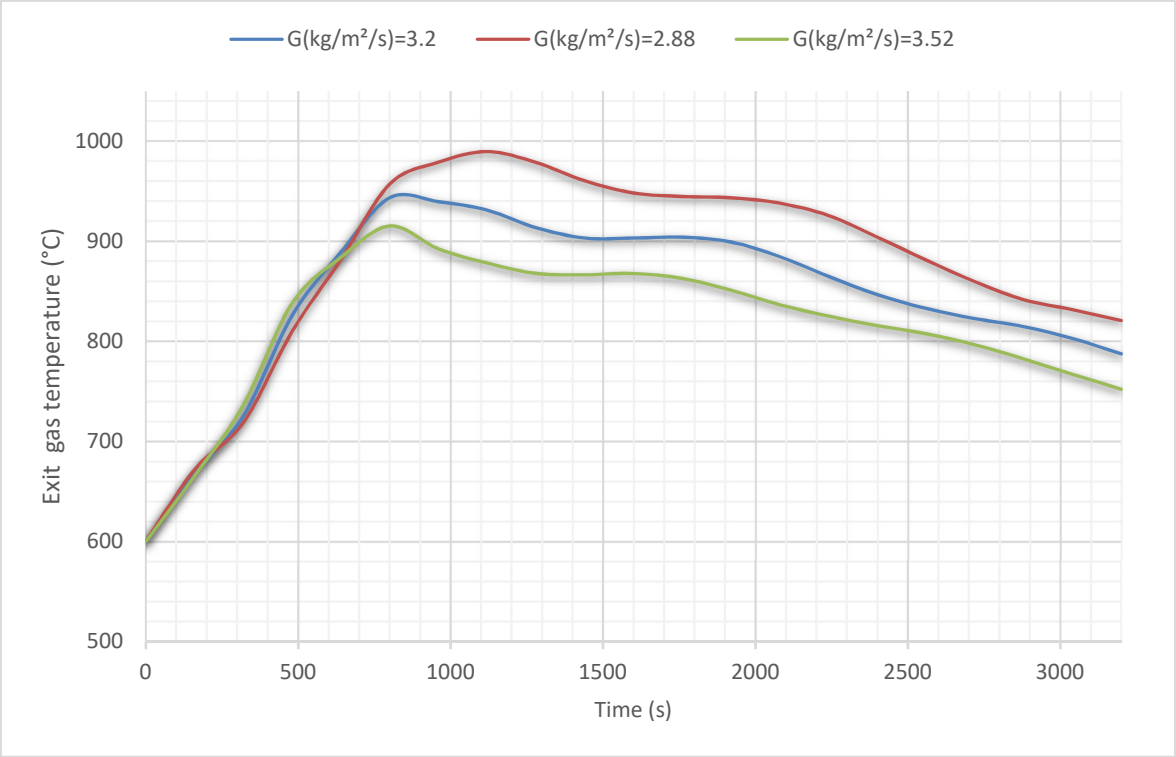

Figure 10 Effect of varying the inlet air mass flux on the exit temperature profile during the oxidation stage

Figure 10 shows that higher temperatures are reached when lower inlet air mass fluxes are fed during the oxidation stage. Oxygen is so highly abundant throughout the duration of the oxidation stage that a reduction in the reaction rate due to a decrease in the inlet mass flux does not create significant effects on the overall process. Thus, the difference between the peaks is due to a minor drop in temperature caused by lower mass flux convection; hence, a crucial aspect in the reactor's performance is maintaining an air mass flux that allows the heat transfer from the exothermic reaction to be greater than the cooling caused by the air mass flux moving within the reactor. Therefore, by lowering the inlet mass flux the exit gas temperature can be maintained at relatively high values for a longer period of time; thus promoting the heat recovery in the downstream turbine.

For the reduction stage, lower inlet mass fluxes would translate into less fuel slip at the reactor outlet. Although higher mass fluxes would ameliorate the reaction rate and the OC conversion, it simultaneously creates a higher fuel slip resulting in lower CO_2 capture efficiency. To analyse the effect of the inlet methane mass flux on the reactor's performance, a change of +/- 10% on this parameter is considered.

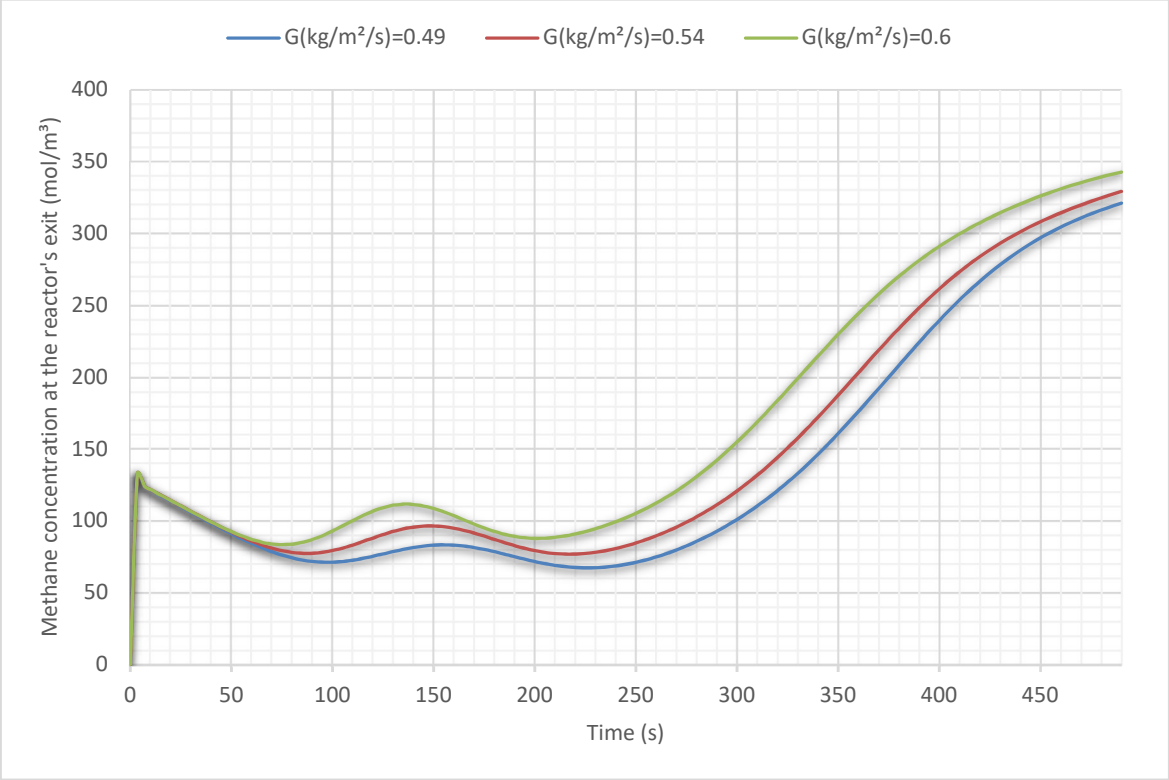

Figure 11. Effect of varying the inlet methane mass flux on the methane concentration at the reactor's exit during the reduction stage

Figure 11 shows a decrease of fuel slip at the reactor's exit by reducing the inlet mass flux. The results show a steady increment during the second half of the simulation time; as expected, the amount of unreacted methane leaving the reactor increases due to

an augmentation in OC conversion. Similarly, the sudden peak at the beginning of the simulation time describes the faster rate of methane diffusion and convection across the bed than the reaction rate of methane consumption. Furthermore, changes in the methane mass flux to reduce that peak on the exit mol concentration show no impact; the changes are more evident after 70 s of simulation. Nevertheless, an important operational aspect to consider is the manipulation of the inlet methane mass flux, in order to keep a minimum methane slip at the reactor's outlet; by lowering the mass flux, the residence time of the methane is increased allowing for its full conversion to take place.

3.7.2 Effect of the inlet gas stream temperature

Selecting the suitable inlet temperature for the gas streams feeding the CLC reactor may be instrumental in the CLC process. For instance, a higher inlet air temperature during oxidation would translate into greater heat recovery since the cooling of the packed bed would be reduced. Moreover, a higher inlet methane temperature during the reduction stage would also reduce the cooling of the packed bed, thus enhancing the Arrhenius-type reaction rate as shown in section 3.3. To analyse the effect of the inlet gas temperature on the reactor's performance, a change of +/- 10% on this parameter is considered during the oxidation and reduction stages.

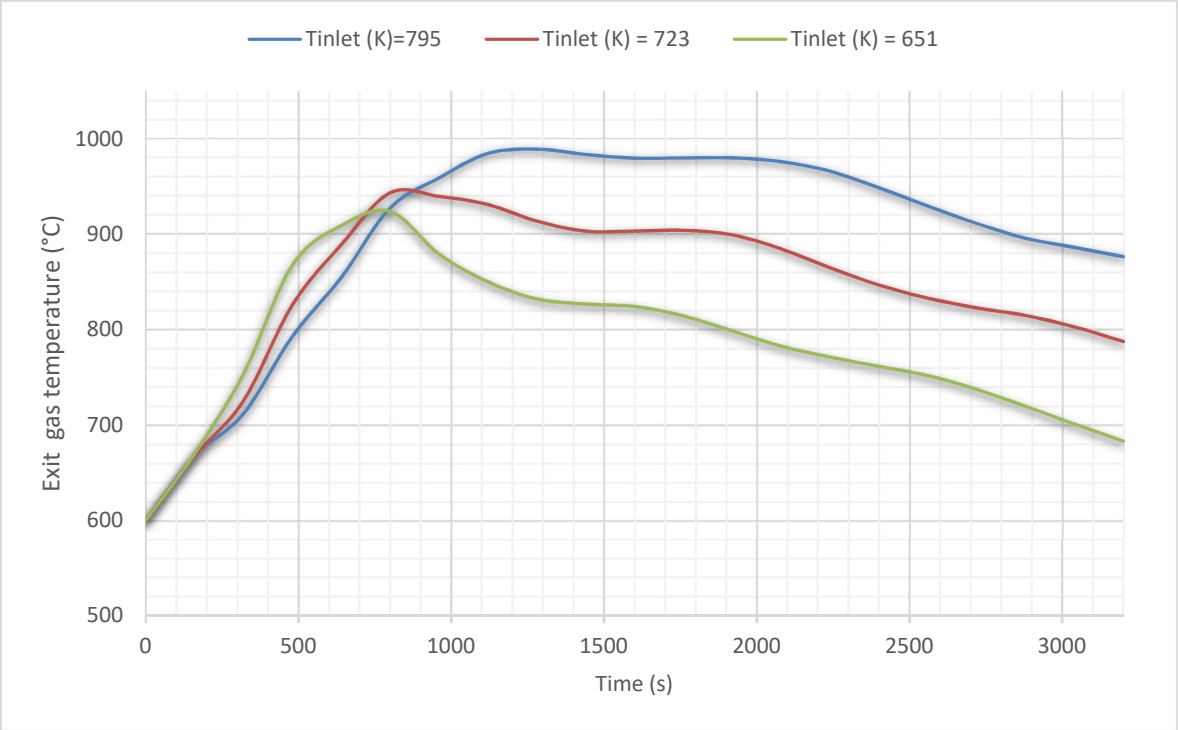

Figure 12. Effect of varying the inlet air temperature on the exit temperature profile during the oxidation stage

Figure 12 shows that increasing the inlet air temperature would not only increase the maximum exit temperature, but also extend the generation time of this hot outlet stream. The peak mismatch between the curves can be explained by the change in mol concentration, since the temperature increments are inversely proportional to the oxygen concentration within the reactor, affecting the reaction rate and therefore the exothermic temperature reached. Furthermore, as expected, Figure 12 depicts that a low inlet air temperature would rapidly drop the hot stream production, due to a greater cooling of the packed bed caused by the greater temperature gradient.

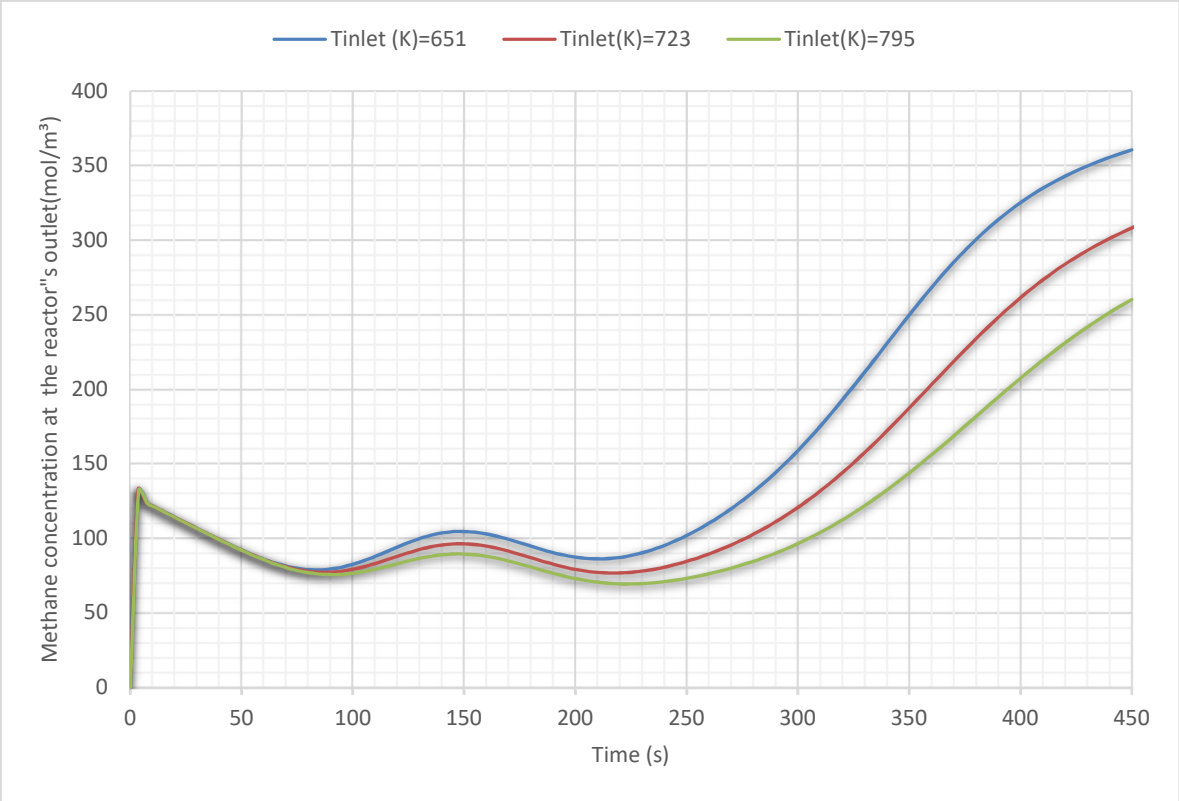

Figure 13. Effect of varying the inlet methane temperature on the methane concentration at the reactor's exit during the reduction stage

Figure 13 shows the inversely proportional impact that the inlet temperature has on the exit methane concentration during the reduction stage. By increasing the inlet gas temperature, the inlet mol concentration is reduced (ideal gas behaviour) thus reducing the concentration of exit methane in the reactor. Moreover, since the temperature gradient between the packed bed and the inlet stream is lower at higher inlet fuel temperatures, the cooling of the reactor is less drastic; hence, the reaction rates are enhanced and the result is more methane reacted by the OC.

The inlet gas temperatures can be adjusted by manipulating the preheating process, which could be configurated as shown in Figure 5, where the exhaust from the turbines are

used to preheat the aforementioned feeding streams into the reactor. Although the integration of the turbines and the CLC reactor is beyond the scope of this study, it is worth mentioning the importance of properly coupling the CLC reactor with the complete combined cycle.

3.7.3 Effect of the reactor's length

The dimensions of the reactor are considered next. The use of a 1-dimensional model only allows to analyze the length of the CLC reactor. Nevertheless, the effects of OC load within the reactor can be studied by varying the reactor's length. This parameter is variated by +/- 10% in both the oxidation and reduction stages.

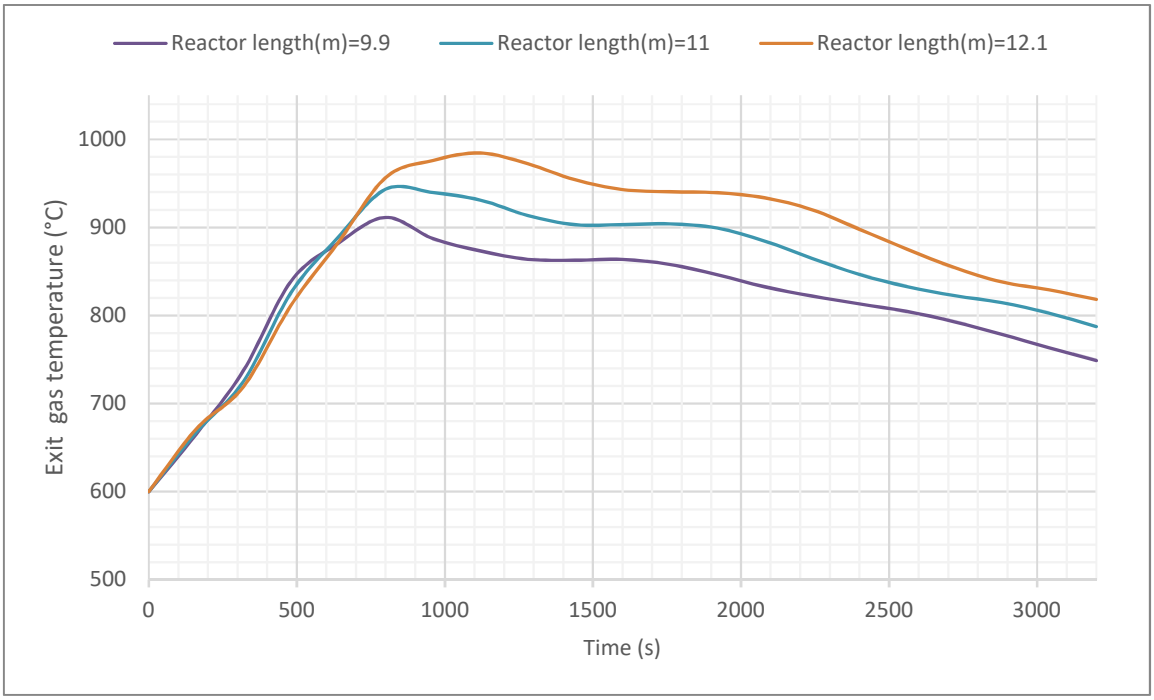

Figure 14. Effect of the reactor's length on the exit gas temperature during the oxidation stage

Figure 14 shows the impact of the reactor's length on the oxidation stage. It is possible to achieve higher temperatures when using larger reactors, which is expected since the heat front is highly dependent on the spatial axial domain of the reactor. Moreover, the peak temperature occurs at different times according to the different reactor size, with 300 s the maximum difference between the peaks. The latter impacts the timing of the switch from the oxidation stage to the heat recovery stage, i.e. the heat recovery comes after the desired high temperature is reached. If switching happens too late in the process, wasted energy production in the gas turbine could happen; conversely, if the switch happens too early, damage to the turbine could occur since lower temperatures are fed which increases the risk of thermal stress.

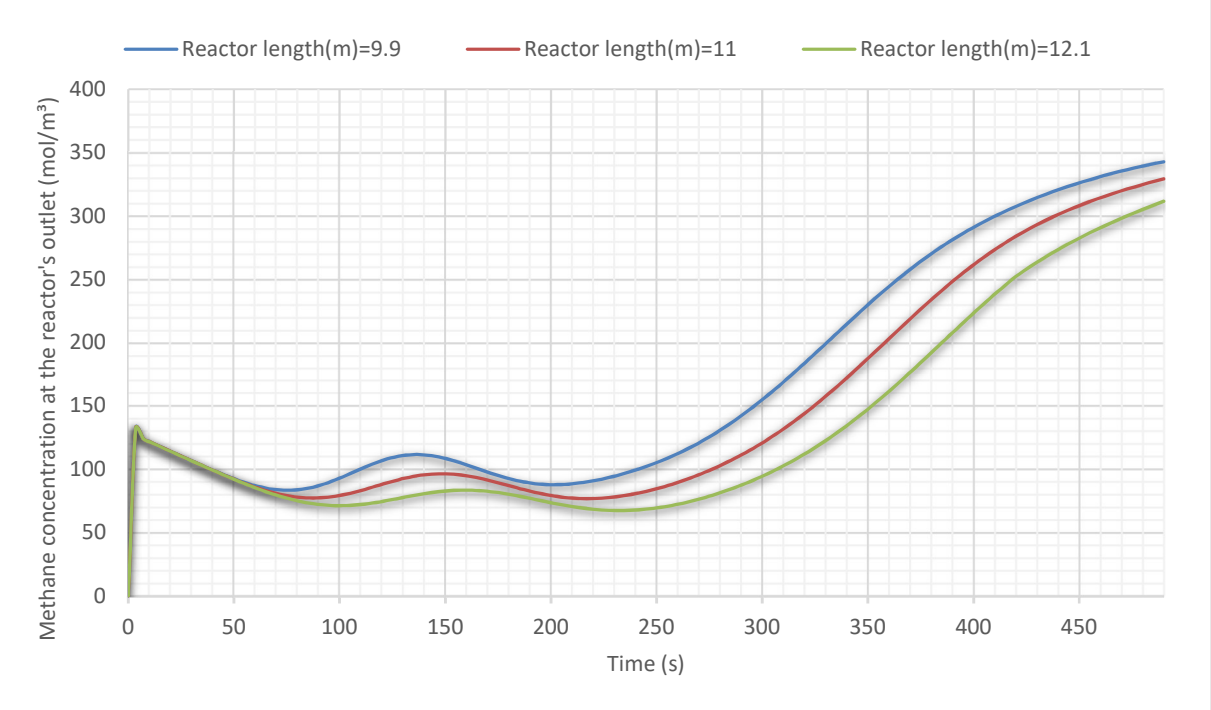

Figure 15. Effect of the reactor's length on the methane concentration at the reactor's exit during reduction

Figure 15 shows how a change in the reactor's length affects methane concentrations in the reduction stage. As expected, an increment in the length results in a lower concentration of exit methane; this result is reasonable because the surface area and the OC load of the packed bed are increased proportionately with the length, allowing more methane to react within the OC.

3.7.4 Effect of the pressure

The pressure at which the CLC reactor operates is a key aspect not only for the reactor's performance, but also for the overall performance of the combined cycle (CC). Setting a proper operating pressure would also affect secondary equipment in the CLC-CC; thus, the operating conditions of the HRSG, turbines and preheaters connected to the system would also need to be modified accordingly. To analyse the effect of pressure on the CLC PBR during the oxidation stage, changes of +/- 25% on this parameter are conducted.

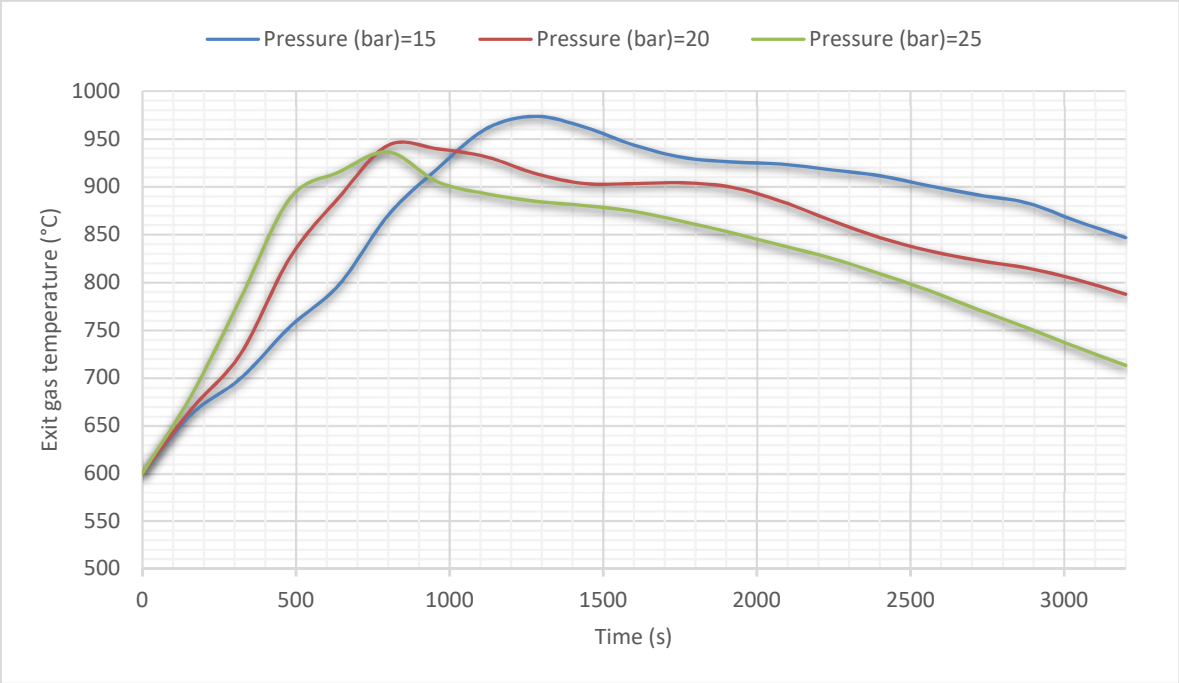

Figure 16. Effect of varying the operating pressure on the exit gas temperature during oxidation

Figure 16 shows the inversely proportional effect of decreasing the operating pressure on the exit gas temperature. Although the difference between peak temperatures is about 35°C, the time span of a high exit gas temperature (i.e. above 900°C) is considerably larger at lower pressures. The decrease in the inlet pressure also lowered the inlet mole concentration; therefore, limiting the exothermic reaction due to lack of available oxygen. Hence, operating at higher pressures enhances the OC conversion rate, which would shorten the stage time and the heat recovery process. Nevertheless, lower pressures would maintain a constant hot exit gas production and the turbine's safety would not be affected; on the other hand, a lower pressure ratio will be available for the gas turbine thus producing less energy.

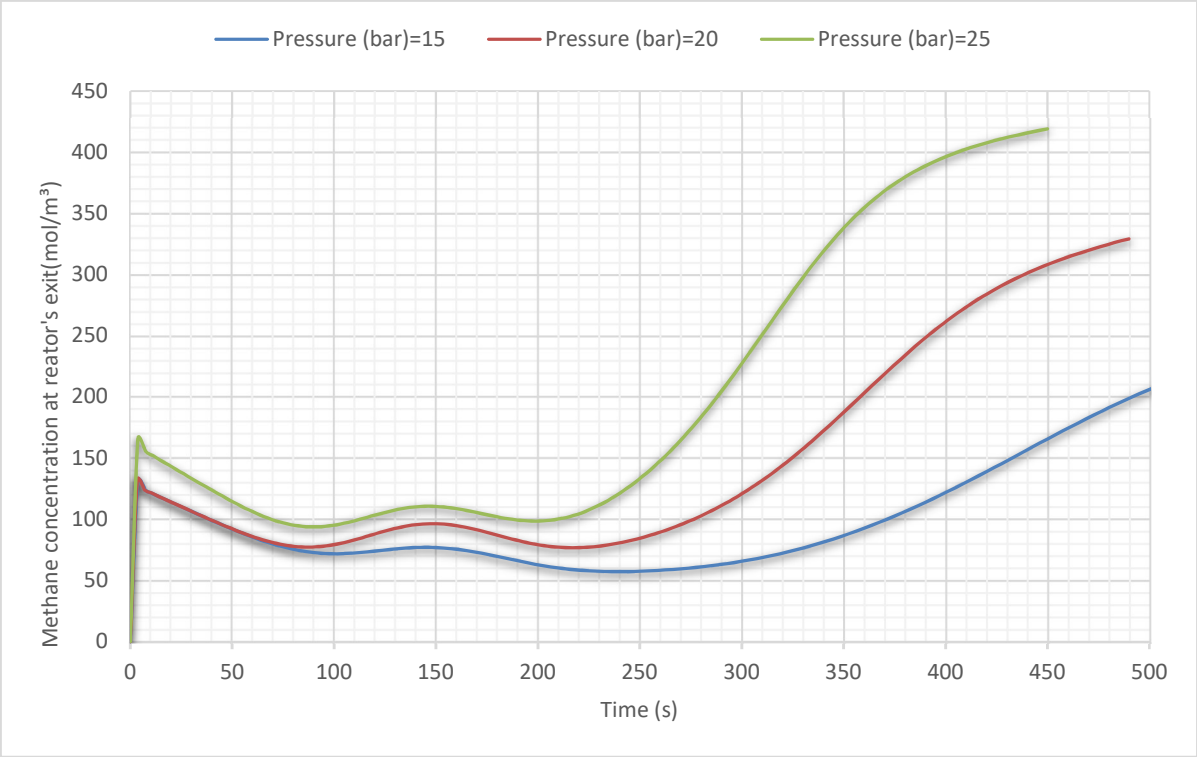

Figure 17. Effect of varying the operating pressure on the methane concentration at the reactor's exit during the reduction

Figure 17 shows the effects of changing the operating pressure on the exit methane concentration during the reduction stage. The expected results are obtained, simultaneous increases in operating pressure and mole concentration indicated that an excess of unreacted methane moves within the reactor. Furthermore, lowering the pressure would also translate into less OC conversion during the same timespan; thus, extending the timeframe necessary to allow for a full OC conversion. This time extension during the reduction stage would also affect the switching between stages and potentially delay the reactor entering into the oxidation stage at the optimal moment. Notwithstanding the changes in operating conditions, all the times required for full reduction of the OC studied in this section are lower

than the time required for full oxidation of the OC. Therefore, no delay is expected to occur between stages for this CLC packed bed configuration.

An adequate control in the oxidation process would translate into a more efficient energy production by the downstream turbine, thus diminishing the energy penalty that CCS entails. Moreover, controlling the methane slip from the reactor and hence allowing more fuel conversion would improve the CO_2 capture efficiency. According to the sensitivity analysis presented above, it is concluded that changes in the inlet mass flux at various stages is indeed the most practical approach in order to obtain the design objectives of the CLC process, i.e. maintaining a high exit temperature and low fuel slip during the oxidation and reduction stages, respectively. This conclusion is also supported by best practice in the field, as changing the mass flux is a more common control engineering practice compared to changing the operating pressure of a reactor.

3.8 Chapter summary

A 1-dimensional heterogeneous model for a packed bed CLC reactor was presented in this chapter. A base case was selected in accordance with data obtained from the literature for a large-scale CLC reactor. The model was validated against data reported in the literature. The results are to be in reasonable agreement with the reported data; thus, showing that the model captures the behaviour of a CLC PBR. Moreover, a sensitivity analysis was performed for the reduction and oxidation stages. The effects of various mass flux changes were analyzed, showing that less inlet moles to the reactor would translate into lower fuel slip; moreover, a better control in the state variables, such as concentration and temperature, was also observed when changing the inlet mass fluxes. Additionally, the current study analyzed the effect of the inlet stream temperature and effectively depicted

that greater heat recovery can be obtained at higher temperatures. Likewise, the mole concentration is affected by the above change and therefore dictates the corresponding modified duration of the stage. Moreover, the effect of the reactor's length on the oxidation and reduction stages was also studied. By increasing the reactor's length, the load of OC in the pack bed changes requiring more time for full conversion. Similarly, increases in length result in increases in the heat front and the methane consumption during the oxidation and reduction stages, respectively. Furthermore, the effect of the operating pressure was analyzed and it was shown that this parameter is directly related to the inlet mole concentration. Whereas increases in pressure during the oxidation stage enhance the peak and maintenance of the hot temperature in the exit air stream, during reduction stage, the same pressure changes initiated a major fuel slip at the reactor's exit.

By analyzing various parameters and performing a sensitivity analysis, it has been effectively demonstrated the implementation of a dynamic model and selected the proper controlled and manipulated variables necessary to perform dynamic optimization for the CLC PBR.

Chapter 4
Dynamic optimization of the CLC PBR

The aim of this section is to evaluate the controllability of the CLC PBR stages during operation using dynamic optimization. During the oxidation process, the goal is to keep a constant exit gas temperature, with the intention to extend the heat recovery process in the downstream turbine, while adjusting the inlet air mass flux. Whereas for the reduction stage, the objective is to keep a fuel conversion greater than 95% while adjusting the inlet fuel mass flux. In addition, the purge between the oxidation and reduction stages has to be not only effective, but also to be performed as quickly as possible. The organization of the following chapter is as follows: a solution based on step-wise changes in the manipulated variables is presented as an initial attempt to address the aforementioned objectives for each state. An optimal control problem expressed as a dynamic optimization formulation is proposed next; by defining a set point in every stage in the CLC process sequence the goal is to depict the adeptness of implementing this control technique. Furthermore, based on the sensitivity analysis presented in Chapter 3, two optimal control scenarios are proposed and solved using dynamic optimization formulations. Note that part of the work presented in this Chapter has been submitted for publication [129].

4.1 Introduction

The process control system allows flexibility in every unit operation in chemical engineering; the nominal operating conditions inside the process can be easily disrupted by unexpected disturbances and the process control system therefore allows to maintain those

conditions at their target values. Regarding the design and operating conditions for a CLC PBR, very few works have been published in the literature [87], [89], [123]. In this limited body of research, the design of a network of PBRs for a large-scale power plants (350-400 MWth) was performed using a simplified analytical solution of a 1-D mechanistic model; the number and size of the reactors, as well as their related process operating conditions were considered, with the goal of achieving continuous operation in the downstream turbine. Furthermore, studies regarding process control and dynamic optimization are scarce within this limited body of research. To the author's knowledge, the work presented by Han et al. [13] is the only available study that considers controllability for the CLC PBR process, as discussed in Section 2.6.2. This chapter will therefore propose a control strategy based on dynamic optimization of all stages in the CLC PBR sequence in an attempt to fill in the current gaps in this subject area (see Figure 4). It will be considered, the operating conditions and dimensions of a large-scale process with a specific focus on the control actions that best maintain the operation of the entire CLC process while also improving the performance and efficiency at every stage.

4.2 Manual step changes in the inlet mass flux

The goal of controlling the dynamic operation of a CLC PBR during oxidation is to avoid temperature fluctuations, which can harm the downstream turbine due to thermal stress and differential expansion between stationary and rotating parts [89], [124]. Whereas in the reduction stage, the objective is to maximize the OC conversion while maintaining high CO_2 capture efficiency [13]. To accomplish these goals, the present scenario performs manual step changes in the inlet mass fluxes during the oxidation and reduction stages in an attempt to enhance their performance.

The nominal case operation presented in section 3.4 will be used as framework to perform this study. Hence, a feasibility problem is formulated with user-defined step changes in the inlet mass flux as input variable. These variables were adjusted accordingly to improvements observed in control variables for each stage, such as temperature and mole concentration. The timing of the increments or decrements in the mass fluxes was defined on a trial and error basis through performing simulations.

The oxidation stage is comprised of a heat recovery process, which can be defined as the period during which the reactor's exit gas temperature has reached a certain value that makes the outlet stream suitable for feeding the downstream turbine. Once the value drops below the minimum turbine inlet temperature (TIT), the recovery process and the oxidation stage have both ended. Based on the operation range of gas turbines presented in previous works [82], [106], the TIT selected for this study was 900 °C which also corresponds to Han's work [13].

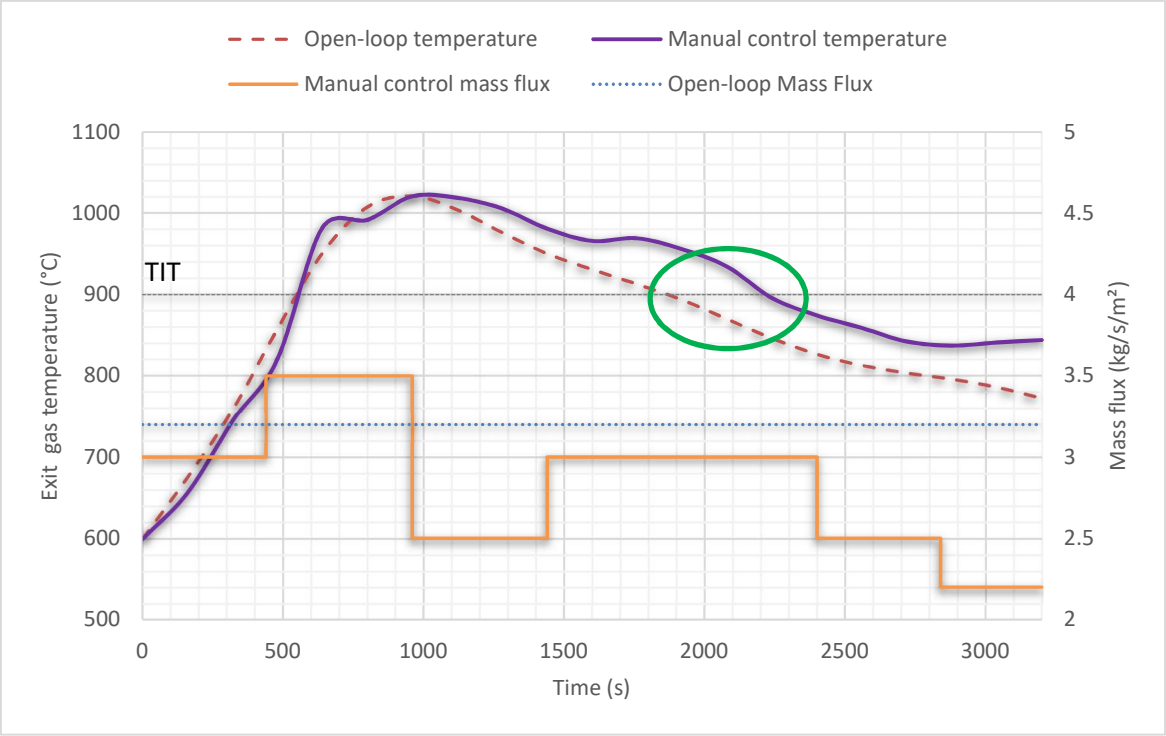

Figure 18. Exit gas temperature time profile with manual step changes in the inlet mass flux during the oxidation stage.

Figure 18 shows a comparison between the exit gas temperature for the base case presented in Section 3.4 and that obtained with step changes. The base case, which considers a constant mass flux throughout the entire stage, crosses the TIT barrier after 1,900 s. of simulation time; alternatively, in the step change scenario the exit gas temperature falls below the TIT set-point after 2,200 s, showing an improvement of 300 s in the time duration of the heat recovery process. This would automatically translate into more energy in the downstream turbine as the manual step change scenario recovers 22.5 MW-h of energy, compared to 19.7 MW-h for the base case. This control approach indicates that the energy production during the oxidation stage can be enhanced by making online adjustments to the mass flux; nevertheless, the timing of this adjustment requires precision

since executing the change in an inaccurate manner could result in overshooting or undershooting the set-point of the exit temperature which, as discussed previously, could damage either the OC particles or the turbine.

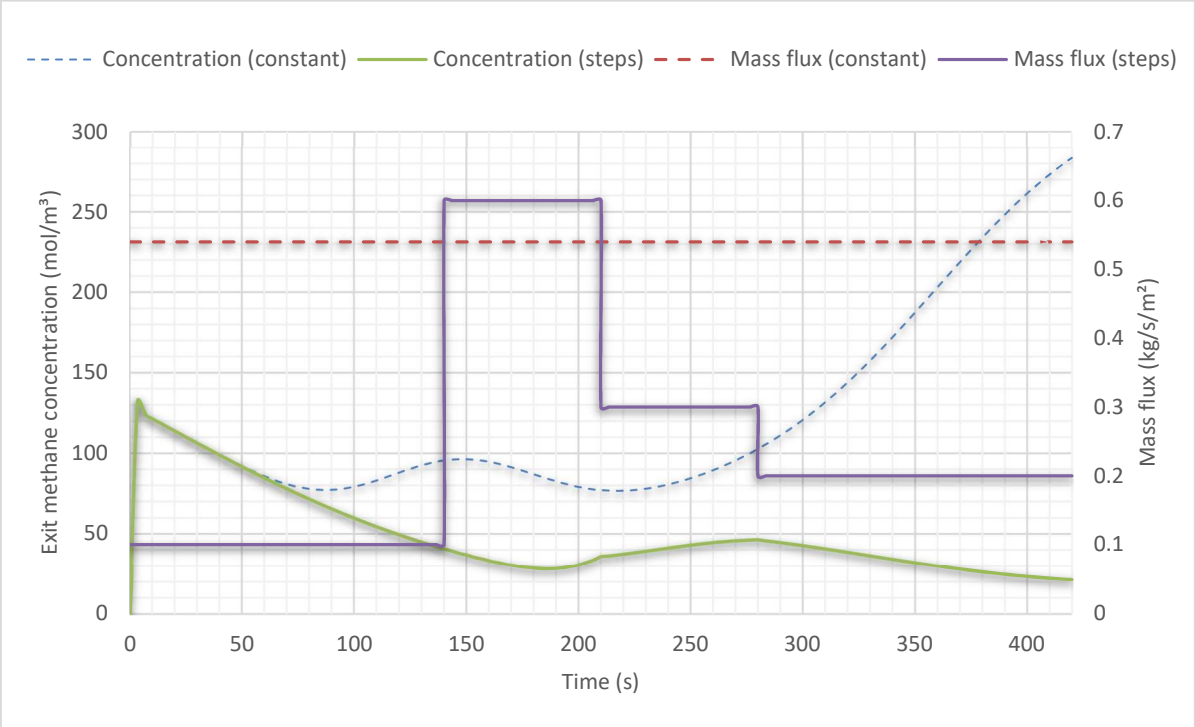

Figure 19. Exit methane concentration time profile with manual step changes in the fuel mass flux during the reduction stage

The methane concentration at the reactor's outlet should be kept as low as possible in order to carry out a more efficient reduction stage, i.e. increase CO_2 recovery efficiency. Figure 19 shows the reduction stage comparison between the base case, which considers constant inlet mass flux during the timespan, against performing manual step changes in the input variable. As in the oxidation stage, the manual step changes aimed to keep the

methane concentration under 50 mol/m³. This concentration represents an 85% methane (fuel) conversion rate and it can be used as target control value for the reduction stage. Figure 19 effectively indicates that performing step changes result in less fuel slip during the simulation timespan. Conversely, a larger fuel slip is seen in the base case operation as the methane concentration value is close to 290 mol/m³ at the end of the reduction stage. This indicates an almost full reduction of the OC since it is no longer reacting with methane. Additionally, one can observe in Figure 19 that the set-point is achieved after 120 s; before this point, any further decrease in the inlet mass flux has no major effect on the exit methane concentration. This is due to the fact that it takes time for the methane to fully diffuse into all the OC particles, allowing complete utilization of the surface area in the reaction. Before reaching this diffused state, the exit methane concentration will not decrease despite decrements in the inlet mass flux. In the step change scenario depicted in Figure 19, a 90% fuel (methane) conversion rate was not obtained, despite the fact that this is widely considered the minimal rate required for an efficient CCS process [8]. However, the step change scenario was useful in showing that it is possible to maintain an exit methane concentration under the desired set-point during a time span of 300 s, thus confirming the impact of this control approach.

Based on the above, making manual changes in the key input variables improves the overall process performance. Furthermore, the step changes considered in this analysis produced the expected outcome, i.e. and extension of the energy production in the oxidation stage and an enhancement of the methane conversion in the reduction stage. These results motivate the seek for optimal control strategies that can further improve the expected performance of this process.

4.3 Dynamic optimization

Based on the results presented in the previous section, the aim of this section is to present an optimal control study on the CLC packed bed reactor using the inlet mass flux as the manipulated variable for both stages. As in the previous section, the goal is to extend heat recovery by maintaining the exit gas temperature at a minimum of 900°C during the oxidation process and by maintaining the fuel conversion above 90 % to ensure a more efficient CO_2 capture process in the reduction stage. Additionally, the purge stages are included in the analysis in order to analyze the possibility of shortening their duration while also proposing a better utilization of the purge gas stream.

The oxidation stage optimal control problem can be formulated as a dynamic optimization problem as follows:

$$\min_{G_j(k_j\Delta t)\in G_j} \sum_{k_j=0}^{K_j}\left(T_{\text{exit}} - T(k_j\Delta t)\right)^2 \tag{4.1}$$

Subject to:

CLC packed bed model (3.1-3.11), reaction equations (3.12,3.13,3.20-3.23)

$t_j = \left[0, \Delta t, \ldots\ldots, k_j\Delta t, \ldots\ldots, K_j\Delta t\right] \;\forall\; j = oxidation\ stage$

$2.0 \le G_j\left(k_j\Delta t\right) \le 4.7 \quad \forall\, k_j = 0, \ldots\ldots, K_j$

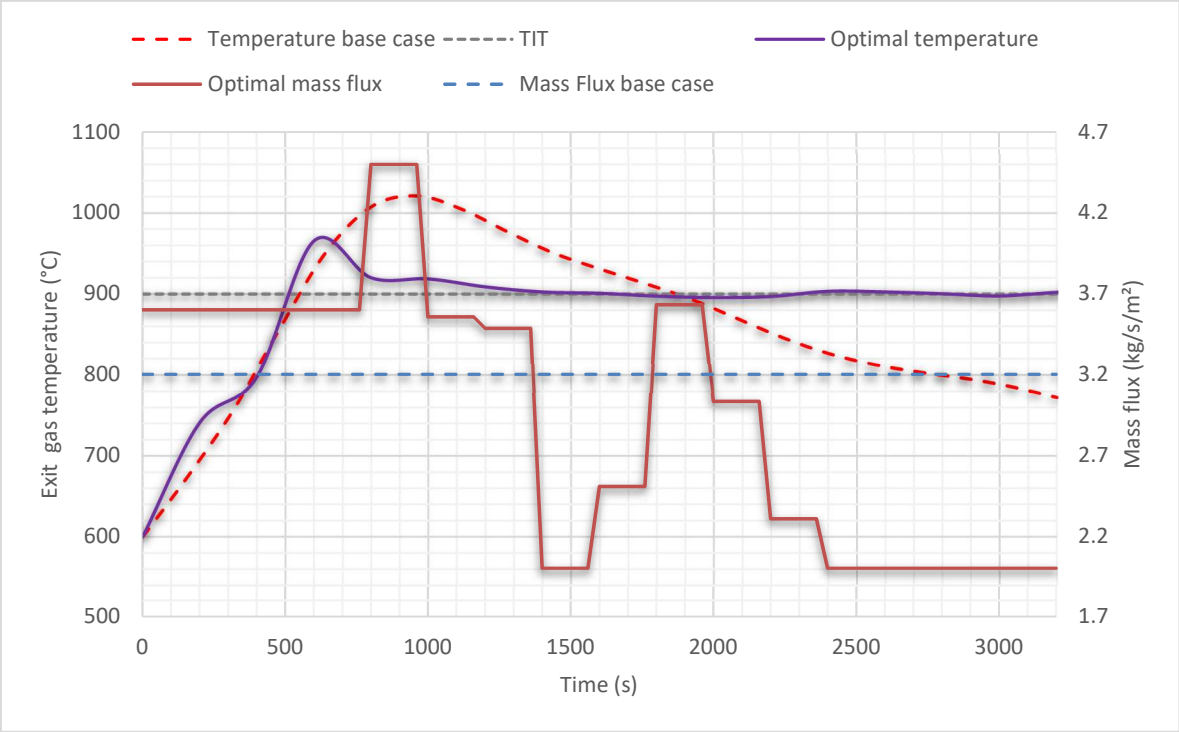

Figure 20. Optimal exit gas temperature and inlet mass flux time profiles during the oxidation stage

The problem shown in equation 4.1 searches for the control actions that need to be implemented in the inlet mass flux for the oxidation stage at each time interval k_j that would minimize the deviations between the reactor's outlet temperature set-point (T_{exit}) and the actual exit gas temperature. The proposed formulation is subject to the CLC PBR model presented in Chapter 3. Using the direct transcription dynamic optimization approach, alongside centered difference discretization as discussed in Section 3.5, the resulting optimal control problem consisted of 48,573 non-linear equations with 48,593 optimization variables. This problem converged to local optimal solution in 450 s using the interior-point optimization algorithm.

Figure 20 shows a comparison between the exit gas temperature for the base case scenario with constant inlet mass flux and the optimal control profiles identified from the solution of problem (4.1). The results show that an optimal control profile is able to maintain the $T_{\text{exit}} = 900°C$ in a fairly constant manner, whereas, the base case solution shows an initial peak of 1,020°C in the exit gas temperature with a quick decrement afterwards. Furthermore, the optimal control strategy defines a non-trivial inlet air mass flux profile since it depends on the stage of the oxidation process, e.g. the time at which the system reaches the set-point for the first time. Thus, by lowering the mass flux the cooling of the packed bed caused by convection of the moving air stream across the reactor is hindered. Han et al. [13] showed similar results when they performed a multi-period optimization by manipulating the air inlet flow rate (mass flux) as decision variable on every period and maximizing the heat recovery stage. A key difference is that they assume that the air mass flux would remain constant throughout the oxidation process. This work demonstrates that the efficiency in the heat recovery process can be further improved if optimal time-dependent control profiles are implemented during the oxidation process. Moreover, using the equation found on NASA's website [130] to calculate the power generated by the downstream gas turbine, the base case produces 19.7 MW-h of heat during a shorter period of time during which the exit gas is above 900°C; whereas in the present optimal control strategy, a heat production of 31.7 MW-h is achieved under the same criteria and the displayed time span in the figure, which is equivalent to a 60.8% improvement.

As described in Section 4.2, the objective in the reduction stage is to reduce the fuel slip at the reactor's outlet; by controlling this parameter the fuel conversion within the reactor would be increased, as well as the CO_2 captured. Thus, the reduction stage optimal control problem can be formulated as a dynamic optimization problem and is as follows:

$$\min_{G_j(k_j\Delta t)\in G_j} \sum_{k_j=0}^{K_j}\left(C_{Fs} - C_{methane|z=L}(k_j\Delta t)\right)^2 \quad (4.2)$$

Subject to:

CLC packed bed model (3.1-3.11), reaction equations (3.14-3.22,3.24)

$t_j = [0, \Delta t, .., k_j\Delta t, \dots\dots, K_j\Delta t] \quad \forall\, j = reduction\ stage$

$0.1 \le G_j(k_j\Delta t) \le 0.8 \quad \forall\, k_j = 0, \dots.., K_j$

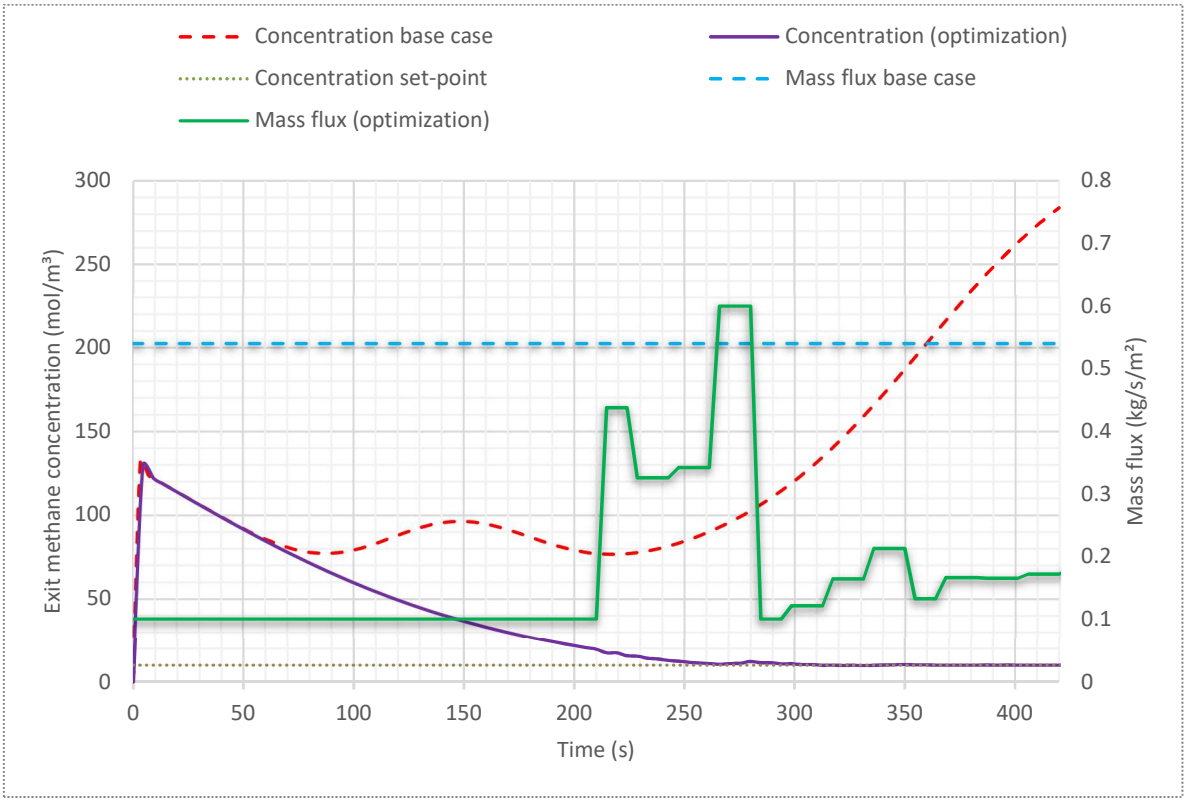

Figure 21. Optimal exit methane concentration and inlet fuel mass flux time profiles during the reduction stage

In the same manner, the solution to the problem shown in equation 4.2 specifies the optimal control actions in the inlet fuel mass flux that minimizes the deviations between

desired and actual concentrations of the fuel at the outlet. After performing discretization of the PDE's and implementing the direct transcription dynamic optimization approach, the resulting optimal control problem consisted of 42,527 equations with 42,557 decision variables that converged after 1296 s.

As shown in Figure 21, the exit methane concentration for the base case scenario with constant inlet methane mass flux is compared with the corresponding optimal control strategy obtained from the solution of problem (4.2). The set-point value for the optimal control case (equation 4.2) was C_{Fs}= 10 mol/m³, which corresponds to a 97% fuel conversion, which is the same used in Han's study [13]. As shown in this figure, the optimal control profile is able to maintain a fairly constant value on the set-point. Moreover, the methane mass flux profile depends on the stage of the reduction; e.g. at the moment when the system reaches the set-point for the first time, the aggressive changes are made in the mass flux to avoid undershooting the target value. Similarly, towards the end of the reduction process, the mass flux is reduced as the OC conversion increases, which is the expected behaviour of the OC since fuel intake has decreased due to the abatement in the unreacted OC surface area. These results show that during the first time periods of the reduction stage, despite the fact that the mass flux control is at the lower-bound, the set-point has not been met due to a fast diffusion and convection of the methane across the bed thus resulting in a large fuel slip.

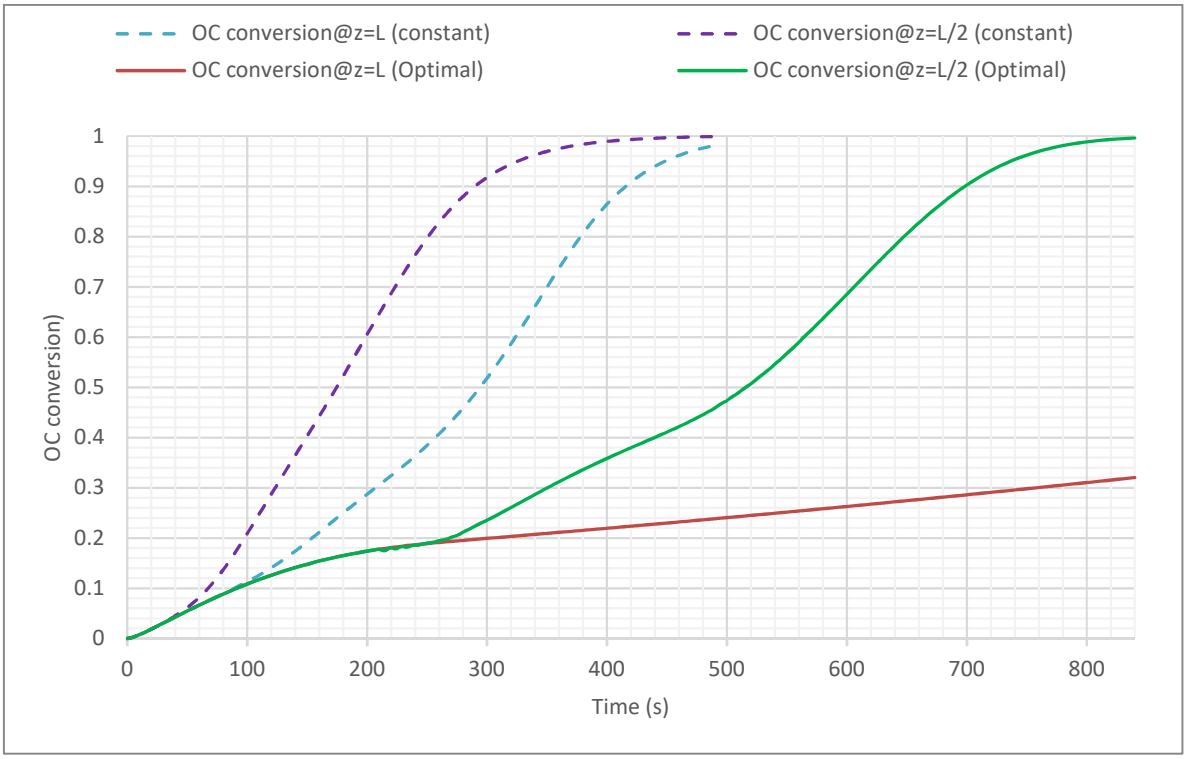

Figure 22. Constant and optimal OC conversion time profile at different bed positions during the reduction stage

Figure 22 shows a comparison of the OC conversion time profile between the base case scenario with constant mass flux and the proposed optimal control strategy. As expected, the decrease in the inlet fuel mass flux during the optimal control strategy hampers the full reduction of the OC at the rector's outlet; although the middle of the packed bed is fully converted into the reduced form, the OC particles closer to the outlet, and therefore farther away from the inlet mass flux, are not yet converted due to reactant limitations (fuel). Accordingly, Figure 22 depicts that a longer simulation time is required to reach full reduction of the entire packed bed which could potentially delay the beginning of the oxidation stage

when multibed configuration is implemented; therefore jeopardized the downstream turbine operation.

Given that the steadfast lower-bound value of the inlet mass flux hampers any further decrease in the exit methane concentration during the optimal control case operation, a possible alternative to increase the fuel conversion of the first half of the reduction process could be recirculating or redirecting the outlet stream to an intermediate vessel for momentaneous storage, in order to avoid a decrement in CO_2 purity. This is beyond the scope of this work and left for future studies.

A typical purge stage for CLC PBR process, in terms of time span or mass flux rate, is usually defined by common engineering practices. Thus far, the defined criteria to execute the purge stage was based on the number of reactor volumes to remove the undesired gas compounds from the packed bed [13], [87]. This criterion uses a steadfast time span during which a constant inlet mass flux of the inert compound is fed to the reactor. In the present study a different approach is considered by using dynamic optimization and formulating the purge as an optimal control problem with the goal of decreasing the amount of inert compound (argon), as well as the timespan required to completely eliminate the undesired gases inside the reactor.

The purge after the oxidation optimal control problem can be stated as follows:

$$\min_{G_j(k_j\Delta t)\in G_j} \sum_{k_j=0}^{K_j}\left(C_{OS} - C_{oxygen|z=L}(k_j\Delta t)\right)^2 \tag{4.3}$$

Subject to:

CLC packed bed model (3.1-3.11), reaction equations (3.12,3.13,3.20-3.23)

$t_j = \left[0, \Delta t, \ldots\ldots, k_j\Delta t, \ldots\ldots, K_j\Delta t\right] \quad \forall\ j = purge_1\ (after\ oxidation\ stage)$

$0.3 \leq G_j(k_j\Delta t) \leq 0.55\ \forall\ k_j = 0, \ldots\ldots, K_j$

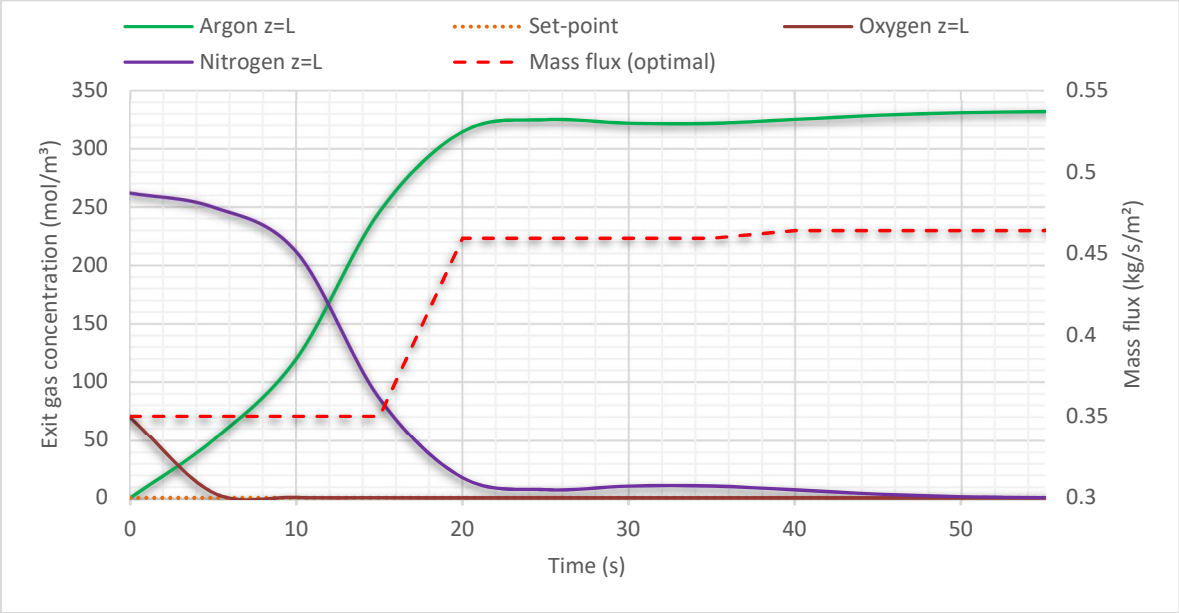

Figure 23. Optimal exit gas concentration and inlet argon mass flux time profiles for the purge after oxidation

The problem shown in equation 4.3 aims to find the control actions in the inlet argon mass flux values at each time interval for the purge after oxidation stage that minimizes the square deviations between the desired and actual concentration of oxygen at the reactor's outlet. Likewise, the optimal control problem was solved using the direct transcription approach as in the previous optimization problems; resulting in 55,146 equations with 55,166 decision variables which correspond to each inlet mass flux at every k_j. Moreover, using the interior-point optimization algorithm the problem converged after 187 s.

The idea for the purge after oxidation is to reduce or eliminate the oxygen that could potentially mix with the fuel used in the reduction and may eventually generate NOx products, which would only exacerbate the process of CO_2 separation before sequestration. Therefore, the purge optimal control strategy uses the final values of the state variables (e.g.

concentration and temperature) specified from the oxidation stage as initial conditions for the purge stage. Figure 23 shows the resulting argon inlet mass flux profile for the purge's optimal control strategy after the oxidation stage when the oxygen slip is set at C_{OS}=0.0 mol/m³. Whereas the oxygen concentration decreases relatively fast, the argon the concentration reaches its peak after 50 s, as shown in Figure 23. Additionally, the increment in inlet mass flux proposed by the optimal control strategy after 15 s is in order to numerically achieved 0.0 mol/m³ at the reactor outlet and minimize even more the square differences with the defined set-point. Despite the fact that the argon mass flux used during this study remained below the 1.3 kg/s/m² used in previous works [87], the oxygen concentration was effectively reduced to the desired C_{OS} set-point value during the purge stage. Moreover, the timespan required to remove all the oxygen from the PBR is shorter than that reported by Spallina et al. [87], i.e. a purge stage lasting 300 s. Due to the length of the purge stage, Spallina's work reported a total of 9,195 kg of argon used, which is 15 times more than the 605 kg required in this study.

The purge after the reduction optimal control problem can be stated as follows:

$$\min_{G_j(k_j\Delta t)\in G_j} \sum_{k_j=0}^{K_j}\left(C_{MS} - C_{methane|z=L}(k_j\Delta t)\right)^2 \tag{4.4}$$

Subject to:

CLC packed bed model (3.1-3.11), reaction equations (3.14-3.22,3.24)

$t_j = \left[0, \Delta t, \ldots\ldots, k_j\Delta t, \ldots\ldots, K_j\Delta t\right] \;\; \forall \; j = purge_2 \; (after \; reduction \; stage)$

$0.35 \leq G_j(k_j\Delta t) \leq 0.5 \;\; \forall \, k_j = 0, \ldots\ldots, K_j$

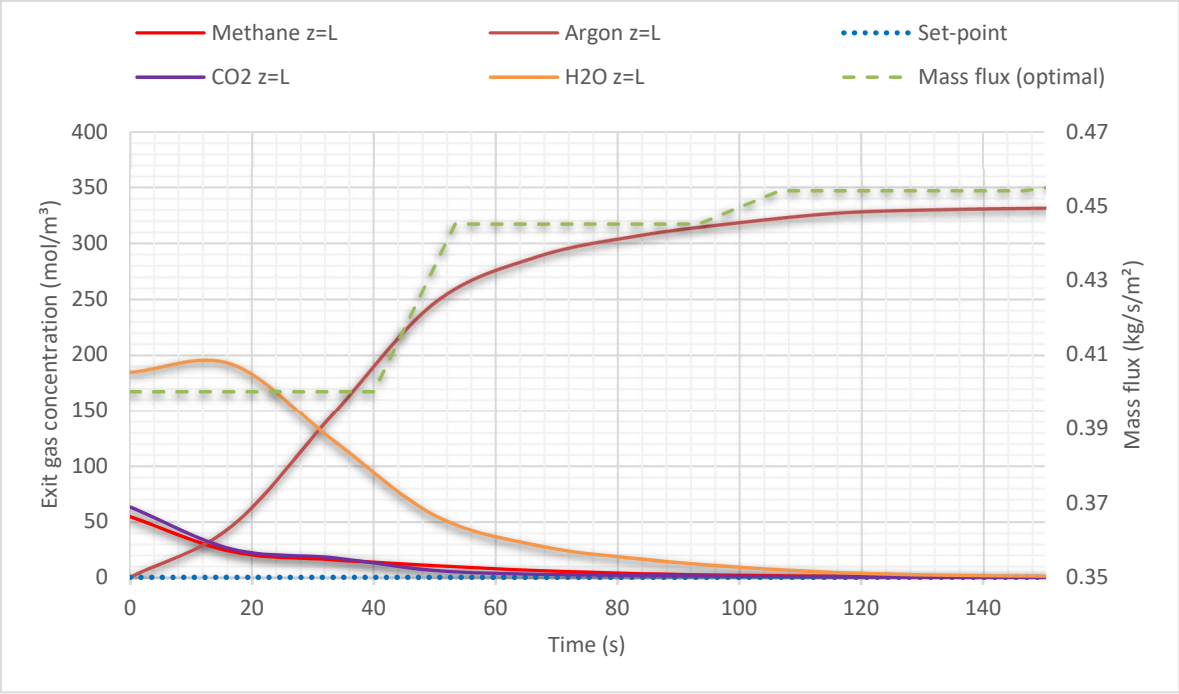

Figure 24. Optimal exit gas concentration and inlet argon mass flux time profiles for the purge after the reduction stage

The problem shown in equation 4.4 was solved using the same approach described above for the purge stage after oxidation but this time the difference between the set-point and the exit methane concentration of the reactor was the objective. The optimal control problem was solved using the direct transcription approach as in the previous optimization problems, resulting in 36,355 equations with 36,370 decision variables that correspond to each inlet mass flux at every k_j. Moreover, using the interior-point optimization algorithm the problem found a local optimal solution after 92 s of CPU time.

The purge after the reduction stage aims to remove the remaining unreacted gases that are still inside the packed bed, specifically methane. Therefore, the initial conditions of the purge optimal control problem are the final values of the state variables (e.g.

concentration and temperature) from when the reduction stage is completed. Figure 24 shows the resulting time profiles of the exit methane and argon concentrations when the methane slip is set at C_{MS}=0.0 mol/m³; additionally, the inlet argon mass flux transient profile is presented. As expected, the figure depicts how the exit methane concentration decreases rapidly (i.e. in a timeframe shorter than 100 s), due to mass transport convection and the consumption with the remaining unreacted OC particles. Likewise, the exit argon concentration reaches its maximum value at 150 s, indicating that the removal of all undesired gases has been completed. Moreover, the amount of argon specified by the optimal control strategy did not surpass the 1.3 kg/s/m² indicated by Spallina et al. [87]; hence, the resulting total amount of argon used for this work was 75.4 kg, which represents an amount 5 times smaller than the 9,195 kg required in Spallina's study.

This last section not only showed improvements in reduced amounts of inert gas used, but also shorter time durations for the purge stages. These changes would also translate into smaller heat losses due to convection and which would result in warmer packed bed temperatures for the reactions that were to follow. Having a higher temperature in the packed bed enhances both reactions (oxidation and reduction), as shown in the sensitivity analysis (Figure 12 and Figure 13); thus, improving the net process efficiency.

4.4 Dynamic optimization: optimistic and worst-case scenarios

The aim of this section is to present the results of optimal operation of the CLC PBR during optimistic and worst-case scenarios, which have been selected based on the results obtained from this study. The initial conditions, inlet temperatures, operating pressures, etc. were selected from previous works in the existing body of literature [8], [87], [89]; moreover, the sensitivity analysis presented in Chapter 3 showed the effect of varying these operating

conditions on the performance of the oxidation and reduction stages. In this section, the oxidation and reduction stages undergo assessment in a proposed optimistic scenario, where the operating conditions favour the performance of both stages. Likewise, a worst-case scenario is also presented in which the operating conditions diminish the performance of those stages. The key idea is to show that the use of dynamic optimization in both scenarios would enhance the performance of each stage, thus demonstrating that operational flexibility of a CLC PBR can be attained despite drastic changes in operational conditions.

The solution of these two new scenarios was executed using the direct transcription approach and centered difference discretization, as discussed in Section 3.5. Additionally, the NFE used for every domain and the number of equations, decision variables and manipulated variables remained the same as their equivalent in the Dynamic optimization section (4.3).

Table 9 shows the values selected for the optimistic scenario and the worst-case scenario.

Table 9 Optimistic and worst-case scenarios conditions

Oxidation			
	Base case	Optimistic	Worst-case
Operating pressure (bar)	20	15	25
Inlet temperature (°C)	450	522	377
Reduction			
Operating pressure (bar)	20	15	25
Inlet temperature (°C)	450	522	377

4.4.1 Optimistic scenario

The sensitivity analysis carried out in Section 3.7 was used to identify the parameters that play a significant role in the CLC PBR process. As previously discussed, the inlet gas temperature and the operating pressure were identified as parameters that affect the inlet stream mole concentration. By decreasing the operating pressure and increasing the inlet stream temperature, the inlet mole concentration diminishes, which would curb both reaction rates. Moreover, feeding inlet streams at higher temperatures would also mean a lesser temperature gradient within the packed bed; hence, delaying the cooling of the reactor, specifically during the oxidation stage.

This optimistic scenario is performed to show that optimal control strategies can result in larger energy production and lower fuel slip for the oxidation and reduction stages, respectively. Since larger temperatures are expected, an increase in the TIT set-point is performed. Based on the operational range of gas turbines presented in previous works [13], [82], [106], the TIT set-point value is set to 950°C for this scenario. Thus, the oxidation stage optimal control strategy for the optimistic scenario can be found from equation 4.1 using the data shown in

Table 9 and with $T_{\text{exit}} = 950$. The solution of this optimistic scenario converged after 530 s.

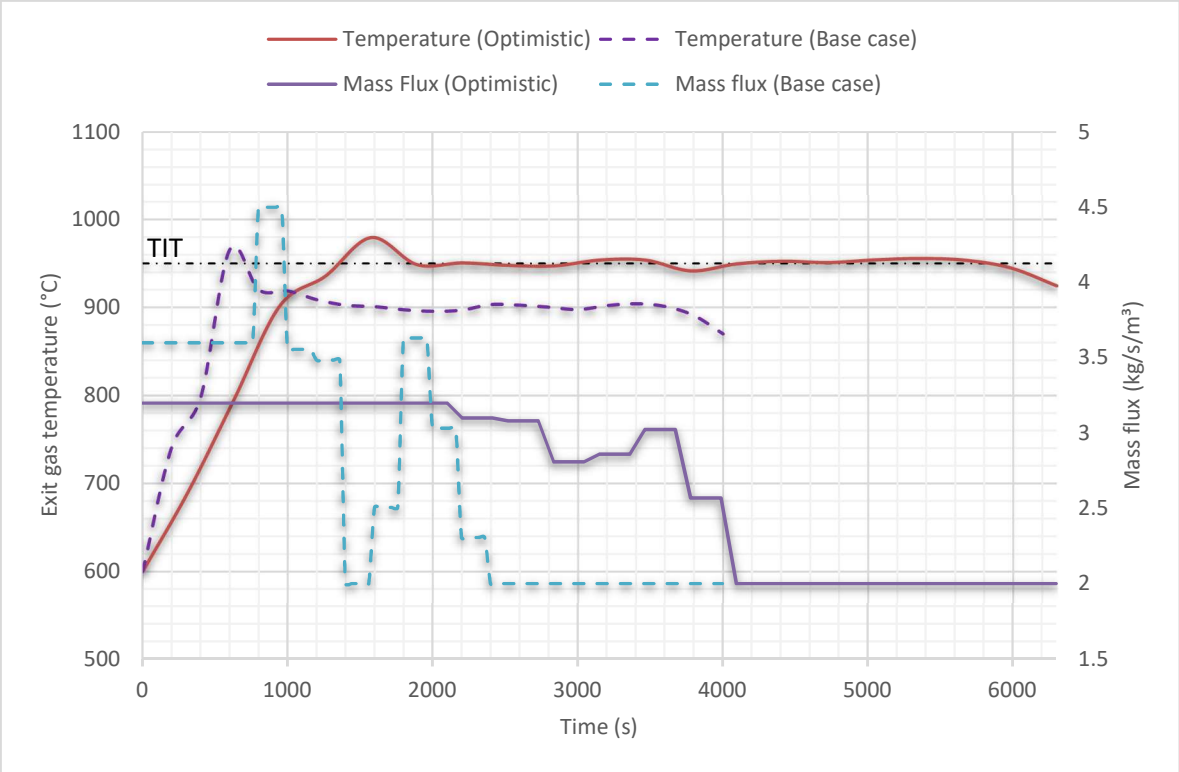

Figure 25. Optimistic case optimal exit gas temperature and mass flux time profiles during the oxidation stage

As shown in Figure 25, the exit gas temperature profiles for the base case optimization problem are compared against the equivalent for the optimistic case optimization problem; additionally, the mass flux profiles for both problems are presented. As shown in this figure, a longer heat recovery process is observed for the optimistic scenario; the exit gas temperature is maintained for an additional time of approximately 2,000 s. The time extension can be attributed to lower oxidation rate of the OC; caused by the changes in the inlet stream conditions affecting the inlet mol concentration being fed into the reactor. Likewise, the cooling of the PBR caused by convection with the gas phase is decreased due to a higher inlet stream temperature. Furthermore, when the OC is about to

reach its full oxidation and the mass flux has reached its lower bound, the exit gas temperature started to decrease. Additionally, the mass flux control profiles show differences; for instance, in the base case the mass flux moves from the lower to the upper bound, but in the optimistic case the mass flux is steadily lowered. Nevertheless, both profiles show a non-trivial solution. Regarding the energy produced, the base case optimization solution is able to generate 36.6 MW-h; whereas the optimistic case optimization generates 45.9 MW-h, which represents a 26% increase for the time span displayed.

The strategy of increasing the inlet temperature and reducing the operating pressure looks promising, however, it is also crucial to remain conscientious of the fact that there are limitations to how much these values can be adjusted. For instance, the inlet gas temperature depends on the preheating system that, at the same time, depends on the gas turbine performance. The same situation is observed with the operating pressure since this is also fundamental for the performance of the gas turbine. Caution when selecting the operating conditions and the inclusion of manufacturer data of the gas turbine are both recommended in order to better understand the entire system.

According to the sensitivity analysis, the exit methane concentration is expected to be lower in order to increase the fuel conversion and therefore the CO_2 sequestration during the optimistic scenario. Hence, the reduction stage optimistic optimal control strategy is formulated as per problem 4.2 with a C_{Fs}=5.0 mol/m³. The solution of this optimization problem converged after 2400 s.

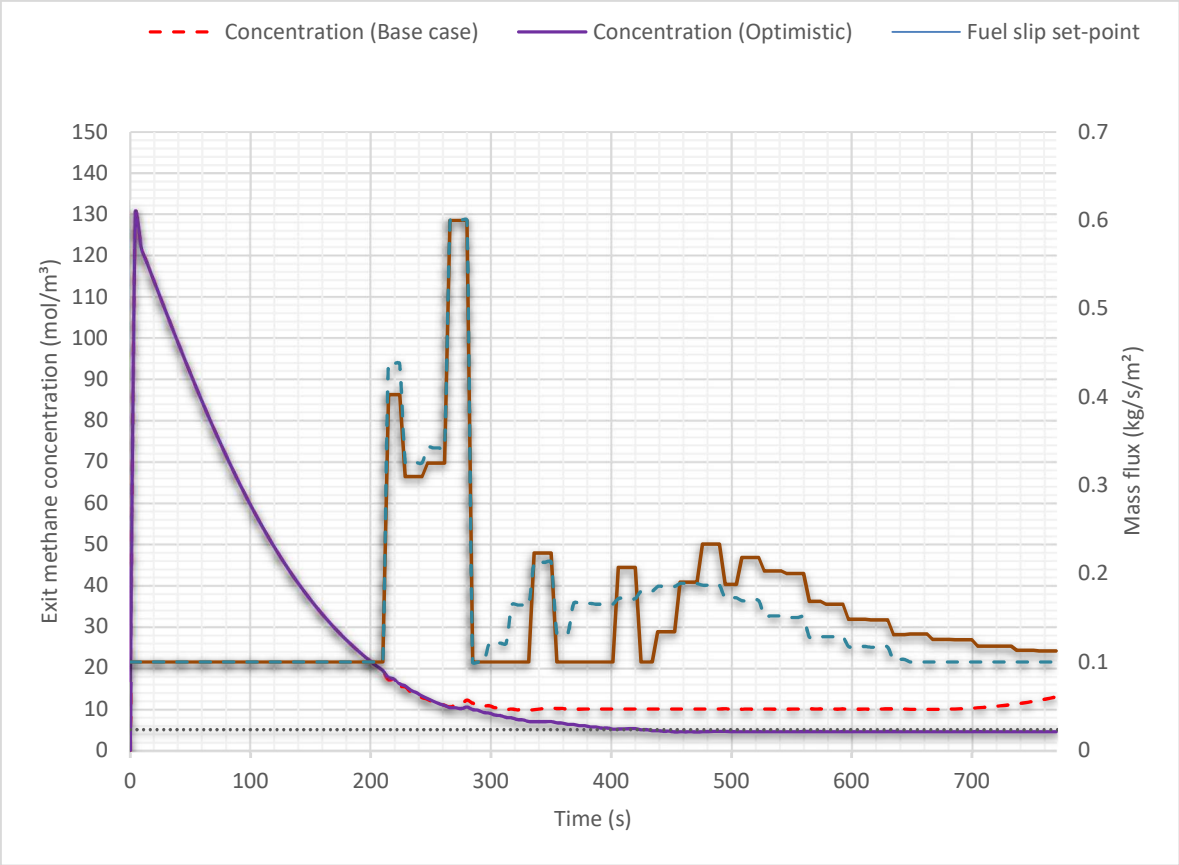

Figure 26. Optimistic case optimal exit methane concentration and inlet fuel mass flux time profiles during the reduction stage.

Figure 26 depicts a comparison between the exit methane concentration profiles in the base case optimization and the optimistic case optimization for the reduction stage. As shown in this figure, the methane exit concentration remains reasonably equal in both cases before reaching each set-point; therefore, the mass flux time profiles are almost the same during the same timespan. The major difference between the base case strategy and the optimistic case is the stage time duration. While the methane concentration in the base case trespasses the 10 mol/m³ barrier at approximately 720 s, the concentration in the optimistic scenario is kept on the set-point (5 mol/m³) for a longer period of time. This can be attributed

to the OC conversion, which in the base case strategy has reached almost full reduction, and to the control actions in the inlet methane mass flux, which cannot compensate for the low fuel intake by the OC after reaching its lower bound. Hence, the increment of unreacted methane exiting the PBR is more discernible towards the end of the reduction stage. This stage time extension difference would affect the time switching between stages, which might convolute the operation if more reactors would be operating in parallel. Nevertheless, as long as the total time of the reduction stage remains lower than the time of the oxidation stage time, no overlapping between stages is expected for a two CLC PBR parallel configuration during continuous operation of the gas turbine. Furthermore, the optimistic scenario shows a 98% fuel conversion compared to the 97% rate from the base case; effectively corroborating the suggestion that the proper operation of a CLC PBR will assist in curbing CO_2.

4.4.2 Worst-case scenario

As discussed in the previous section, the sensitivity analysis guided us to identify operating conditions that would thwart the oxidation and reduction stages. Thus, the present scenario aims to detect optimal operating strategies under extreme (worst-case) operating conditions for the CLC PBR. The purpose of choosing this scenario is to show that by performing an optimal control, a fair energy production and low fuel slip could still be obtained for the CLC PBR. For this worst-case scenario, the inlet gas temperature and the operating pressure were changed to produce a lower heat recovery and a higher fuel slip during the oxidation and reduction stage, respectively. Hence, the inlet mole concentration would be raised by simultaneously increasing the operating pressure and decreasing the inlet stream temperature. This would produce that the reaction rates in the oxidation and

reduction stages are enhanced. Similarly, a large temperature gradient between the inlet gas stream and the packed bed is expected to increase the cooling of the reactor due to convection.

Table 9 shows the operating conditions selected for the worst-case scenario.

Since lower temperatures are expected during oxidation, the TIT set-point value is set to 850°C, which still is an acceptable operating condition for this process [82]. The oxidation optimal control strategy can be obtained by solving problem 4.1 with $T_{\text{exit}} = 850$ and the operating conditions specified in

Table 9. The solution of this new optimization problem converged after 500 s.

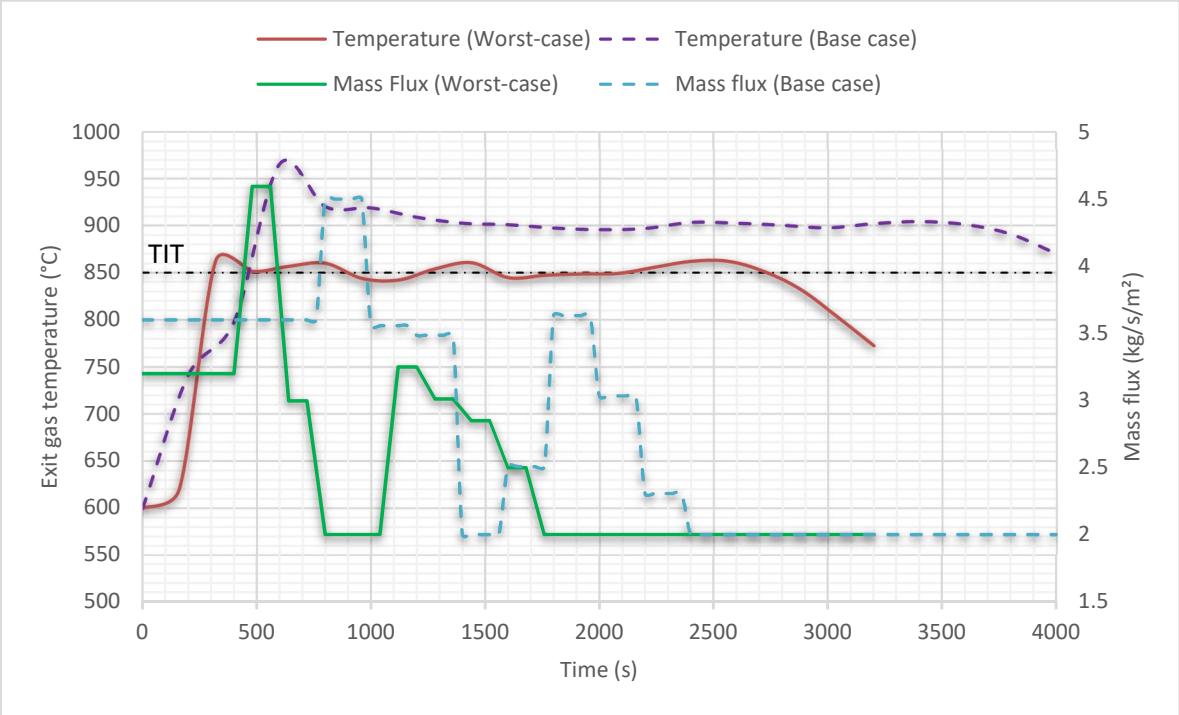

Figure 27. Worst-case optimal exit gas temperature and mass flux time profiles during the oxidation stage

Figure 27 shows a qualitative comparison between the exit gas temperature profiles for base case optimization against the worst-case scenario. During the worst-case scenario the set-point of 850 °C is reached faster than in the base case, as expected; likewise, the set-point can only be maintained for 2,400 s, which is 1,200 s less than in the base case scenario. The latter can be explained by the changes in the operating conditions that resulted in an increment in inlet moles to the reactor; hence, increasing the OC conversion rate reduces the duration of the oxidation stage. Moreover, the inlet mass flux profile in both scenarios show similar trends, i.e. a peak in the inlet mass flux is observed after the set-point is reached; afterwards, a staggered decrement in the manipulated variable is observed. The energy production for the present scenario is 26.9 MW-h, which is a 27% reduction compared to the base case scenario. Despite the lower energy production from this scenario, the control of the exit gas temperature was maintained for a reasonable period of operation, thus safe operation of the downstream turbine is guaranteed.

The increase in operating pressure and decrease on the inlet methane temperature would translate into more moles per second across the reactor, which would promote a higher fuel slip. Notwithstanding, a set-point of 8 mol/m³, which is 20% lower than the one in the base case, was defined at the reactor's outlet in order to maintain a high fuel conversion and CO_2 recovery efficiency. Thus, the reduction stage optimal control strategy for the worst-case scenario can be obtained by solving problem 4.2 with C_{Fs}=8.0 and the operating conditions listed in

Table 9. This optimization problem converged after 2,850 s.

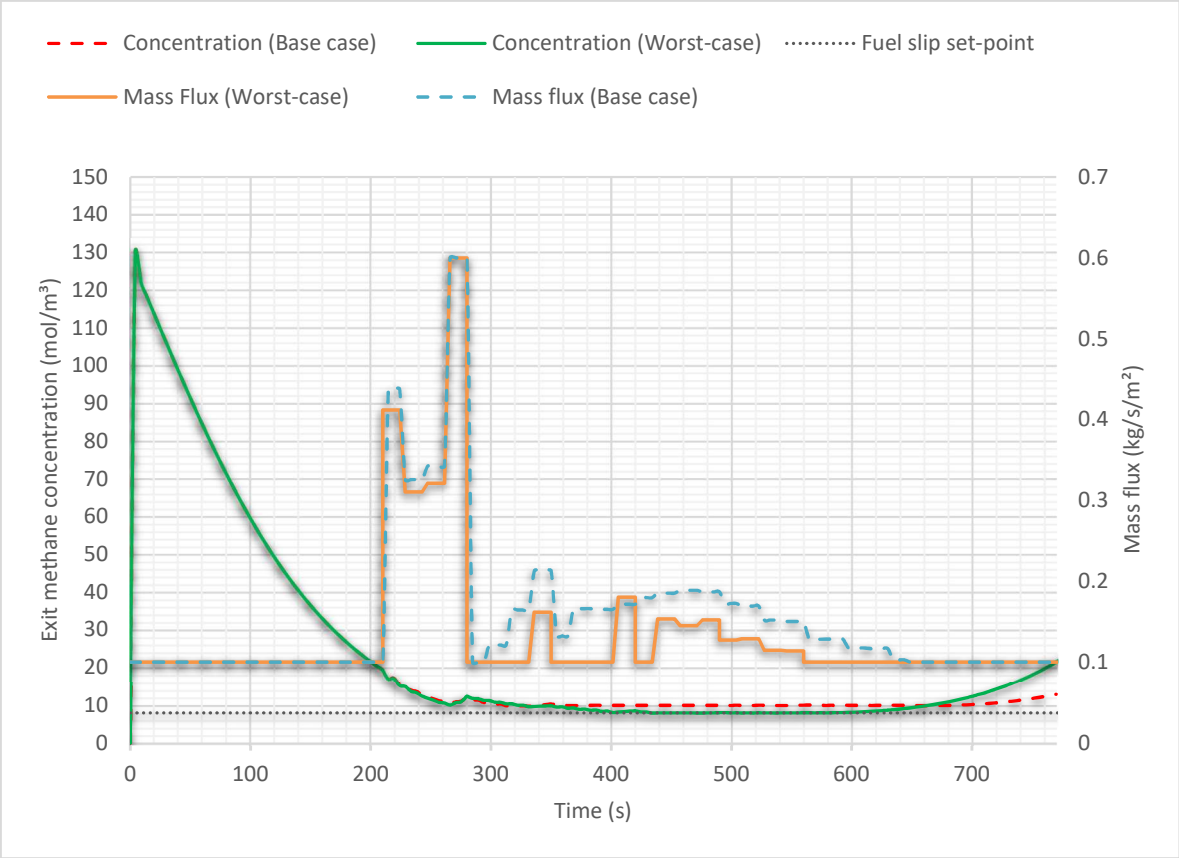

Figure 28. Worst-case optimal exit methane concentration and inlet fuel mass flux time profiles during the reduction stage

In Figure 28, a comparison of the exit methane concentration for the base case and the worst-case scenarios is presented. The results show that the fuel slip set-point is trespassed 80 s earlier in the worst-case scenario than in the base case; the earlier fuel slip can be attributed to an almost full OC conversion as the inlet mass flux controller cannot compensate the low methane intake by the OC. Moreover, in both scenarios the non-trivial control profiles show very similar trends regarding the mass flux value; additionally, during the worst-case scenario the manipulated variable reached its lower bound sooner than in the base case scenario, which is an expected behaviour since the reaction rate is enhanced

by the new operating conditions. Note that methane conversion in the worst-case remains at 98% during the timeframe at the methane concentration was at the requested set-point (not shown for brevity).

Based on the above, the results obtained for both scenarios confirmed that the heat recovery process as well as a low fuel slip can still be achieved in both the oxidation and reduction stages, respectively. The implementation of optimal control strategies to solve these two scenarios allowed the system to reach the desirable set-points which would entail a continuous energy production in the downstream turbine and a high fuel conversion, which enhances the CO_2 recovery system.

In summary, this chapter presented the advantages of performing manual step changes instead of keeping a constant inlet mass flux in the stages of the CLC PBR process. The results showed an improvement in heat recovery and a lower fuel slip during the oxidation and reduction stages, respectively. Moreover, the oxidation and reduction stages were studied using dynamic optimization; where set-points were defined for each stage. The results from the dynamic optimization showed better heat recovery in the oxidation and higher fuel conversion in the reduction; additionally, smooth control of the state variables was observed and the timespan of each reaction stage was increased. Furthermore, two new scenarios were presented based on the sensitivity analysis performed in Chapter 3, i.e. an optimistic and worst-case scenario. The optimal control strategies obtained from those scenarios showed significant improvements in fuel conversion and energy production; but most importantly, it demonstrated that flexibility in the operation of the CLC PBR can be achieved using online optimal control.

Chapter 5
Conclusions and recommendations

5.1 Conclusions

The goal of this thesis was to contribute to the current literature on chemical-looping combustion in a packed bed reactor intended for carbon capture and sequestration. Specifically, the scope of this thesis included the study of transient operation of each one of the CLC stages through the use of a 1-dimensional mechanistic heterogeneous dynamic model.

The adapted dynamic mechanistic model was presented. It described the mass and energy balances of the OC particles and the reactor. A base case from the literature was selected and was subsequently subjected to a sensitivity analysis in order to demonstrate the effect of certain parameters such as: inlet mass flux, operating pressure and reactor length, during the oxidation and reduction stages in the process. The main results of the sensitivity study are as follows:

- Both lower inlet mass fluxes and operating pressures, as well as, higher inlet air temperatures and larger reactor lengths, were all proven to be part of an increase in exit gas temperatures and the duration of the oxidation stage.
- Similarly, the combination of lower inlet mass fluxes and operating pressures, as well as, higher inlet fuel temperatures and larger reactor lengths, were identified as a strategy to reduce the amount of fuel slip at the reactor's exit during the reduction stage.

The sensitivity analysis demonstrated that the inlet mass fluxes are variables that can be manipulated and therefore, they were used in this study to perform manual step changes while controlling state variables, such as temperature and concentration. In this regard, the present study effectively showed that inlet mass fluxes are feasible control variables in the CLC process. By benchmarking against the base case, the online manual-changes were aimed towards improving the energy production and the fuel conversion of the oxidation and reduction stages, respectively. The main results of this open-loop manual control study are as follows:

- The energy produced during the oxidation stage was increased by extending the duration of the heat recovery process when step-changes in the inlet air mass flux were performed.
- The fuel slip was substantially diminished during the reduction stage when step-changes in the inlet methane mass flux were performed.

Similarly, dynamic optimization was implemented to solve each one of the stages in the CLC sequence of the base case problem while using the same manipulated variables to meet the same objectives as before. Contrasting the results obtained from this study against the base case operation, the main conclusions resulting from the dynamic optimization are as follows:

- During the oxidation stage, an ample improvement in energy production and stage duration was attained when a set-point of 900 °C was maintained in the exit gas temperature while manipulating the inlet air mass flux.

- During the reduction stage, a substantial increment in fuel conversion was accomplished when a methane concentration set-point of 10 mol/m³ at the reactor's exit was maintained while manipulating the inlet methane mass flux.
- The time duration and total amount of argon used during the purges was reduced considerably when a set-point of 0 mol/m³ of undesired concentrations in the reactor were defined while manipulating the inlet argon mass flux.
- The implementation of dynamic optimization for the control of a CLC PBR is an attractive alternative in order to achieve an energy and fuel-efficient CCS process.

Similarly, dynamic optimization was implemented on an optimistic and a worst-case scenario for the oxidation and reduction stages, in order to confirm that flexibility in the CLC PBR operation is attainable. Comparing the results of this study against their equivalent from dynamic optimization of the base case, the following conclusions can be drawn:

- The optimistic scenario showed further improvements in energy produced during the oxidation stage and fuel conversion during the reduction stage
- The worst-case scenario showed a reasonable decrease in energy production during oxidation while maintaining a near full methane conversion into CO_2 and H_2O during the reduction stage

Thus, this thesis demonstrates that flexibility in the CLC PBR can be attained while keeping an adequate heat recovery process and a high fuel conversion during the oxidation and reduction stages, respectively. Moreover, these results bolster the importance of the CLC process as an attractive CCS technology that would reduce the energy penalty normally entailed in CO_2 sequestration.

5.2 Recommendations

The research presented in this thesis can be extended to further the development and implementation of CO_2 capture and sequestration technologies. The recommendations to be followed in future works are as follows:

- In the present work, the dynamic simulation and optimization of every single stage in the CLC PBR sequence was performed individually. Implementing the same mechanistic model to perform the simulation and optimization of the complete integrated sequence will produce a more complete insight into the CLC operation, specifically, in determining the optimal switching time points between the stages of the PBR.
- A single large-scale packed bed reactor was considered in this study. Incorporating more PBRs working in parallel will help to comprehend the best heat management strategy required by a large-scale power plant. This will guarantee a constant and safe operation of the downstream turbine. Moreover, finding the optimal solution for this problem would simultaneously entail the solution of a large number of partial differential equations.
- The full integration of an integrated gasification combined cycle with CLC will provide more knowledge of the operating conditions surrounding the CLC PBR's and how they impact their operation. The integration will have to address manufacturer data for the compressor and turbines, as well as the heat recovery system generator (HRSG). Moreover, the CO_2-H_2O

separation phase at the end of the process sequence will have to be included for a more complete process.

- The present study detected that the oxidation and reduction kinetic values in a CLC process depend greatly on the conditions under which they were tested and therefore obtained; moreover, the kinetic data varies from one study to another. Therefore, implementing dynamic optimization while considering uncertainty in these parameters will provide a more realistic operating scenario for both reaction processes.

.

Bibliography

[1] D. Archer, “Fate of fossil fuel CO2 in geologic time,” J Geophys Res 2005; vol. 110, no. March, pp. 1–6, 2005.

[2] L. Riboldi and O. Bolland, “Overview on Pressure Swing Adsorption (PSA) as CO2Capture Technology: State-of-the-Art, Limits and Potentials,” *Energy Procedia*, vol. 114, no. 1876, pp. 2390–2400, 2017.

[3] J. Adanez, A. Abad, F. Garcia-labiano, P. Gayan, and L. F. De Diego, “Progress in Chemical-Looping Combustion and Reforming technologies,” vol. 38, 2012.

[4] http://www.iea.org/etp/publications/etp2012/, “International Energy Agency: Energy Technology Perspectives ,2012,” 2012.

[5] IPPC, *IPCC Special Report on Carbon Dioxide Capture and Storage. Cambridge University Press*. 2005.

[6] Y. Yuan, H. You, and L. Ricardez-Sandoval, “Recent advances on first-principles modeling for the design of materials in CO 2 capture technologies,” *Chinese Journal of Chemical Engineering*. 2019.

[7] D. C. Thomas, “Carbon Dioxide Capture for Storage in Deep Geologic Formations – Results from the CO2 Capture Project,” *Contract*, vol. 1, p. 660, 2005.

[8] S. Noorman, M. V. S. Annaland, and H. Kuipers, “Packed Bed Reactor Technology for Chemical-Looping Combustion,” pp. 4212–4220, 2007.

[9] S. Noorman, F. Gallucci, M. V. S. Annaland, and J. A. M. Kuipers, “A theoretical investigation of CLC in packed beds . Part 1 : Particle model,” vol. 167, pp. 297–307, 2011.

[10] S. Noorman, F. Gallucci, M. V. S. Annaland, and J. A. M. Kuipers, “A theoretical investigation of CLC in packed beds . Part 2 : Reactor model,” vol. 167, pp. 369–376, 2011.

[11] L. Han, Z. Zhou, and G. M. Bollas, “Heterogeneous modeling of chemical-looping combustion . Part 1 : Reactor model,” vol. 104, pp. 233–249, 2013.

[12] L. Han, Z. Zhou, and G. M. Bollas, “Heterogeneous modeling of chemical-looping combustion . Part 2 : Particle model,” *Chem. Eng. Sci.*, vol. 113, pp. 116–128, 2014.

[13] L. Han and G. M. Bollas, “Dynamic optimization of fi xed bed chemical-looping combustion processes,” *Energy*, vol. 112, pp. 1107–1119, 2016.

[14] L. Han, “Dynamic Simulation , Optimization , and Control of Flexible Chemical-Looping Combustion Processes,” 2016.

[15] International Energy Agency, “World Energy Outlook 2018 Summary,” 2018.

[16] D. Figueroa, T. Fout, S. Plasynski, H. Mcilvried, and R. D. Srivastava, “Advances in CO 2 capture technology — The U . S . Department of Energy ’ s Carbon Sequestration Program §,” vol. 2, pp. 9–20, 2008.

[17] E. J. A. M.E. Boot-Handford, J.C. Abanades, “Carbon capture and storage update,” pp. 130–189, 2014.

[18] T. Nittaya, P. L. Douglas, E. Croiset, and L. A. Ricardez-Sandoval, “Dynamic modelling and control of MEA absorption processes for CO 2 capture from power plants,” *Fuel*, vol. 116, pp. 672–691, 2014.

[19] T. Nittaya, P. L. Douglas, E. Croiset, and L. A. Ricardez-Sandoval, “Dynamic modeling and evaluation of an industrial-scale CO2 capture plant using monoethanolamine absorption processes,” *Ind. Eng. Chem. Res.*, vol. 53, no. 28, pp. 11411–11426, 2014.

[20] D. Jansen, M. Gazzani, G. Manzolini, and E. Van Dijk, “Pre-combustion CO2 capture,” *Int. J. Greenh. Gas Control*, vol. 40, pp. 167–187, 2015.

[21] F. Casella and P. Colonna, “Dynamic modeling of IGCC power plants,” *Appl. Therm. Eng.*, vol. 35, no. 1, pp. 91–111, 2012.

[22] M. Hossein Sahraei, D. McCalden, R. Hughes, and L. A. Ricardez-Sandoval, “A survey on current advanced IGCC power plant technologies, sensors and control systems,” *Fuel*, vol. 137. pp. 245–259, 2014.

[23] Z. He and L. A. Ricardez-Sandoval, “Dynamic modelling of a commercial-scale CO2 capture plant integrated with a natural gas combined cycle (NGCC) power plant,” *Int. J. Greenh. Gas Control*, vol. 55, pp. 23–35, 2016.

[24] M. Bee, “High efficiency electric power generation : The environmental role,” vol. 33, pp. 107–134, 2007.

[25] E. R. Lewis, W.K., Gilliland, “PRODUCTION OF PURE CARBON DIOXIDE,” 1954.

[26] H. J. RICHTER and K. F. KNOCHE, “Reversibility of Combustion Processes,” 1983, pp. 71–85.

[27] M. Ishida, D. Zheng, and T. Akehata, “Evaluation of a chemical-looping-combustion power-generation system by graphic exergy analysis,” *Energy*, vol. 12, no. 2, pp. 147–154, 1987.

[28] M. Ishida and H. Jin, “A new advanced power-generation system using chemical-looping combustion,” *Energy*, vol. 19, no. 4, pp. 415–422, 1994.

[29] M. Ishida and H. Jin, “A Novel Combustor Based on Chemical-Looping Reactions and Its Reaction Kinetics,” *J. Chem. Eng. Japan*, vol. 27, no. 3, pp. 296–301, 1994.

[30] A. Lyngfelt, B. Kronberger, J. Adanez, J. X. Morin, and P. Hurst, “The grace project: Development of oxygen carrier particles for chemical-looping combustion. Design and operation of a 10 kW chemical-looping combustor,” in *Greenhouse Gas Control Technologies*, 2005, pp. 115–123.

[31] J. Adánez, F. García-Labiano, L. F. de Diego, P. Gayán, A. Abad, and J. Celaya, “Development of Oxygen Carriers for Chemical-Looping Combustion,” in *Carbon Dioxide Capture for Storage in Deep Geologic Formations*, 2005, pp. 587–604.

[32] A. Lyngfelt and H. Thunman, “Construction and 100 h of Operational Experience of A 10-kW Chemical-Looping Combustor,” in *Carbon Dioxide Capture for Storage in Deep Geologic Formations*, 2005, pp. 625–645.

[33] T. Mattisson, F. García-Labiano, B. Kronberger, A. Lyngfelt, J. Adánez, and H. Hofbauer, “Chemical-looping combustion using syngas as fuel,” *Int. J. Greenh. Gas Control*, vol. 1, no. 2, pp. 158–169, 2007.

[34] H. J. Ryu, G. T. Jin, and C. K. Yi, “Demonstration of inherent CO2 separation and no NOx emission in a 50kW chemical-looping combustor: Continuous reduction and oxidation experiment,” in *Greenhouse Gas Control Technologies*, 2005, pp. 1907–1910.

[35] Juan Adánez, P. Gayán, Javier Celaya, Luis F. de Diego, A. Francisco García-Labiano, and A. Abad, “Chemical Looping Combustion in a 10 kWth Prototype Using a CuO/Al2O3 Oxygen Carrier: Effect of Operating Conditions on Methane Combustion,” 2006.

[36] L. F. De Diego, F. Garcı, M. Palacios, and J. Ada, “Operation of a 10 kWth chemical-looping combustor during 200 h with a CuO – Al 2 O 3 oxygen carrier,” vol. 86, pp. 1036–1045, 2007.

[37] C. Linderholm, A. Abad, T. Mattisson, and A. Lyngfelt, “160 h of chemical-looping combustion in a 10 kW reactor system with a NiO-based oxygen carrier,” *Int. J. Greenh. Gas Control*, vol. 2, no. 4, pp. 520–530, 2008.

[38] S. Rifflart, A. Hoteit, M. M. Yazdanpanah, W. Pelletant, and K. Surla, “Construction and operation of a 10kW CLC unit with circulation configuration enabling independent solid flow control,” in *Energy Procedia*, 2011, vol. 4, pp. 333–340.

[39] S. Wang, G. Wang, F. Jiang, M. Luo, and H. Li, “Chemical looping combustion of coke oven gas by using Fe<inf>2</inf>O<inf>3</inf>/CuO with MgAl<inf>2</inf>O<inf>4</inf>as oxygen carrier,” *Energy Environ. Sci.*, vol. 3, no. 9, 2010.

[40] L. Shen, J. Wu, J. Xiao, Q. Song, and R. Xiao, “Chemical-looping combustion of biomass in a 10 kWth reactor with iron oxide as an oxygen carrier,” *Energy and Fuels*, vol. 23, no. 5, pp. 2498–2505, 2009.

[41] L. Shen, J. Wu, Z. Gao, and J. Xiao, “Reactivity deterioration of NiO/Al2O3 oxygen carrier for chemical looping combustion of coal in a 10 kWth reactor,” *Combust. Flame*, vol. 156, no. 7, pp. 1377–1385, 2009.

[42] L. S. Fan, *Chemical Looping Systems for Fossil Energy Conversions*. 2010.

[43] P. Kolbitsch, J. Bolhàr-Nordenkampf, T. Pröll, and H. Hofbauer, “Operating experience with chemical looping combustion in a 120 kW dual circulating fluidized bed (DCFB) unit,” *Int. J. Greenh. Gas Control*, vol. 4, no. 2, pp. 180–185, 2010.

[44] J. Bolhàr-Nordenkampf, T. Pröll, P. Kolbitsch, and H. Hofbauer, “Performance of a NiO-based oxygen carrier for chemical looping combustion and reforming in a 120

kW unit," in *Energy Procedia*, 2009, vol. 1, no. 1, pp. 19–25.

[45] P. Ohlemüller, J. Ströhle, and B. Epple, "Chemical looping combustion of hard coal and torrefied biomass in a 1 MWth pilot plant," *Int. J. Greenh. Gas Control*, vol. 65, pp. 149–159, 2017.

[46] F. Alobaid, P. Ohlemüller, J. Ströhle, and B. Epple, "Extended Euler–Euler model for the simulation of a 1 MWth chemical–looping pilot plant," *Energy*, vol. 93, pp. 2395–2405, 2015.

[47] H. E. Andrus, J. H. Chiu, P. R. Thibeault, and A. Brautsch, "Alstom ' s Calcium Oxide Chemical Looping Combustion Coal Power Technology Development," 2009.

[48] H. E. Andrus Jr., J. H. Chiu, P. R. Thibeault, and C. Miller, "ALSTOM's chemical looping combustion coal power technology development prototype.," *Proc. - Annu. Int. Pittsburgh Coal Conf.*, vol. 26th, p. a29/1-a29/14, 2009.

[49] H. You, Y. Yuan, J. Li, and L. R. Sandoval, "A Multi-scale model for CO2 capture: A Nickel-based oxygen carrier in Chemical-looping Combustion," *IFAC-PapersOnLine*, vol. 51, no. 18, pp. 97–102, 2018.

[50] S. C. Bayham *et al.*, "Iron-Based Coal Direct Chemical Looping Combustion Process: 200-h Continuous Operation of a 25-kW $_{th}$ Subpilot Unit," *Energy & Fuels*, vol. 27, no. 3, pp. 1347–1356, Mar. 2013.

[51] P. Markström, C. Linderholm, and A. Lyngfelt, "Chemical-looping combustion of solid fuels – Design and operation of a 100 kW unit with bituminous coal," *Int. J. Greenh. Gas Control*, vol. 15, pp. 150–162, Jul. 2013.

[52] M. Rydén, D. Jing, M. Källén, H. Leion, A. Lyngfelt, and T. Mattisson, "CuO-Based Oxygen-Carrier Particles for Chemical-Looping with Oxygen Uncoupling – Experiments in Batch Reactor and in Continuous Operation," *Ind. Eng. Chem. Res.*, vol. 53, no. 15, pp. 6255–6267, Apr. 2014.

[53] T. Berdugo Vilches, F. Lind, M. Rydén, and H. Thunman, "Experience of more than 1000 h of operation with oxygen carriers and solid biomass at large scale," *Appl. Energy*, vol. 190, pp. 1174–1183, Mar. 2017.

[54] P. Hallberg, M. Hanning, M. Rydén, T. Mattisson, and A. Lyngfelt, "Investigation of a

calcium manganite as oxygen carrier during 99 h of operation of chemical-looping combustion in a 10 kWth reactor unit," *Int. J. Greenh. Gas Control*, vol. 53, pp. 222–229, Oct. 2016.

[55] A. Nandy, C. Loha, S. Gu, P. Sarkar, M. K. Karmakar, and P. K. Chatterjee, "Present status and overview of Chemical Looping Combustion technology," *Renew. Sustain. Energy Rev.*, vol. 59, pp. 597–619, 2016.

[56] J. Adanez, A. Abad, F. Garcia-labiano, P. Gayan, and L. F. De Diego, "Progress in Chemical-Looping Combustion and Reforming technologies," vol. 38, 2012.

[57] B. Leckner, T. Mattisson, and A. Lyngfelt, "A fluidized-bed combustion process with inherent CO2 separation; application of chemical-looping combustion," *Chemical Engineering Science*, vol. 56, no. 10. pp. 3101–3113, 2001.

[58] Z. Zhou, L. Han, and G. M. Bollas, "Model-based analysis of bench-scale fixed-bed units for chemical-looping combustion," *Chem. Eng. J.*, vol. 233, pp. 331–348, 2013.

[59] L. F. De Diego, J. Ada, A. Abad, P. Gaya, and M. L. Casta, "Reduction and Oxidation Kinetics of a Copper-Based Oxygen Carrier Prepared by Impregnation for Chemical-Looping Combustion," no. 2, pp. 8168–8177, 2004.

[60] J. Adánez, F. García-Labiano, L. F. De Diego, P. Gayán, J. Celaya, and A. Abad, "Nickel-copper oxygen carriers to reach zero CO and H2emissions in chemical-looping combustion," in *Industrial and Engineering Chemistry Research*, 2006, vol. 45, no. 8, pp. 2617–2625.

[61] J. Adánez, L. F. De Diego, F. García-Labiano, P. Gayán, A. Abad, and J. M. Palacios, "Selection of oxygen carriers for chemical-looping combustion," *Energy and Fuels*, vol. 18, no. 2, pp. 371–377, 2004.

[62] C. Dueso *et al.*, "Reduction and oxidation kinetics of nickel-based oxygen-carriers for chemical-looping combustion and chemical-looping reforming," vol. 188, no. x, pp. 142–154, 2012.

[63] J. Adánez, C. Dueso, L. F. De Diego, F. García-Labiano, P. Gayán, and A. Abad, "Effect of fuel gas composition in chemical-looping combustion with Ni-based oxygen carriers. 2. Fate of light hydrocarbons," *Ind. Eng. Chem. Res.*, vol. 48, no. 5, pp. 2509–

2518, 2009.

[64] M. Ishida and H. Jin, “A novel chemical-looping combustor without NOx formation,” *Ind. Eng. Chem. Res.*, vol. 35, no. 7, pp. 2469–2472, 1996.

[65] A. Abad, T. Mattisson, A. Lyngfelt, and M. Rydén, “Chemical-looping combustion in a 300 W continuously operating reactor system using a manganese-based oxygen carrier,” *Fuel*, vol. 85, no. 9, pp. 1174–1185, 2006.

[66] Y. Matsumura and T. Nakamori, “Steam reforming of methane over nickel catalysts at low reaction temperature,” *Appl. Catal. A Gen.*, vol. 258, no. 1, pp. 107–114, 2004.

[67] H. J. Ryu, N. Y. Lim, D. H. Bae, and G. T. Jin, “Carbon deposition characteristics and regenerative ability of oxygen carrier particles for chemical-looping combustion,” *Korean J. Chem. Eng.*, vol. 20, no. 1, pp. 157–162, 2003.

[68] R. Villa *et al.*, “Ni based mixed oxide materials for CH4 oxidation under redox cycle conditions,” *J. Mol. Catal. A Chem.*, vol. 204–205, pp. 637–646, 2003.

[69] E. Jerndal, T. Mattisson, I. Thijs, F. Snijkers, and A. Lyngfelt, “Investigation of NiO/NiAl2O4 oxygen carriers for chemical-looping combustion produced by spray-drying,” *Int. J. Greenh. Gas Control*, vol. 4, no. 1, pp. 23–35, 2010.

[70] P. Gayán, C. Dueso, A. Abad, J. Adanez, L. F. de Diego, and F. García-Labiano, “NiO/Al2O3 oxygen carriers for chemical-looping combustion prepared by impregnation and deposition-precipitation methods,” *Fuel*, vol. 88, no. 6, pp. 1016–1023, 2009.

[71] M. Ishida, H. Jin, and T. Okamoto, “A fundamental study of a new kind of medium material for chemical-looping combustion,” *Energy and Fuels*, vol. 10, no. 4, pp. 958–963, 1996.

[72] S. R. Son and S. D. Kim, “Chemical-looping combustion with NiO and Fe2O3 in a thermobalance and circulating fluidized bed reactor with double loops,” in *Industrial and Engineering Chemistry Research*, 2006, vol. 45, no. 8, pp. 2689–2696.

[73] P. Cho, T. Mattisson, and A. Lyngfelt, “Comparison of iron-, nickel-, copper- and manganese-based oxygen carriers for chemical-looping combustion,” *Fuel*, vol. 83, no. 9, pp. 1215–1225, 2004.

[74] T. Mattisson, A. Järdnäs, and A. Lyngfelt, “Reactivity of some metal oxides supported on alumina with alternating methane and oxygen - Application for chemical-looping combustion,” *Energy and Fuels*, vol. 17, no. 3, pp. 643–651, 2003.

[75] S. Y. Chuang, J. S. Dennis, A. N. Hayhurst, and S. A. Scott, “Development and performance of Cu-based oxygen carriers for chemical-looping combustion,” *Combust. Flame*, vol. 154, no. 1–2, pp. 109–121, 2008.

[76] S. Y. Chuang, J. S. Dennis, A. N. Hayhurst, and S. A. Scott, “Kinetics of the oxidation of a co-precipitated mixture of cu and Al 2O3 by O2 for chemical-looping combustion,” *Energy and Fuels*, vol. 24, no. 7, pp. 3917–3927, 2010.

[77] A. Abad, J. Adánez, F. García-Labiano, L. F. de Diego, P. Gayán, and J. Celaya, “Mapping of the range of operational conditions for Cu-, Fe-, and Ni-based oxygen carriers in chemical-looping combustion,” *Chem. Eng. Sci.*, vol. 62, no. 1–2, pp. 533–549, 2007.

[78] P. Cho, T. Mattisson, and A. Lyngfelt, “Carbon formation on nickel and iron oxide-containing oxygen carriers for chemical-looping combustion,” *Ind. Eng. Chem. Res.*, vol. 44, no. 4, pp. 668–676, 2005.

[79] A. Abad, F. García-Labiano, L. F. de Diego, P. Gayán, and J. Adánez, “Reduction kinetics of Cu-, Ni-, and Fe-based oxygen carriers using syngas (CO + H2) for chemical-looping combustion,” *Energy and Fuels*, vol. 21, no. 4, pp. 1843–1853, 2007.

[80] S. F. Håkonsen and R. Blom, “Chemical looping combustion in a rotating bed reactor - Finding optimal process conditions for prototype reactor,” *Environ. Sci. Technol.*, vol. 45, no. 22, pp. 9619–9626, 2011.

[81] S. F. Håkonsen, C. A. Grande, and R. Blom, “Rotating bed reactor for CLC: Bed characteristics dependencies on internal gas mixing,” *Appl. Energy*, vol. 113, pp. 1952–1957, 2014.

[82] F. J. Brooks, “GE Gas Turbine Performance Characteristics,” *GE Power Syst.*, pp. 1–16, 2006.

[83] J. I. Baek *et al.*, “Highly attrition resistant oxygen carrier for chemical looping

combustion," in *Energy Procedia*, 2011, vol. 4, pp. 349–355.

[84] A. Thon, M. Kramp, E.-U. Hartge, J. Werther, and S. Heinrich, "The Role of Attrition and Solids Recovery in a Chemical Looping Combustion Process," *Oil Gas Sci. Technol. – Rev. d'IFP Energies Nouv.*, vol. 66, no. 2, pp. 277–290, 2011.

[85] O. Brandvoll and O. Bolland, "Inherent CO[sub 2] Capture Using Chemical Looping Combustion in a Natural Gas Fired Power Cycle," *J. Eng. Gas Turbines Power*, vol. 126, no. 2, p. 316, 2004.

[86] J. Wolf, M. Anheden, and J. Yan, "Performance analysis of combined cycles with chemical looping combustion for CO2 capture," in *Prof. 18th Annual Int Pittsburg Coal Conf. Newcastle, New South Wales, Australia*, 2001, pp. 1122–1139.

[87] V. Spallina *et al.*, "Reactor design and operation strategies for a large-scale packed-bed CLC power plant with coal syngas," *Int. J. Greenh. Gas Control*, vol. 36, pp. 34–50, 2015.

[88] S. Noorman, M. van Sint Annaland, and J. A. M. Kuipers, "Experimental validation of packed bed chemical-looping combustion," *Chem. Eng. Sci.*, vol. 65, no. 1, pp. 92–97, 2010.

[89] V. Spallina, F. Gallucci, M. C. Romano, P. Chiesa, G. Lozza, and M. V. S. Annaland, "Investigation of heat management for CLC of syngas in packed bed reactors," vol. 225, pp. 174–191, 2013.

[90] Z. Zhou, L. Han, and G. M. Bollas, "Overview of Chemical-Looping Reduction in Fixed Bed and Fluidized Bed Reactors Focused on Oxygen Carrier Utilization and Reactor Efficiency Overview of Chemical-Looping Reduction in Fixed Bed and Fluidized Bed Reactors Focused on Oxygen Carrier Utilizatio," no. January 2014, 2015.

[91] F. Gallucci, H. P. Hamers, M. van Zanten, and M. van Sint Annaland, "Experimental demonstration of chemical-looping combustion of syngas in packed bed reactors with ilmenite," *Chem. Eng. J.*, vol. 274, pp. 156–168, 2015.

[92] S. Noorman, F. Gallucci, M. V. S. Annaland, and J. A. M. Kuipers, "Experimental Investigation of Chemical-Looping Combustion in Packed Beds : A Parametric Study," pp. 1968–1980, 2011.

[93] Z. Deng, R. Xiao, B. Jin, and Q. Song, “Numerical simulation of chemical looping combustion process with CaSO4 oxygen carrier,” *Int. J. Greenh. Gas Control*, vol. 3, no. 4, pp. 368–375, 2009.

[94] K. Mahalatkar, J. Kuhlman, E. D. Huckaby, and T. O’Brien, “CFD simulation of a chemical-looping fuel reactor utilizing solid fuel,” *Chem. Eng. Sci.*, vol. 66, no. 16, pp. 3617–3627, 2011.

[95] X. Wang, B. Jin, W. Zhong, Y. Zhang, and M. Song, “Three-dimensional simulation of a coal gas fueled chemical looping combustion process,” *Int. J. Greenh. Gas Control*, vol. 5, no. 6, pp. 1498–1506, 2011.

[96] A. Abad, P. Gayán, L. F. de Diego, F. García-Labiano, and J. Adánez, “Fuel reactor modelling in chemical-looping combustion of coal: 1. model formulation,” *Chem. Eng. Sci.*, vol. 87, pp. 277–293, 2013.

[97] A. Abad, J. Adánez, L. F. de Diego, P. Gayán, F. García-Labiano, and A. Lyngfelt, “Fuel reactor model validation: Assessment of the key parameters affecting the chemical-looping combustion of coal,” *Int. J. Greenh. Gas Control*, vol. 19, pp. 541–551, 2013.

[98] L. F. De Diego, F. Garcı, J. Ada, A. Abad, and P. Gaya, “Fuel reactor modelling in chemical-looping combustion of coal : 1 . model formulation,” vol. 87, pp. 277–293, 2013.

[99] P. Gayán, A. Abad, L. F. de Diego, F. García-Labiano, and J. Adánez, “Assessment of technological solutions for improving chemical looping combustion of solid fuels with CO2capture,” *Chem. Eng. J.*, vol. 233, pp. 56–69, 2013.

[100] L. F. De Diego, P. Gaya, A. Abad, J. Ada, and F. Garcı, “Fuel reactor modelling in chemical-looping combustion of coal : 2 — simulation and optimization,” vol. 87, pp. 173–182, 2013.

[101] P. Kolbitsch, J. Bolhàr-Nordenkampf, T. Pröll, and H. Hofbauer, “Comparison of two Ni-based oxygen carriers for chemical looping combustion of natural gas in 140 kw continuous looping operation,” *Ind. Eng. Chem. Res.*, vol. 48, no. 11, pp. 5542–5547, 2009.

[102] H. Kruggel-Emden, S. Rickelt, F. Stepanek, and A. Munjiza, “Development and testing of an interconnected multiphase CFD-model for chemical looping combustion,” *Chem. Eng. Sci.*, vol. 65, no. 16, pp. 4732–4745, 2010.

[103] H. P. Hamers, F. Gallucci, P. D. Cobden, E. Kimball, and M. Van Sint Annaland, “CLC in packed beds using syngas and CuO/Al2O3: Model description and experimental validation,” *Appl. Energy*, vol. 119, pp. 163–172, 2014.

[104] L. Han, Z. Zhou, and G. M. Bollas, “Model-Based Analysis of Chemical-Looping Combustion Experiments . Part I : Structural Identifiability of Kinetic Models for NiO Reduction *,” vol. 62, no. 7, pp. 2419–2431, 2016.

[105] E. Jerndal, T. Mattisson, and A. Lyngfelt, “Thermal analysis of chemical-looping combustion,” *Chem. Eng. Res. Des.*, vol. 84, no. 9 A, pp. 795–806, 2006.

[106] T. K. Ibrahim, M. M. Rahman, O. M. Ali, F. Basrawi, and R. Mamat, “Optimum Performance Enhancing Strategies of the Gas Turbine Based on the Effective Temperatures,” *MATEC Web Conf.*, vol. 38, p. 01002, 2016.

[107] B. Erlach, M. Schmidt, and G. Tsatsaronis, “Comparison of carbon capture IGCC with pre-combustion decarbonisation and with chemical-looping combustion,” *Energy*, vol. 36, no. 6, pp. 3804–3815, 2011.

[108] U.S. Deparment of Energy, “Cost and Performance Baseline for Fossil Energy and Natural Gas to Electricity Volume 1: Bituminous Coal Plants,” *J. Philos. Log.*, vol. 38, no. 3, pp. 6657–6670, 2016.

[109] O. Nordness, L. Han, Z. Zhou, and G. M. Bollas, “High-Pressure Chemical-Looping of Methane and Synthesis Gas with Ni and Cu Oxygen Carriers,” 2016.

[110] A. Abad, J. Adánez, F. García-Labiano, L. F. De Diego, and P. Gayán, “Modelling of the Chemical-Looping Combustion of Methane using a Cu-based Oxygen-Carrier,” *Combust. Flame*, vol. 157, pp. 602–615, 2010.

[111] M. Lucio and L. Ricardez-Sandoval, “Dynamic Optimization Applied for Modelling and Optimal Control of a Packed Bed Reactor for Chemical-Looping Combustion,” *IFAC-PapersOnLine*, vol. 52, no. 1, pp. 850–855, Jan. 2019.

[112] R. Naqvi and O. Bolland, “Optimal performance of combined cycles with chemical

looping combustion for CO2 capture," *Proc. Asme Turbo Expo, Vol 3*, no. 2, pp. 117–125, 2007.

[113] J. Wolf, M. Anheden, and J. Yan, "Comparison of nickel- and iron-based oxygen carriers in chemical looping combustion for CO2 capture in power generation," *Fuel*, vol. 84, no. 7–8, pp. 993–1006, 2005.

[114] S. Consonni, G. Lozza, G. Pelliccia, S. Rossini, and F. Saviano, "Chemical-Looping Combustion for Combined Cycles With CO[sub 2] Capture," *J. Eng. Gas Turbines Power*, vol. 128, no. 3, p. 525, 2006.

[115] I. Iliuta, R. Tahoces, G. S. Patience, S. Rifflart, and F. Luck, "Chemical-looping combustion process: Kinetics and mathematical modeling," *AIChE J.*, vol. 55, no. 8, p. NA-NA, 2010.

[116] R. . Perry and D. Green, *Perry's Chemichal Engineers's Handbook*. 2007.

[117] L. F. de Diego, M. Ortiz, F. García-Labiano, J. Adánez, A. Abad, and P. Gayán, "Hydrogen production by chemical-looping reforming in a circulating fluidized bed reactor using Ni-based oxygen carriers," *J. Power Sources*, vol. 192, no. 1, pp. 27–34, 2009.

[118] Z. Zhou, L. Han, and G. M. Bollas, "ScienceDirect Kinetics of NiO reduction by H 2 and Ni oxidation at conditions relevant to chemical-looping combustion and reforming," vol. 9, 2014.

[119] K. E. Sedor, M. M. Hossain, and H. I. De Lasa, "Reduction kinetics of a fluidizable nickel-alumina oxygen carrier for chemical-looping combustion," *Can. J. Chem. Eng.*, vol. 86, no. 3, pp. 323–334, 2008.

[120] M. M. Hossain and H. I. de Lasa, "Chemical-looping combustion (CLC) for inherent CO2 separations-a review," *Chemical Engineering Science*, vol. 63, no. 18. pp. 4433–4451, 2008.

[121] W. E. Hart, "Python optimization modeling objects (Pyomo)," *Oper. Res. Comput. Sci. Interfaces Ser.*, vol. 47, pp. 3–19, 2009.

[122] J. D. Hogg, J. A. Scott, and H. Oxford, "HSL_MA97 : a bit-compatible multifrontal code for sparse symmetric systems," *Rutherford Applet. Lab. Tech. Reports*, 2011.

[123] H. P. Hamers, F. Gallucci, P. D. Cobden, E. Kimball, and M. Van Sint Annaland, “A novel reactor configuration for packed bed chemical-looping combustion of syngas,” *Int. J. Greenh. Gas Control*, vol. 16, pp. 1–12, 2013.

[124] A. Ticâ, H. Guéguen, D. Dumur, D. Faille, and F. Davelaar, “Design of a combined cycle power plant model for optimization,” *Appl. Energy*, vol. 98, pp. 256–265, 2012.

[125] K. B. Bischoff and O. Levenspiel, “Fluid dispersion-generalization and comparison of mathematical models-II comparison of models,” *Chem. Eng. Sci.*, vol. 17, no. 4, pp. 257–264, 1962.

[126] J. B. Butt, “Mass transfer in heterogeneous catalysis, C. N. Satterfield, Massachusetts Institute of Technology Press, Cambridge, Mass.(1970). 267 pages,” *AIChE J.*, vol. 16, no. 3, pp. 509–510, 2004.

[127] H. S. Fogler, “Elements of Chemical Reaction Engineering Elements of Chemical Reaction Engineering,” in *Elements of Chemical Reaction Engineering Elements of Chemical Reaction Engineering*, vol. 3, 1999, pp. 1–535.

[128] T. R. Marrero and E. A. Mason, “Gaseous Diffusion Coefficients,” *J. Phys. Chem. Ref. Data*, vol. 1, no. 1, pp. 3–118, 1972.

[129] Lucio M., Ricardez-Sandoval L., " Dynamic Modelling and Optimal Control Strategies for Chemical-Looping Combustion in an Industrial-Scale Packed Bed Reactor, Fuel

[130] Glenn Reasearch Center, Turbine Thermodynamics, NASA website, https://www.grc.nasa.gov/WWW/K-12/airplane/powtrbth.html

Appendix A

Mass and heat transfer correlations and physical properties

The effective axial dispersion coefficient ($D_{ax\,i,j}$) is calculated with following equation [125]:

$$Pe_{a\,i,j} = \frac{v_{0\,j} D_p}{D_{ax\,i,j}} \quad \forall\ i = \{O_2, CH_4, H_2,\ CO, CO_2, H_2O, Ar\},\ j = \{oxidation,\ reduction,\ purge1, purge2\} \tag{1}$$

Where:

$$\frac{1}{Pe_{a\,i,j}} = \frac{\varepsilon_b}{\tau\ Re_{p\,j}\, Sc_{\,i,j}} + \frac{0.45}{(1+(7.3/(Re_{p\,j}\, Sc_{\,i,j}))} \tag{2}$$

$$Re_{p\,j} = \frac{v_{0j}\, D_p\, \rho_{\,j}}{(1-\varepsilon_b)\mu_j} \tag{3}$$

$$Sc_{i,j} = \frac{\mu_j}{\rho_{\,j} D_{m\,i,j}} \tag{4}$$

$$v_{0\,j} = \frac{G_j}{\rho_{\,j}} \tag{5}$$

where $Pe_{a\,i,j}$ is the axial Peclet number, $v_{0\,j}$ is the superficial velocity at the inlet (m/s), D_p is the diameter of the OC (m); τ is the pore tortuosity, $Re_{p\,j}$ is the Reynolds number based on initial superficial velocity, $Sc_{\,i,j}$ is the Schmidt number; μ_j (N s/m²) and $\rho_{\,j}$ (kg/m³) are the viscosity and the density of the gas mixture, respectively.

The effective axial thermal conductivity ($\lambda_{ax\,j}$) is calculated with the following equation:

$$\frac{\lambda_{ax\,j}}{\lambda_{m\,j}} = \frac{\lambda_e^0}{\lambda_{m\,j}} + 0.7 Pr_j Re_{p\,j} \quad \forall \quad j = \{oxidation,\ reduction,\ purge1, purge2\} \tag{6}$$

Where:

$$Pr_j = \frac{C_{pf\,j} * \mu_j}{\lambda_{m\,j}} \tag{7}$$

where Pr_j is the Prandtl number, λ_e^0 is the static contribution to effective thermal conductivity (W/m /K), $\lambda_{m\,j}$ is the thermal conductivity of the gas mixture (W/m/K) and $C_{pf\,j}$ is the specific heat of the gas mixture (J/Kg/K)

The mass $k_{c\,i,j}$ and heat $h_{f\,j}$ transfer coefficients are estimated as [126]:

$$k_{c\,i,j} = 0.357 Re_j^{-0.359} Sc_{i,j}^{-2/3} \frac{G_j}{\rho_{j^*}\,\varepsilon_b} \quad \forall\ i = \{O_2, CH_4, H_2,\ CO, CO_2, H_2O, Ar\},\ j = \{oxidation,\ reduction,\ purge1, purge2\} \tag{8}$$

$$h_{f\,j} = 1.37 \frac{0.357}{\varepsilon_b} C_{pf\,j}\, G_j Re_j^{-0.359} Sc_{i,j}^{-2/3} \quad \forall\ i = \{O_2, CH_4, H_2,\ CO, CO_2, H_2O, Ar\},\ j = \{oxidation,\ reduction,\ purge1, purge2\} \tag{9}$$

Where:

$$G_j = \frac{F_{in\,j}}{A_c} \frac{C_j}{\rho_j} \tag{10}$$

where G_j is the gas phase mass flux (kg/m²/s).

The bed porosity ε_b for the spherical OC and surface area per unit volume are calculated with [127]:

$$\varepsilon_b = \frac{1.0}{(D_t/D_p)^2} + 0.375 \tag{11}$$

$$a_v = 6(1 - \varepsilon_b)/D_p \tag{12}$$

where D_t is the diameter of the reactor tube (m) and D_p is the diameter of the oxygen-carrier particle.

The effective diffusion coefficient of species *i* ($D_{e\,i,j}$) calculates the true diffusion path from the molecular diffusivity and Knudsen diffusivity ($D_{k,i}$), as follows [116]:

$$\frac{1}{D_{e\,i,j}} = \frac{\tau}{\varepsilon_b}\left(\frac{1}{D_{m\,i,j}} + \frac{1}{D_{k\,i,j}}\right) \forall\ i = \{O_2, CH_4, H_2,\ CO, CO_2, H_2O, Ar\},\ j = \{oxidation,\ reduction,\ purge1, purge2\} \tag{13}$$

Where:

$$D_{m\,i,j} = \frac{1 - y_i}{\sum_{w \neq i} y_v / D_{w,i,j}} \tag{14}$$

$$D_{k\,i,j} = \frac{d_{pore}}{3\sqrt{8R_g T_j / \pi M_i}} \tag{15}$$

where $D_{m\,i,j}$ is the diffusion coefficient of component *i* in the mixture (m²/s), y_i mole fraction of species *i*, $D_{w,i,j}$ binary gas phase diffusivities (m²/s); R_g ideal gas constant (kg m²/s²/K/gmol), M_i is the molecular weight.

Binary gas phase diffusivities for a wide range of temperatures and pressures are estimated through published correlations [126], [128], Table 10 shows the component pairs used for this work.

Table 10 Binary gas phase diffusivities for components pairs [cm²/s]

Pair	A	B	C	D	E	Equation
H_2-CO	15.39e-3	1.548	0.316e8	-2.8	1067	1
H_2-CO_2	3.14e-5	1.75	-	11.7	-	2
CO-CO_2	0.577e-5	1.803	-	-	-	2
CO_2-H_2O	9.24e-5	1.5	-	307.9	-	2
H_2-CH_4	3.13e-5	1.765	-	-	-	2
Ar-H_2	23.5e-3	1.519	0.488e8	39.8	-	1
Ar-CH_4	0.748e-5	1.785	-	-	-	2
Ar-CO	0.904e-5	1.752	-	-	-	2
Ar-CO_2	1.74e-5	1.646	-	89.1	-	2
H_2-H_2O	-	0.927	-	-	-	3
CH_4-H_2O	-	0.361	-	-	-	3
CH_4-CO_2	-	0.153	-	-	-	3

Note that D_{12}=D_{21}. The parameters shown above are for the following expressions:

Equation 1 : $$D_{w,i,j} = \left(\frac{A*{T_j}^B}{P}\right)\left[ln\left(\frac{C}{T_j}\right)\right]^{-2} exp\left(-\frac{D}{T_j}-\frac{E}{{T_j}^2}\right) \quad (16)$$

Equation 2: $$D_{w,i,j} = \left(\frac{A*{T_j}^B}{P}\right) exp\left(-\frac{D}{T_j}\right) \quad (17)$$

Equation 3: $$D_{w,i,j} = \left(\frac{A*T_j+B}{P}\right) \quad (18)$$

The gas phase heat capacity ($C_{pf\ j}$) is taken as a molar average of the gas component heat capacity ($C_{p\ i,j}$), which is estimated using Perry's chemical engineer handbook [116] and shown in Table 11.

Table 11 Gas phase heat capacity constants for relevant species [J/kmol/K]

	A	B	C	D	E
CH_4	33,298	79,933	2,086.9	41,602	991.96
H_2	27,617	9,560	2,466	3,760	567.6
H_2O	33,363	26,790	2,610.5	8,896	1169
CO	29,108	8,773	3,085.1	8,455.3	1538.2
CO_2	29,370	34,540	1,428	26,400	588
Ar	20,105	-	-	-	-

The parameters shown above are for the following expression:

Equation : $$Cp_{i,j} = A + B * \frac{C}{T_j * \sinh\left(\frac{C}{T_j}\right)^2} + D * \frac{E}{T_j * \sinh\left(\frac{E}{T_j}\right)^2} \quad (19)$$

The gas phase viscosity (μ_j) is estimated by the Wilke method with Herning and Zipperer approximation.

$$\mu_j = \sum_{i=1}^{\#comp} \frac{y_i \mu_{i,j}}{\sum_{k=1}^{\#\ comp} y_j \sqrt{M_j/M_i}} \quad (20)$$

The gas phase viscosity ($\mu_{i,j}$) of the species can be calculated using Perry's chemical engineer handbook [116] and shown in Table 12.

Table 12 Gas phase viscosity constants for selected species

	A	B	C	D
CH_4	5.255e-7	0.59006	105.67	-
H_2	1.797e-7	0.685	-0.59	140
H_2O	1.710e-8	1.1146	0	-
CO	1.113e-6	0.5338	94.7	-
CO_2	2.148e-6	0.46	290	-
Ar	9.212e-7	0.60529	83.24	-

The parameters shown above are for the following expression:

Equation: $\mu_{i,j} = A * {T_j}^B/(1 + \frac{C}{T_j} + D/{T_j}^2)$ (21)

The physical properties of the solids are taken from [77] and shown in Table 13.

Table 13 Physical properties of the solids

Active material/inert	**Thermal conductivity, $\lambda_{s\,j}$ (W/m/K)**	**Heat capacity, C_{ps} (J/kg/k)**				**Solid density, ρ_s (kg/m³)**
		Cp_0	Cp_1	Cp_2	Cp^b	
Ni	75	347	2.71e-1	-5.52e-5	596	8900
NiO	13	790	-2.06e-1	1.43e-4	752	6670
γ-Al_2O_3	7	843	5.40e-1	-1.61e-4	1263	3965

The parameters for calculating the heat capacity of the solid species showed above are for the following expression:

Equation: $Cps^a = Cp_0 + Cp_1\,T_j + Cp_2{T_j}^2\ ;\ Cp^b\ at\ Tref = 1223\ K$ (22)

The heat capacity of the OC heat capacity ($C_{ps\ j}$) is taken as the mass proportion of each solid component times its heat capacity (Cps^{a}). Similarly, the thermal conductivity ($\lambda_{s\ j}$) and density ($\rho_{s\ j}$) of the OC are taken as the mass proportion of each component times its thermal conductivity and solid density, respectively.